INTERPLAY BETWEEN P-GLYCOPROTEIN-MEDIATED EFFLUX AND CYTOCHROME P4503A-MEDIATED METABOLISM IN THE INTESTINE

Beverly M. Knight

A dissertation submitted to the faculty of the University of North Carolina at Chapel Hill in partial fulfillment of the requirements for the degree of Doctor of Philosophy in the School of Pharmacy

Chapel Hill
2007

Approved by:

Advisor: Dr. Dhiren R. Thakker

Reader: Dr. Gary M. Pollack

Reader: Dr. Mary F. Paine

Reader: Dr. Joseph Polli

Reader: Dr. Anthony Hickey

ABSTRACT

BEVERLY M. KNIGHT: INTERPLAY BETWEEN P-GLYCOPROTEIN EFFLUX AND CYTOCHROME P4503A-MEDIATED METABOLISM IN INTESTINE

(Under the direction of Dhiren R. Thakker, Ph.D.)

Intestinal metabolism and drug efflux are recognized as two important barriers to drug absorption. The interactions between these factors may also be an important consideration in evaluating the drug-drug interaction potential of a given compound. Presented here are mechanistic studies that examine the interaction between the most germane metabolic enzyme/efflux transporter pair: cytochrome P4503A (CYP3A) and P-glycoprotein (P-gp).

In order to study this interaction, two model systems and two dual CYP3A/P-gp substrates were selected. The first model used was the CYP3A-expressing Caco-2 cell system. This system allowed for detailed mechanistic studies, with few confounding factors. The second system utilized was fresh mouse intestine (from P-gp competent and deficient mice) in a side-by-side diffusion chamber model. This model provided more physiologically relevant results with the caveat of increased complexity. The two drugs selected for study were terfenadine (an antihistamine) and loperamide (an antidiarrheal). In order to study the interplay between P-gp efflux and metabolism, the metabolism of each compound was measured during

absorptive transport across Caco-2 cell monolayers and mouse tissue, in the presence or absence of P-gp activity.

In the Caco-2 cell system, the results varied between the two compounds. Loperamide showed an increase in metabolism in the presence of the P-gp inhibitor GW918, while terfenadine showed no change. The lack of effect for terfenadine may be due to the action of a second transporter. In the mouse intestine, both compounds showed a higher metabolic rate in the absence of P-gp expression. For both systems, the effects were seen only within the low dose range, below about 50 μM. This study also showed that terfenadine is metabolized about 60% by an enzyme that is inhibitable by quinidine (possibly CYP2D22) and only 40% by CYP3A in mouse intestine.

The results presented in this dissertation indicate that P-gp efflux effectively decreases metabolism in intestine by decreasing intracellular concentrations. This conclusion is also supported by the pharmacokinetic modeling and simulations presented. The mechanistic information collected can provide insight into the nature of the CYP3A/P-gp interaction and can help in developing better models to predict *in vivo* intestinal drug-drug interactions.

DEDICATION

I dedicate this dissertation to myself, for succeeding despite everything.

ACKNOWLEDGEMENTS

I would like to thank my advisor, Dr. Dhiren Thakker for all of his patience, advice and guidance.

I would also like to thank my committee members for their participation and feedback. In particular, I am grateful to Dr. Mary Paine for providing materials and for her assistance with the induction studies.

I would like to thank J. Cory Kalvass for his support and for all of the time we spent in coffee shops studying, writing, and discussing.

I am grateful to GSK for loaning us equipment and to Pfizer and for funding my project, and to GSK and the PhRMA Foundation for providing fellowships.

TABLE OF CONTENTS

LIST OF TABLES

LIST OF FIGURES

ABBREVIATIONS

A-to-B	Apical to Basolateral
B-to-A	Basolateral to Apical
BCRP	Breast Cancer Resistance Protein
BCS	Biopharmaceutics Classification System
C	Concentration
CYP3A	Cytochrome P4503A
ER	Extraction Ratio
HIM	Human Intestinal Microsomes
J_{max}	Maximum rate of efflux
kDa	Kilodaltons
K_m	Concentration at which half of the maximum rate is achieved
KO	P-gp deficient mouse
MDR	Multidrug Resistance Protein
mdr1a(+/+)	P-gp competent mouse
mdr1a(-/-)	P-gp deficient mouse
MIM	Mouse Intestinal Microsomes
M_{in}	Amount of compound that is available to be cleared
MLM	Mouse Liver Microsomes
M_{out}	Amount of compound lost to metabolism, i.e. $M_{metabolites}$
M_{parent}	Amount of intracellular parent drug
MRP	Multidrug Resistance Associated Protein
OATP	Organic Anion Transporting Polypeptide

PEPT1	Peptide Transporter
P_{app}	Apparent permeability
P-gp	P-glycoprotein
WT	Normal (P-gp competent) mouse
V_{max}	Maximum rate of metabolism

CHAPTER 1: DECONVOLUTING THE EFFECT OF P-GP EFFLUX ON CYP3A-MEDIATED METABOLISM IN INTESTINE: A MAJOR CHALLENGE

Beverly M. Knight, Matthew D. Troutman and Dhiren R. Thakker

Current Opinion in Pharmacology, 2006

A. ABSTRACT

Metabolism by Cytochrome P4503A (CYP3A) and P-glycoprotein-mediated efflux transport are two important biochemical barriers to drug absorption from the intestine. CYP3A, the most abundant subfamily of drug-metabolizing enzymes, shares many substrates with the efflux transporter P-glycoprotein (P-gp). While the impact of each of these systems on drug disposition is routinely assessed individually, the effect of both systems acting in concert during intestinal absorption is difficult to ascertain. Researchers have published conflicting findings on how efflux affects metabolism. Pharmacokinetic theory predicts that the effect of efflux on overall metabolism depends on substrate concentrations relative to the respective kinetic parameters of these processes (i.e. affinities for transport and metabolism as well as capacities of these processes). In contrast, the *in vitro* parameters (e.g. extraction ratio, ER) that have been used to explain or predict the effect of P-gp-mediated efflux on CYP3A-mediated metabolism of dual substrates are more relevant for describing overall changes to extraction efficiency of the system (intestinal epithelium), rather than deconvoluting the effect of P-gp on CYP3A-mediated metabolism. Developing a more refined way to understand this interplay and its potential relevance to drug absorption is an important goal, as a large proportion of marketed drugs and many modern drug discovery candidates are known to be affected by one or both of these proteins. Also, since many modern

drug discovery candidates are substrates for these processes, a more detailed understanding of how these barriers can ultimately influence oral absorption is needed for better decision-making for compound progression.

B. ORAL DRUG ABSORPTION

The oral route is the preferred route of delivery for most therapeutic agents. Despite this, there are still some gaps in our understanding of the mechanisms involved in oral absorption. There are many physical and biochemical factors associated with the liver and intestine that can introduce variability in the extent of drug absorption. Further study is, therefore, needed in order to more accurately predict the absorptive properties of new drug candidates.

B.1. Intestinal Epithelium

During absorption, drugs must traverse the intestinal epithelium. The intestinal epithelium is a highly specialized barrier that is composed of a continuous single layer of polarized cells, or enterocytes (Figure 1.1). The epithelium is folded into villi, which provide a large surface area for absorption of nutrients; the enterocytes also have microvilli on the apical (lumenal) side to maximize surface area. The spaces between the cells are bridged by tight junctions, which limit the paracellular permeability of most compounds, except those that are very small and hydrophilic. Therefore, most compounds are absorbed transcellularly by first crossing the apical membrane of the enterocyte by either diffusing passively or by transport using

carrier proteins. Then the compound must diffuse through the cell and cross the basolateral membrane (actively or passively) to be absorbed into the bloodstream.

B.2. Bioavailability

Optimization of drug bioavailability is an important aspect of oral delivery of human therapeutic agents. Bioavailability is defined as the rate and extent of drug absorption into the systemic circulation (Gilbaldi and Perrier, 1982). Ideally, the bioavailability of a therapeutic agent should be high, with low intersubject variability; this would help to ensure predictable safety and efficacy. During drug discovery, a great deal of emphasis is placed on improving intestinal absorption by optimizing drugs' physicochemical properties; however, many biological factors can also significantly influence a therapeutic agent's oral bioavailability, including intestinal permeability, lumenal contents/pH, GI motility and metabolism by enzymes in the intestine.

In order to predict which drugs will be affected by these factors, a model termed the Biopharmaceutics Classification System (BCS) has been developed (Amidon et al., 1995). Drugs were placed into four classes based on solubility and permeability values (Table 1.1). For the compounds in BCS Class I, the high solubility results in saturation of drug efflux and metabolism, so these drugs are likely to have high bioavailability values that correlate well with *in vitro* predictions from dissolution data. The compounds in BCS Classes II and III are likely to be substrates for transporters

and metabolic enzymes. For example, many substrates of P-gp are lipophilic and therefore fall into Class II: they have high permeability and low aqueous solubility (Seelig, 1998). Thus, the bioavailability of these Class II and III drugs may be difficult to predict using physicochemical analyses (Wu and Benet, 2005). Class IV contains drugs with undesirable properties for oral delivery, and therefore relatively few drugs from this class have been developed into orally administered products. The following discussion will primarily be relevant to the compounds in Classes II and III; i.e., the drugs for which current models are unable to accurately predict the absorptive behavior.

C. BIOCHEMICAL BARRIERS TO DRUG ABSORPTION

In addition to the physicochemical parameters that determine the rate at which a compound crosses the epithelium, many biochemical processes can affect the rate of absorption and the amount of compound that reaches the portal vein. For most drugs, a primary factor of concern is “first pass” extraction of drugs by metabolism in the intestine and liver and biliary excretion in the liver. Both the liver and intestine are rich in drug-metabolizing enzymes, including peptidases, hydrolases, alkaline phosphatases, and CYP enzymes. In addition, uptake transporters in the intestinal epithelium such as OATP and PEPT1 can facilitate absorption of compounds, while efflux transporters such as P-glycoprotein (P-gp), multidrug resistance associated proteins (MRPs) and breast cancer resistance protein (BCRP) can play a role in reducing the bioavailability and pharmacokinetic profiles of substrates.

As substrates translocate from the apical side (facing the intestinal lumen) of the cells to the basolateral (blood) side, efflux transporters (e.g., P-gp) in the apical membrane function to prevent the drug from entering enterocytes, resulting in an effective reduction of the compound’s permeability; if this barrier is overcome, the drug can then be subject to oxidative metabolism by enzymes, most notably, CYP3A, within the smooth endoplasmic reticulum of the enterocyte. Any drug within the enterocyte that is not metabolized or effluxed can diffuse across the basolateral membrane and enter the bloodstream, where it is subsequently carried to the liver for processing.

It is also worth noting that, if solubility is high, a drug may be able to overcome the barriers of metabolism and efflux, since both processes are saturable; this may be more likely to occur in the proximal intestine, where drug concentrations are often higher. Ultimately, drug bioavailability depends on physical properties of the compound and on both hepatic and intestinal first-pass clearance mechanisms.

C.1. Intestinal CYP3A

CYP3A is the most highly expressed subfamily of CYP enzymes in both human small intestine and liver (Paine et al., 1997; Paine et al., 2006; Shimada et al., 1994). CYP3A enzymes are NADPH-dependent hemoproteins with a wide range of substrates, which tend to be relatively lipophilic (Bu, 2006). Although bound to the membranes of endoplasmic reticulum, CYP3A enzymes are in close proximity to the apical membrane of enterocytes (Figure 1.4) where P-gp resides (Cummins et al., 2001). CYP3A enzymes are involved in the metabolism of a majority of the drugs that are on the market and have most frequently been implicated in drug-drug interactions (Dresser et al., 2000). Drugs such as ketoconazole, erythromycin and clarithromycin are well known inhibitors of CYP3A that increase the plasma concentrations of coadministered CYP3A substrates to toxic levels. Although *in vitro* assays are often used during drug development in an effort to identify these types of interactions for a given compound, the reliability of these predictions is still somewhat limited (Obach et al., 2006).

CYP3A acts similarly in the intestine and liver (Watkins, 1997), but the average intestinal content of CYP3A has been estimated to be only 70 nmoles in humans, much less than the average hepatic content of 5000 nmoles (Paine et al., 1997). Nevertheless, for certain drugs, intestinal metabolism is at least as extensive as hepatic metabolism. This phenomenon may be explained by better access to the enzymes in intestine because of the large absorptive surface area, and also could be due to reduced access to hepatic enzymes because of potential binding to proteins in portal blood (Hall et al., 1999).

One group of researchers was able to show, using an intestinal perfusion technique in humans, an equivalent extent of metabolism of the CYP3A substrate verapamil in the intestine and liver (extraction ratios were 0.49 and 0.48, respectively) (von Richter et al., 2001). Other investigators have taken a more direct approach. For example, in an experiment conducted during liver transplant surgery, it was demonstrated that 43% of an intraduodenal midazolam dose was metabolized by intestinal CYP3A during the anhepatic phase of the surgery (Paine et al., 1996). These studies demonstrate the importance of intestinal metabolism as well as the complexities involved in studying this process clinically. In addition, intestinal CYP3A content varies between patients and is susceptible to inhibition and/or induction by co-administered drugs, which may lead to toxicity or a lack of efficacy; therefore, understanding the true role of drug metabolism in determining gut bioavailability is essential (Lampen et al., 1996). Unfortunately, there are currently few robust methods for determining this contribution.

C.2. Intestinal P-glycoprotein (P-gp)

The drug transporting protein P-gp (ABCB1) was first discovered as an efflux pump that is highly expressed in multidrug-resistant cells, conferring the MDR phenotype (Juliano and Ling, 1976). Two members of the MDR gene family have been identified in humans. The MDR3 gene encodes a phospholipid "flippase", while the MDR1 gene encodes the better known drug efflux transporter P-gp (van Helvoort et al., 1996). This 170 kDa protein consists of 12 membrane-spanning domains and two ATPase catalytic sites that drive drug efflux. The substrate binding site(s) of the protein are thought to be located within the plasma membrane (Gottesman and Pastan, 1993), since most P-gp substrates are lipophilic in nature, but the mechanism of drug efflux is still under debate. A "vacuum cleaner" model has been proposed by which P-gp siphons drug out of the membrane and extrudes it into the extracellular space (Raviv et al., 1990).

Another possible mechanism is the "flippase" model, which theorizes that P-gp flips the drug from the inner to the outer leaflet of the membrane (Higgins and Gottesman, 1992). This is plausible since P-gp has been shown to interact with a broad range of membrane lipids (van Helvoort et al., 1996; Romsicki and Sharom, 1999) and since drug efflux can be modulated by various agents which perturb the membrane (e.g., PEGs (Shen et al., 2006)).

P-gp is now known to be constitutively expressed in many cells of the body including hepatocytes, epithelial cells of the placenta and kidney, the capillary endothelium that comprises the blood-brain barrier, and the columnar cells of intestinal epithelium. It plays a protective role in many tissues, including the small intestine. P-gp resides in the apical membranes of intestinal enterocytes (Thiebaut et al., 1987), where it modulates apical to basolateral (luminal to blood) permeability by effluxing compounds from enterocytes back into the intestinal lumen. It should be noted that this is opposite to the direction of flux in the liver, where drugs enter hepatocytes from the portal blood across the basolateral (sinusoidal) membrane and can be metabolized within the cell or pumped into bile by efflux transporters at the apical (canalicular) membrane (Figure 1.1). Consequently, the role of P-gp differs in these two organs: in the liver, it can act as a clearance mechanism competing with metabolism, while in intestine it can reduce the rate and extent of absorption.

The effect of P-gp on drug absorption has been clearly established in mice deficient for the P-gp gene(s) (Smit et al., 1998). In addition, a subpopulation of collie dogs deficient in functional P-gp has been shown to exhibit toxicity after oral ingestion of the antiparasitic drug, ivermectin (Paul et al., 1987) (Roulet et al., 2003). A growing body of evidence supports the importance of P-gp in intestinal drug-drug interactions (Endres et al., 2006). For example, rifampin has been shown to induce P-gp in the intestine, decreasing the area under the curve (AUC) of orally dosed digoxin, in healthy volunteers (Achira et al., 1999). Another clinical study found a significant inverse correlation between intestinal P-gp expression and cyclosporine A

maximum plasma concentration (C_{max}) in 25 renal transplant patients (Lown et al., 1997). A third clinical study concluded that an interaction between rifampin and oral erythromycin was most likely caused by P-gp induction (Paine et al., 2002). In rats, ketoconazole was shown to increase digoxin AUC approximately 5-fold after oral dosing by inhibiting intestinal P-gp (Salphati and Benet, 1998). Studies comparing P-gp-deficient mice to normal mice have also shown increases in drug bioavailability and systemic exposure of P-gp substrates in the absence of P-gp expression (Chen et al., 2003). It is probable that many drug-drug interactions that were previously attributed to CYP3A are at least in part due to the activity of intestinal P-gp, as was shown previously for cyclosporine A (Lown et al., 1997).

D. METABOLISM/TRANSPORTER INTERPLAY

Some investigators have considered the possibility of functional interplay between drug transporters and metabolic enzymes in the intestine and its effect on drugs that are substrates for both proteins (Cummins et al., 2002). Although there are many efflux transporters and metabolic enzymes that can affect drug absorption, most studies in this area have focused on the interaction between P-gp and CYP3A due to their wide and overlapping substrate specificities (Table 1.2), co-localization, and similarity of (protective) function.

In addition to location, P-gp and CYP3A have overlapping, yet not identical, regulatory pathways (Schuetz et al., 1996) and, as mentioned above, share many of the same substrates (Table 1.2). These observations have led to the hypothesis that transport and metabolic processes work cooperatively to reduce absorption of dual substrates across the enterocyte layer. However, the literature is not quite unified on how these two proteins interact with each other to attenuate the oral bioavailability of their dual substrates.

This type of functional interaction is not without precedent. P-gp activity has previously been shown to decrease metabolism of dual substrates in the liver. In a previous study, P-gp deficient mice (mdr1a/1b(–/–)) and mice expressing P-gp (mdr1a/1b(+/+)) were compared with regards to erythromycin metabolism by hepatic CYP3A. The assay utilized, the erythromycin breath test, has been considered to be

primarily a measure of hepatic CYP3A metabolism. Although the two strains of mice showed equivalent levels of CYP3A expression, and equivalent CYP3A activity in liver microsomes, the deficient mice showed about a 2-fold higher AUC (area under the curve) and increased maximum $^{14}CO_2$ exhalation rate (a measure of hepatic CYP3A activity) (Lan et al., 2000), suggesting that P-gp efflux can attenuate hepatic CYP3A metabolism. However some recent evidence has suggested that the erythromycin breath test may also reflect P-gp activity (Kurnik et al., 2006). The authors showed that the P-gp inhibitor taquidar could increase the $^{14}CO_2$ exhalation rate, independent of CYP3A activity. Therefore, the results from this study may need to be reassessed in light of the recent reports of the effect of P-gp on this assay.

The first group to study the P-gp/CYPA interaction *in vitro* noted that oxidative metabolism of the dual substrate cyclosporine A was greater during absorptive transport (apical to basolateral) than during secretory transport (basolateral to apical) across Caco-2 cell monolayers (an immortalized human colon carcinoma cell line used as an *in vitro* model of human intestinal epithelium), implying an enhancement of metabolism in the absorptive direction due to P-gp efflux. These authors proposed that extension of cellular transit time was the underlying mechanism by which the efflux activity of P-gp at the apical membrane could influence metabolism (Gan et al., 1996). Subsequently, several studies have been performed to investigate the mechanism of this interaction, leading to the hypothesis that transport and metabolic processes, catalyzed by P-gp and CYP3A respectively,

work cooperatively to reduce absorption of dual substrates across intestinal epithelium (Gan et al., 1996; Hochman et al., 2000; Cummins et al., 2001; Cummins et al., 2002; Benet et al., 2004).

D.1. Current *In Vitro* Approaches for Understanding CYP3A/P-gp Interplay

There are a few *in vitro* methods that have been used to elucidate the interactions between P-gp and CYP3A, in attempts to clarify their combined effect on the intestinal absorption of dual substrates. The Caco-2 cell model (Figure 1.2) is used to study drug transport due to its morphological and biochemical similarity to the intestinal epithelium, including expression of P-gp. Unlike enterocytes, quiescent Caco-2 cells do not normally express CYP3A4. However, methods have been adapted to allow study of both transport and metabolism either by transfection with the CYP3A gene or by treating cells with 1α, 25-dihydroxyvitamin D_3, which induces functionally active CYP3A (Schmiedlin-Ren et al., 1997). For compounds that are dual CYP3A/P-gp substrates, the interaction between transport and metabolism is often assessed by comparing the extent of metabolism relative to drug transported, in the presence versus absence of a P-gp inhibitor. However, there is still some uncertainty as to which parameters should be used in interpreting the results of these studies. Hochman, et al. used the following equation to calculate the extent of metabolism in cell transport studies (Hochman et al., 2000):

$$Metabolite/parent\ ratio = \frac{\sum M_{metabolites}}{M_{out}} \qquad \text{Equation 1}$$

where $M_{metabolites}$ is the cumulative mass of all metabolites from all compartments at time *t* and M_{out} is the mass of parent compound appearing in the receiver compartment at time *t*.

Another parameter, the extraction ratio (ER), has been proposed by Fisher et al. (Fisher et al., 1999):

$$ER = \frac{\sum M_{metabolites}}{\sum M_{metabolites} + M_{out}} \qquad \text{Equation 2}$$

Subsequently, Benet et al. (Benet et al., 2004) modified this definition to include the amount of intracellular parent drug (M_{parent}) in the denominator of the above equation to produce equation 3:

$$ER = \frac{\sum M_{metabolites}}{\sum M_{metabolites} + M_{out} + M_{parent}(\text{at time}\, t)} \qquad \text{Equation 3}$$

We feel that this approach of defining ER is not valid because intracellular parent, as defined in equation 3, is not committed to metabolism and/or egress into the basolateral compartment; rather, a fraction is available for efflux back into the apical compartment.

It should be noted that these equations attempt to quantify the efficiency of the cell monolayer in removing the parent drug and to provide a relationship between

how much parent drug is metabolized vs. how much ultimately reaches the receiver compartment intact. However, these relationships have also been used to explain how P-gp efflux affects metabolism. That is, a decrease in ER with P-gp inhibition presumes a decrease in metabolism, implying that active P-gp increases metabolism. For example, Cummins et al. (Cummins et al., 2002) used the CYP3A-expressing Caco-2 cell model to show that the ER (equation 3) of the dual CYP3A/P-gp substrate K77, a cysteine protease inhibitor, decreased from 33% to 14% in the presence of the selective P-gp inhibitor GW918. The authors concluded that P-gp activity enhances the metabolism of K77 by CYP3A using Equation 3, which includes intracellular parent in the denominator of the equation. Measuring intracellular concentrations of parent drug in the K77 study, however, did provide an insight that was perhaps not intended. This data showed that intracellular concentrations of K77 attained upon inhibition of P-gp (estimated >200 µM) may have exceeded the linear range for its CYP3A4-mediated metabolism (based on a reported K_m of ~14 µM for CYP3A metabolism using human liver microsomes (Jacobsen et al., 2000)).

Another Caco-2 cell study, conducted using the dual substrate sirolimus, yielded similar conclusions (Cummins et al., 2004), but the results of this study were also confounded by the inhibitory nature of metabolites of sirolimus. A subsequent K77 study utilizing the perfused rat intestine model also showed a slight decrease in the ER with GW918 treatment but this difference was not significant (Cummins et al., 2003). Another research group corroborated the results by showing that inhibition of

P-gp in CYP3A4-competent Caco-2 cells increased the extraction ratio of indinavir in the A-to-B direction, although the extent of metabolism was unchanged (Hochman et al., 2000) (Hochman et al., 2001); interestingly, cyclosporine A was used as a specific P-gp inhibitor in this study, although it has been used as a CYP3A inhibitor by the previous investigators at the same concentration. In addition, a theoretical model developed by Ito et al. showed that this synergistic effect is enhanced when the diffusion rate of the drug through the cytoplasm is slow (Ito et al., 1999).

D.2. Mathematical Models for Studying CYP3A/P-gp Interplay

Based on their results, Benet et al. proposed a mechanism by which a drug undergoes perpetual cycles of diffusion into and efflux out of the enterocytes as it travels down the intestine, increasing metabolic enzyme exposure, and therefore increasing the extent of metabolism by prolonging the mean residence time (MRT) of drug in the intestine and at the enzyme site (Benet et al., 2004). A pharmacokinetic model was specifically developed to examine this possibility (Tam et al., 2003a); it showed that secretion could increase metabolite formation only under narrowly defined conditions: metabolism must be saturable, apical absorption must be fairly rapid, and drug partitioning at the basolateral compartment must be low. For all other scenarios tested, efflux increased MRT in all compartments but failed to elicit a corresponding increase in metabolite accrual.

Several pharmacokinetic models have been developed which have failed to predict the experimentally observed decrease in extraction ratio with P-gp inhibition, except in the presence of system nonlinearity (Tam et al., 2003a; Tam et al., 2003b) i.e., when drug concentrations within the cell are sufficient to saturate or inhibit metabolism. Theoretical work done by one group demonstrated that efflux and metabolic clearances are not independent; rather, these processes may compete with one another. Therefore, an increase in intrinsic efflux clearance would be expected to result in a decrease in observed metabolic clearance (Tam et al., 2003), i.e., under linear metabolic conditions, drug efflux from cell monolayers would be expected to decrease, not increase, metabolism. However, further work from this group supported the idea that, under nonlinear metabolic conditions, efflux may be able to increase metabolism by decreasing enzyme saturation (Johnson et al., 2003a). In other words, P-gp efflux may increase the efficiency of a compound's metabolism by reducing the parent concentration in the cell, and therefore maintaining linear conditions. This may help explain the unexpectedly high intestinal metabolism of compounds whose clinically dosed concentrations would be expected to produce enzyme saturation.

Another group reached a similar conclusion from experiments that examined the transport of verapamil *in vitro* across rat intestinal mucosa (Ussing chamber) (Johnson et al., 2003a), *in situ* (autoperfused rat jejunum) (Johnson et al., 2003b), and through development of compartmental models to describe these processes.

Their simulations also showed that, in order for P-gp to increase the extraction ratio, nonlinearity must be inherent in the system (Johnson et al., 2003a).

Similarly, a study done with the dual substrate saquinavir in the CYP3A4-expressing Caco-2 cell system showed that inhibition of P-gp increased the rate of metabolism but ER decreased with increasing dose (Table 1.3), implying that the intracellular concentrations of saquinavir achieved by P-gp inhibition were likely to be in the range to saturate metabolism (Mouly et al., 2004). These results confirmed earlier theoretical work, which predicted that a decrease in extraction ratio with P-gp inhibition could occur only in the presence of such a system nonlinearity (Johnson et al., 2001; Johnson et al., 2003a; Tam et al., 2003a; Tam et al., 2003b). While it is recognized that saturation is possible for both efflux and metabolic processes, few studies have accounted for the effect of this nonlinearity when assessing the P-gp/CYP3A interaction.

Recently it was shown that P-gp inhibition increased metabolism of the dual substrate UK-343,664 in both the perfused rat ileum and jejunum (Kaddoumi et al., 2006). The authors had set out to study regional differences in the intestine, which are also an important consideration when evaluating the P-gp/CYP3A4 interaction. CYP3A is most highly expressed in proximal regions of the intestine (Paine et al., 1997), while P-gp appears to be more active distally (Stephens et al., 2001), and wide interindividual variability is observed for both proteins (Lindell et al., 2003).

Some theoretical work has been done to explore the implications of this heterogeneity (Tam et al., 2003b).

Of course, mathematical models cannot substitute for experimental data, but the lack of agreement between these models and observed results may be indicative of a gap in our understanding of these processes.

E. CAN CURRENTLY USED PARAMETERS QUANTIFY THE EFFECT OF EFFLUX ON METABOLISM?

Equations 1-3 can be used to quantify changes in the relative amounts of metabolites versus parent drug appearing on the basolateral side of the cell monolayer, but can they accurately quantify how efflux affects metabolism? These two experimental goals are not the same. To illustrate this difference, Table 1.3 shows the reported (or calculated) ER values for several compounds, as well as the corresponding values for the percent of applied dose metabolized. It is clear that the changes in percent metabolized with P-gp inhibition are very small compared with those reported for ER, and the change can be opposite in direction, leading to different conclusions. In fact, when the amount of metabolites produced is unchanged by P-gp inhibition, a decrease in ER is obtained using this equation. This can occur because P-gp ultimately influences the amount of parent appearing in the receiver compartment, and by definition ER must be affected by P-gp activity, irrespective of its effect on metabolism. Figure 1.3 further illustrates this key point.

The primary action of P-gp-mediated efflux is to reduce the permeability of the substrate across the enterocyte layer. Indeed, P-gp-mediated efflux activity will reduce the (steady-state) flux of a compound across the cell layer rather than prevent it (P-gp in the intestine does not act as a true clearance mechanism). In this regard, P-gp can determine how much of the dose (M_0) ultimately enters the cell (M_{in}) per given time, under sink conditions. M_{in} is the total amount of the drug that can be irreversibly cleared; it can be expressed as amount of metabolites ($M_{metabolites}$) plus the amount of parent drug that reaches the basolateral chamber (M_{out}). It is important to note that $M_{metabolites}$ and M_{out} represent the amount of the parent drug that is no longer subject to metabolic clearance or efflux into the apical compartment. M_{out} is affected by P-gp and CYP3A, but in different ways: P-gp indirectly affects M_{out} by influencing the magnitude of M_{in}, while CYP3A can directly affect M_{out} because the rate of loss to metabolism of M_{in} competes with the rate of appearance of intact drug in the basolateral compartment as M_{out}. Due to the sensitivity of M_{out} to both P-gp and CYP3A activity, relationships that include M_{out} cannot clearly quantify how efflux affects metabolism. Thus ER cannot solely be used to quantify how efflux affects metabolism, but it can be used to gauge how changes to the system (differences in efflux or metabolism) affect the amount of intact drug that crosses the cell monolayer to reach the basolateral compartment.

The definition of ER in equation 2 derives from the following pharmacokinetic definition of extraction ratio:

$$ER = \frac{M_{in} - M_{out}}{M_{in}}$$ Equation 4

where M_{in} is the compound that is available to be cleared and $M_{in} - M_{out}$ is equal to the amount lost to metabolism, i.e. $M_{metabolites}$. While M_{out} and $M_{metabolites}$ are easy to measure, M_{in} cannot be directly measured; therefore, equation 2 can be considered an operationally useful form of equation 4. It is important to note for this type of experiment that M_{in} is not the applied dose (M_0; see Figure 1.3); rather, it is the amount of compound that is available for CYP3A to clear via metabolism or for egress into the basolateral compartment. Again, it is easy to see with Equation 4 and Figure 1.3 that P-gp's influence on M_{in} can confound attempts at understanding the consequences of changes in P-gp activity on metabolism.

Although the ER seems to derive from the E_H (hepatic extraction ratio), there is really little resemblance between the two parameters, so conclusions based on ER should be carefully considered. In an *in vitro* system there are several implicit assumptions for use of this parameter: 1.The system is well-stirred and is at steady-state, so the effect of flow into the cell (permeability x surface area) is ignored. 2. Metabolism occurs within the linear range even when P-gp is inhibited. 3. Paracellular flux is negligible and transcellular flux is not affected by intracellular binding. 4. The amount transported is proportional to the amount metabolized, since both values depend on intracellular concentrations. This last assumption is particularly important, since this implies that the extraction ratio should not change with changes in intracellular concentrations. If a decrease in extraction ratio is

observed with P-gp inhibition, this indicates that the amount transported increased to a greater extent than the amount metabolized, meaning that the assumptions of the model have been violated.

Therefore, the ER cannot be used alone as a surrogate for enterocytic clearance when comparing metabolic efficiencies in the presence versus absence of P-gp efflux, because this violates the assumptions of the model. The ER appears to be more sensitive to changes in efflux than changes in metabolism, i.e. compounds with higher AQ value (absorptive quotient, a measure of the functional effect of P-gp in the absorptive direction (Troutman and Thakker, 2003)) would be expected to produce a more significant change in ER when P-gp is inhibited than those with lower AQ values. Thus the enterocytic metabolic clearance and percent of dose metabolized may be more relevant parameters for assessing this interaction.

F. CONCLUSIONS

It appears that current *in vitro* analyses are insufficient for prediction of the combined effect of CYP3A and P-gp, since the data cannot easily be extrapolated to *in vivo* findings. It is currently very difficult to understand the role of CYP3A4 alone during drug absorption; our lack of understanding of the CYP3A4/P-gp interplay may be partially due to poor understanding of intestinal metabolism and our inability to accurately quantify it. While the Caco-2 cell system represents a valuable model for the study of drug absorption, the experimental conditions commonly used for these cellular assays are likely to cloud the interaction between P-gp and CYP3A, producing misleading conclusions. Furthermore, the parameters used to quantify the purported synergism between the proteins may not be useful for prediction of *in vivo* outcomes. Unfortunately, it is often difficult to extrapolate from the results observed in a reduced *in vitro* system in which certain factors are ignored to the overall complexity of interacting factors seen *in vivo*.

For drugs that are substrates for both P-gp and CYP3A, a better understanding of the mechanisms of interplay between the activities of these two proteins is essential to making informed predictions regarding their effect on absorption of these compounds. Clearly the kinetic complexity of this interaction, and the apparent disagreement between conclusions derived from experimental versus theoretical studies, provide a clear rationale for further mechanistic studies on this subject matter. Indeed, the nature of this interaction can best be understood on a molecular

level in its unique context: intestine or liver. This dissertation asserts that *in vitro* approaches published to date, involving determination of the ER, cannot dissect how P-gp affects CYP3A-mediated metabolism from the overall outcome in terms of intestinal epithelium- or cell monolayer-mediated extraction. Furthermore, application of pharmacokinetic theory supports using the Fisher definition of ER (Fisher et al., 1999) (equation 2) over that proposed by Cummins et al. (Cummins et al., 2002) (equation 3) to understand the overall relevance of P-gp/CYP3A interplay. Nonetheless, percentage of dose metabolized would represent the most relevant parameter for studying this interaction. However, these studies should be conducted over a range of time and intracellular drug concentrations in order to account for non-linearity in transport and metabolism when considering the overall effect of the interplay of P-gp and CYP3A on drug absorption.

Currently used drug screens can identify drug candidates as P-gp or CYP3A substrates, but are unable to address potential interactions between these systems. This is primarily due to the lack of information regarding this interaction, and the inability to scale *in vitro* results to *in vivo* situations. This information is critical for drugs that are substrates for both proteins and have narrow therapeutic indices; a better understanding of the mechanisms of interplay between P-gp and CYP3A is essential to making informed predictions regarding absorption of these compounds. A more thorough examination of the problem is required in order to develop predictive models that can be used in drug discovery and development settings.

G. PROPOSED RESEARCH

The goal of the studies outlined in this dissertation was to test the hypothesis that P-gp efflux decreases the rate of CYP3A-mediated metabolism of dual substrates in the intestine in a concentration-dependent manner. As discussed in this chapter, there is some controversy in this area regarding previously reported data and especially the interpretation of the data. This dissertation aimed to examine the problem more broadly by studying the metabolism of P-gp/CYP3A substrates over a wide concentration range, in the presence and absence of P-gp efflux activity. These studies used *in vitro* models to study the interaction between P-gp and CYP3A on a more mechanistic level.

Although some *in vitro* screens are available to study the properties of new drug entities, these systems determine the susceptibility of a molecule to transport and metabolic processes separately and therefore cannot be used to study transport/metabolism interplay. An *in vitro* system that could be used to simultaneously study transport and metabolism would have significant advantages over existing methodologies. Therefore, two *in vitro* systems that provide the capability of measuring both transport and metabolism were used to study the P-gp/CYP3A interaction: Caco-2 cells (an *in vitro* model derived from human colon carcinoma cells) that express both P-glycoprotein (constitutively) and CYP3A4 (by induction with 1α, dihydroxyvitamin D_3) and fresh mouse intestine from P-gp-competent and -deficient mice. The intestinal tissues were used in a side-by-side

diffusion chamber in order to measure metabolism during absorptive transport across the tissues. Although this model has been used for some time, it has rarely been used for metabolic experiments. In fact, most of the studies done in this area of transport/metabolism interaction have involved cell lines only. The diffusion chamber system is more physiologically relevant than a simple model consisting of only one cell type and therefore provides valuable information about the P-gp/CYP3A interaction. However, potential species differences must be kept in mind when using the mouse model. Chemical inhibitors were used to modulate P-gp in the Caco-2 cell system, while genetic knockout was used for the mouse model. Combination of the data from these two systems afforded enhanced interpretive power as well as better predictions of clinical scenarios.

For this dissertation, two drugs, loperamide and terfenadine, were chosen to study the P-gp/CYP3A interaction. Since drugs with high permeability and low solubility (BCS Class II) are more likely to be affected by metabolism and transport, and are therefore more likely to show the interaction between the two processes, both drugs were selected from this class.

First, the dual P-gp/CYP3A substrate loperamide was selected for study due to its proven affinity for CYP3A (Kim et al., 2004) and its susceptibility to P-gp efflux (Wandel et al., 2002). Loperamide is an opioid derivative that is used as an anti-diarrheal agent. Loperamide is poorly absorbed due to high first-pass and transporter effects: after an oral dose in humans only 0.3% of the dose was found in

the plasma (Heykants et al., 1974). The extensive first-pass metabolism of loperamide made it a good candidate for these experiments, since metabolites were readily detectable. Loperamide has been characterized as a P-gp substrate (Bentz et al., 2005). Central nervous system side effects are uncommon due to the low plasma concentrations attained and due to P-gp efflux at the blood-brain barrier. Brain uptake clearances of loperamide were reported to be approximately 10-fold higher in P-gp-deficient mice than in the wild-type (Dagenais et al., 2004). Loperamide has also been shown to alter the disposition of the well-known P-gp substrate ivermectin: intestinal secretion of ivermectin was decreased in the presence of loperamide, implying competition for the P-gp transporter (Lifschitz et al., 2004). In Caco-2 cell studies, the secretory permeability of loperamide has been reported to be 17-fold higher than absorptive permeability (Crowe and Wong, 2004).

Loperamide has two major metabolites, which are formed from subsequent demethylation reactions. The drug is extensively metabolized, which facilitates detection of metabolites. Loperamide has been shown to be metabolized by several CYP isoforms in human liver microsomes, particularly by CYP3A4 and CYP2C8. A few drug-drug interactions have been reported for this compound. One study reported an increase in AUC with coadministration of ritonavir (a CYP3A inhibitor) (Tayrouz et al., 2001), while another showed that plasma concentrations of loperamide were increased by both CYP3A4 inhibitor itraconazole and CYP2C8 inhibitor gemfibrozil after oral dosing in healthy human volunteers (Niemi et al., 2006). However, CYP3A appears to be predominately responsible for its

metabolism, since 1 μM ketoconazole was shown to inhibit the formation of demethyl-loperamide (DLOP) by 90% in human liver microsomes (Kim et al., 2004).

To help determine the parameters that influence the interaction between P-gp and CYP3A in the intestine, the dual P-gp/CYP3A substrate terfenadine (Ling et al., 1995; Raeissi et al., 1999; Polli et al., 2001) was also selected for study. Terfenadine is a second-generation (non-sedating) antihistamine prodrug that was once widely prescribed but has been removed from the market due to safety concerns. It is known to be extensively metabolized by CYP3A during absorption, resulting in a bioavailability of <1% (Raeissi et al., 1999); this high first-pass metabolism makes the drug particularly susceptible to drug-drug interactions, since inhibition of this enzyme has the potential to increase systemic concentrations of the parent drug substantially. The two main metabolites of terfenadine are fexofenadine and azacyclonol.

Terfenadine is also subject to efflux by P-gp, which represents another barrier to its absorption from the intestine (Raeissi et al., 1999; Polli et al., 2001). Therefore, terfenadine is likely to be affected by both metabolic and efflux transporter processes during absorption. This makes it a good candidate for studying the interplay between P-gp and CYP3A. However, the extent to which its absorption is affected by P-gp is less than that for loperamide. Therefore, a different extent of effect of P-gp on its metabolism was expected.

In summary, two *in vitro* models and two dual P-gp/CYP3A substrates were used to study the interaction between P-gp and CYP3A in intestine. Pharmacokinetic modeling was also used in order to make predictions about the behavior of dual substrates under differing conditions (i.e., in different regions of the intestine) and also to examine the parameters commonly used to assess the P-gp/CYP3A interaction. This combination of approaches allowed prediction of the *in vivo* relevance of the P-gp/CYP3A interaction in intestine.

H. REFERENCES

Achira M, Suzuki H, Ito K and Sugiyama Y (1999) Comparative studies to determine the selective inhibitors for P-glycoprotein and cytochrome P4503A4. *AAPS PharmSci* **1:**E18.

Amidon GL, Lennernas H, Shah VP and Crison JR (1995) A theoretical basis for a biopharmaceutic drug classification: the correlation of in vitro drug product dissolution and in vivo bioavailability. *Pharm Res* **12:**413-420.

Benet LZ, Cummins CL and Wu CY (2004) Unmasking the dynamic interplay between efflux transporters and metabolic enzymes. *Int J Pharm* **277:**3-9.

Bu HZ (2006) A literature review of enzyme kinetic parameters for CYP3A4-mediated metabolic reactions of 113 drugs in human liver microsomes: structure-kinetics relationship assessment. *Curr Drug Metab* **7:**231-249.

Chen C, Liu X and Smith BJ (2003) Utility of Mdr1-gene deficient mice in assessing the impact of P-glycoprotein on pharmacokinetics and pharmacodynamics in drug discovery and development. *Curr Drug Metab* **4:**272-291.

Cummins CL, Jacobsen W and Benet LZ (2002) Unmasking the dynamic interplay between intestinal P-glycoprotein and CYP3A4. *J Pharmacol Exp Ther* **300:**1036-1045.

Cummins CL, Jacobsen W, Christians U and Benet LZ (2004) CYP3A4-transfected Caco-2 cells as a tool for understanding biochemical absorption barriers: studies with sirolimus and midazolam. *J Pharmacol Exp Ther* **308:**143-155.

Cummins CL, Mangravite LM and Benet LZ (2001) Characterizing the expression of CYP3A4 and efflux transporters (P-gp, MRP1, and MRP2) in CYP3A4-transfected Caco-2 cells after induction with sodium butyrate and the phorbol ester 12-O-tetradecanoylphorbol-13-acetate. *Pharm Res* **18:**1102-1109.

Cummins CL, Salphati L, Reid MJ and Benet LZ (2003) In vivo modulation of intestinal CYP3A metabolism by P-glycoprotein: studies using the rat single-pass intestinal perfusion model. *J Pharmacol Exp Ther* **305:**306-314.

Dresser GK, Spence JD and Bailey DG (2000) Pharmacokinetic-pharmacodynamic consequences and clinical relevance of cytochrome P450 3A4 inhibition. *Clin Pharmacokinet* **38:**41-57.

Endres CJ, Hsiao P, Chung FS and Unadkat JD (2006) The role of transporters in drug interactions. *Eur J Pharm Sci* **27:**501-517.

Fisher JM, Wrighton SA, Watkins PB, Schmiedlin-Ren P, Calamia JC, Shen DD, Kunze KL and Thummel KE (1999) First-pass midazolam metabolism catalyzed by 1alpha,25-dihydroxy vitamin D3-modified Caco-2 cell monolayers. *J Pharmacol Exp Ther* **289:**1134-1142.

Gan LS, Moseley MA, Khosla B, Augustijns PF, Bradshaw TP, Hendren RW and Thakker DR (1996) CYP3A-like cytochrome P450-mediated metabolism and polarized efflux of cyclosporin A in Caco-2 cells. *Drug Metab Dispos* **24:**344-349.

Gilbaldi G and Perrier D (1982) *Pharmacokinetics*. Marcel Decker, New York, New York.

Gottesman MM and Pastan I (1993) Biochemistry of multidrug resistance mediated by the multidrug transporter. *Annu Rev Biochem* **62:**385-427.

Hall SD, Thummel KE, Watkins PB, Lown KS, Benet LZ, Paine MF, Mayo RR, Turgeon DK, Bailey DG, Fontana RJ and Wrighton SA (1999) Molecular and physical mechanisms of first-pass extraction, in: *Drug Metab Dispos*, pp 161-166.

Higgins CF and Gottesman MM (1992) Is the multidrug transporter a flippase? *Trends Biochem Sci* **17:**18-21.

Hochman JH, Chiba M, Nishime J, Yamazaki M and Lin JH (2000) Influence of P-glycoprotein on the transport and metabolism of indinavir in Caco-2 cells expressing cytochrome P-450 3A4. *J Pharmacol Exp Ther* **292:**310-318.

Hochman JH, Chiba M, Yamazaki M, Tang C and Lin JH (2001) P-glycoprotein-mediated efflux of indinavir metabolites in Caco-2 cells expressing cytochrome P450 3A4. *J Pharmacol Exp Ther* **298:**323-330.

Ito K, Kusuhara H and Sugiyama Y (1999) Effects of intestinal CYP3A4 and P-glycoprotein on oral drug absorption--theoretical approach. *Pharm Res* **16:**225-231.

Jacobsen W, Christians U and Benet LZ (2000) In vitro evaluation of the disposition of A novel cysteine protease inhibitor. *Drug Metab Dispos* **28:**1343-1351.

Johnson BM, Charman WN and Porter CJ (2001) The impact of P-glycoprotein efflux on enterocyte residence time and enterocyte-based metabolism of verapamil. *J Pharm Pharmacol* **53:**1611-1619.

Johnson BM, Charman WN and Porter CJ (2003a) Application of compartmental modeling to an examination of in vitro intestinal permeability data: assessing the impact of tissue uptake, P-glycoprotein, and CYP3A. *Drug Metab Dispos* **31:**1151-1160.

Johnson BM, Chen W, Borchardt RT, Charman WN and Porter CJ (2003b) A kinetic evaluation of the absorption, efflux, and metabolism of verapamil in the autoperfused rat jejunum. *J.Pharmacol Exp Ther* **305:**151-158.

Juliano RL and Ling V (1976) A surface glycoprotein modulating drug permeability in Chinese hamster ovary cell mutants. *Biochim Biophys Acta* **455:**152-162.

Kaddoumi A, Fleisher D, Heimbach T, Li LY and Cole S (2006) Factors influencing regional differences in intestinal absorption of UK-343,664 in rat: possible role in dose-dependent pharmacokinetics. *J Pharm Sci* **95:**435-445.

Lampen A, Christians U, Bader A, Hackbarth I and Sewing KF (1996) Drug interactions and interindividual variability of ciclosporin metabolism in the small intestine. *Pharmacology* **52:**159-168.

Lan LB, Dalton JT and Schuetz EG (2000) Mdr1 limits CYP3A metabolism in vivo. *Mol Pharmacol* **58:**863-869.

Lindell M, Karlsson MO, Lennernas H, Pahlman L and Lang MA (2003) Variable expression of CYP and Pgp genes in the human small intestine. *Eur J Clin Invest* **33:**493-499.

Lown KS, Mayo RR, Leichtman AB, Hsiao HL, Turgeon DK, Schmiedlin-Ren P, Brown MB, Guo W, Rossi SJ, Benet LZ and Watkins PB (1997) Role of intestinal P-glycoprotein (mdr1) in interpatient variation in the oral bioavailability of cyclosporine, in: *Clin Pharmacol Ther*, pp 248-260.

Mouly SJ, Paine MF and Watkins PB (2004) Contributions of CYP3A4, P-glycoprotein, and serum protein binding to the intestinal first-pass extraction of saquinavir. *J Pharmacol Exp Ther* **308:**941-948.

Obach RS, Walsky RL, Venkatakrishnan K, Gaman EA, Houston JB and Tremaine LM (2006) The utility of in vitro cytochrome P450 inhibition data in the prediction of drug-drug interactions. *J Pharmacol Exp Ther* **316:**336-348.

Paine MF, Hart HL, Ludington SS, Haining RL, Rettie AE and Zeldin DC (2006) The Human Intestinal Cytochrome P450 "Pie". *Drug Metab Dispos*.

Paine MF, Khalighi M, Fisher JM, Shen DD, Kunze KL, Marsh CL, Perkins JD and Thummel KE (1997) Characterization of interintestinal and intraintestinal variations in human CYP3A-dependent metabolism. *J Pharmacol Exp Ther* **283:**1552-1562.

Paine MF, Shen DD, Kunze KL, Perkins JD, Marsh CL, McVicar JP, Barr DM, Gillies BS and Thummel KE (1996) First-pass metabolism of midazolam by the human intestine. *Clin Pharmacol Ther* **60:**14-24.

Paine MF, Wagner DA, Hoffmaster KA and Watkins PB (2002) Cytochrome P450 3A4 and P-glycoprotein mediate the interaction between an oral erythromycin breath test and rifampin. *Clin Pharmacol Ther* **72:**524-535.

Paul AJ, Tranquilli WJ, Seward RL, Todd KS, Jr. and DiPietro JA (1987) Clinical observations in collies given ivermectin orally. *Am J Vet Res* **48:**684-685.

Raviv Y, Pollard HB, Bruggemann EP, Pastan I and Gottesman MM (1990) Photosensitized labeling of a functional multidrug transporter in living drug-resistant tumor cells. *J Biol Chem* **265:**3975-3980.

Romsicki Y and Sharom FJ (1999) The membrane lipid environment modulates drug interactions with the P-glycoprotein multidrug transporter. *Biochemistry* **38:**6887-6896.

Roulet A, Puel O, Gesta S, Lepage JF, Drag M, Soll M, Alvinerie M and Pineau T (2003) MDR1-deficient genotype in Collie dogs hypersensitive to the P-glycoprotein substrate ivermectin. *Eur J Pharmacol* **460:**85-91.

Salphati L and Benet LZ (1998) Effects of ketoconazole on digoxin absorption and disposition in rat. *Pharmacology* **56:**308-313.

Schmiedlin-Ren P, Thummel KE, Fisher JM, Paine MF, Lown KS and Watkins PB (1997) Expression of enzymatically active CYP3A4 by Caco-2 cells grown on extracellular matrix-coated permeable supports in the presence of 1alpha,25-dihydroxyvitamin D3, in: *Mol Pharmacol*, pp 741-754.

Schuetz EG, Beck WT and Schuetz JD (1996) Modulators and substrates of P-glycoprotein and cytochrome P4503A coordinately up-regulate these proteins in human colon carcinoma cells. *Mol Pharmacol* **49:**311-318.

Seelig A (1998) A general pattern for substrate recognition by P-glycoprotein. *Eur J Biochem* **251:**252-261.

Shen Q, Lin Y, Handa T, Doi M, Sugie M, Wakayama K, Okada N, Fujita T and Yamamoto A (2006) Modulation of intestinal P-glycoprotein function by polyethylene glycols and their derivatives by in vitro transport and in situ absorption studies. *Int J Pharm* **313:**49-56.

Smit JW, Schinkel AH, Muller M, Weert B and Meijer DK (1998) Contribution of the murine mdr1a P-glycoprotein to hepatobiliary and intestinal elimination of cationic drugs as measured in mice with an mdr1a gene disruption. *Hepatology* **27:**1056-1063.

Stephens RH, O'Neill CA, Warhurst A, Carlson GL, Rowland M and Warhurst G (2001) Kinetic profiling of P-glycoprotein-mediated drug efflux in rat and human intestinal epithelia. *J Pharmacol Exp Ther* **296:**584-591.

Tam D, Sun H and Pang KS (2003a) Influence of P-glycoprotein, transfer clearances, and drug binding on intestinal metabolism in Caco-2 cell monolayers or membrane preparations: a theoretical analysis. *Drug Metab Dispos* **31:**1214-1226.

Tam D, Tirona RG and Pang KS (2003b) Segmental intestinal transporters and metabolic enzymes on intestinal drug absorption. *Drug Metab Dispos* **31:**373-383.

Thiebaut F, Tsuruo T, Hamada H, Gottesman MM, Pastan I and Willingham MC (1987) Cellular localization of the multidrug-resistance gene product P-glycoprotein in normal human tissues. *Proc Natl Acad Sci U S A* **84:**7735-7738.

Troutman MD and Thakker DR (2003) Novel experimental parameters to quantify the modulation of absorptive and secretory transport of compounds by P-glycoprotein in cell culture models of intestinal epithelium, in: *Pharm Res*, pp 1210-1224.

van Helvoort A, Smith AJ, Sprong H, Fritzsche I, Schinkel AH, Borst P and van Meer G (1996) MDR1 P-glycoprotein is a lipid translocase of broad specificity, while MDR3 P-glycoprotein specifically translocates phosphatidylcholine. *Cell* **87:**507-517.

von Richter O, Greiner B, Fromm MF, Fraser R, Omari T, Barclay ML, Dent J, Somogyi AA and Eichelbaum M (2001) Determination of in vivo absorption, metabolism, and transport of drugs by the human intestinal wall and liver with a novel perfusion technique. *Clin Pharmacol Ther* **70:**217-227.

Watkins PB (1997) The barrier function of CYP3A4 and P-glycoprotein in the small bowel. *Adv Drug Deliv Rev* **27:**161-170.

Wu CY and Benet LZ (2005) Predicting drug disposition via application of BCS: transport/absorption/ elimination interplay and development of a biopharmaceutics drug disposition classification system. *Pharm Res* **22:**11-23.

Table 1.1: Biopharmaceutics Classification System

Class I: High solubility High permeability	**Class II:** Low solubility High permeability
Class III: High solubility Low permeability	**Class IV:** Low solubility Low permeability

Table 1.2. Proposed P-gp/CYP3A4 dual substrates

Amiodarone	Nelfinavir
Amprenavir	Nicardipine
Atorvastatin	Nifedipine
Cephaeline	Nitrendipine
Cerivastatin	Paclitaxel
Colchicine	Pimozide
Cortisol	Prednisolone
Cyclosporin A	Progesterone
Dexamethasone	Quinidine
Diltiazem	Quinine
Ebastine	Ritonavir
Erythromycin	RU486
Etoposide	Saquinavir
Felodipine	Simvastatin
Indinavir	Sirolimus
Itraconazole	Tacrolimus
Ketoconazole	Tamoxifen
Lidocaine	Terfenadine
Loperamide	Testosterone
Lopinavir	Tirilazad
Lovastatin	Verapamil
Methadone	Vincristine
Methylprednisolone	Vinorelbine

Table 1.3. Comparison of percent metabolized and ER for CYP3A/P-gp dual substrates, with or without treatment with P-gp inhibitors.

Substrate	Dose (μM)	% Metabolized (Untreated)	% Metabolized (+Inhibitor)	ER (Untreated)	ER (+Inhibitor)	Reference
K77	10	2.0%	3.3%	33%	14%	6
Indinavir	5	1.4%	1.8%	24%	17%	8
Saquinavir	10	0.2%	0.7%	22%	10%	15
Saquinavir	20	0.2%	0.6%	10%	6%	15
Saquinavir	40	0.2%	0.3%	6%	3%	15

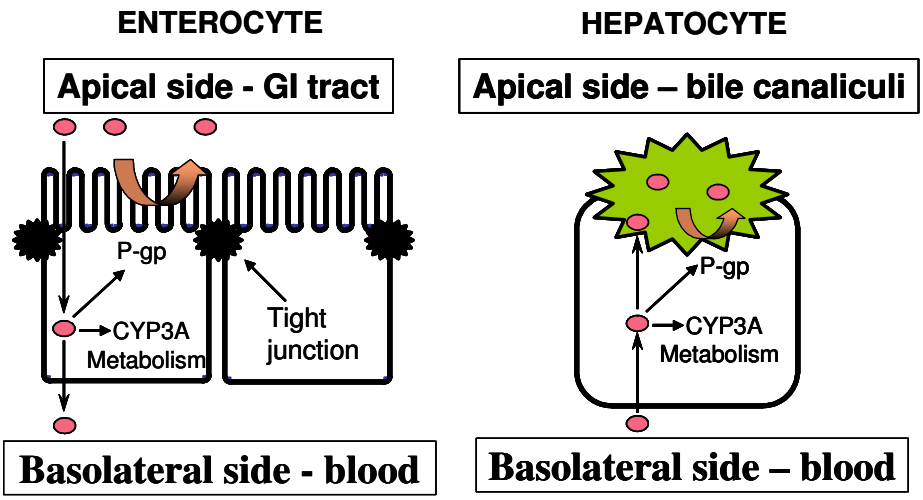

Figure 1.1. Barriers to drug absorption in enterocytes (left) and hepatocytes (right)

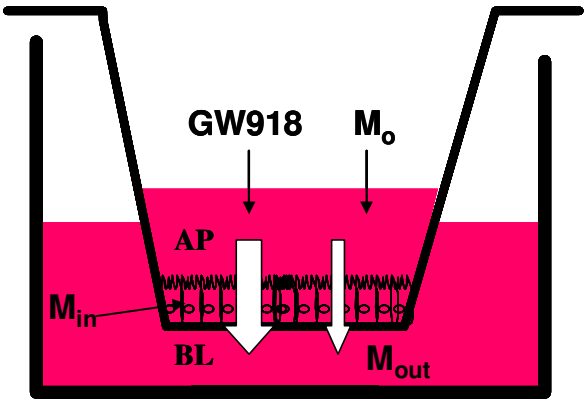

Figure 1.2. Schematic of Caco-2 cell monolayers grown on Transwell ® inserts. Arrow denotes absorptive transport. M_0: parent dose; M_{in}: total amount of the drug that can be irreversibly cleared; M_{out}: amount of parent drug that reaches the basolateral chamber; AP: apical; BL: basolateral

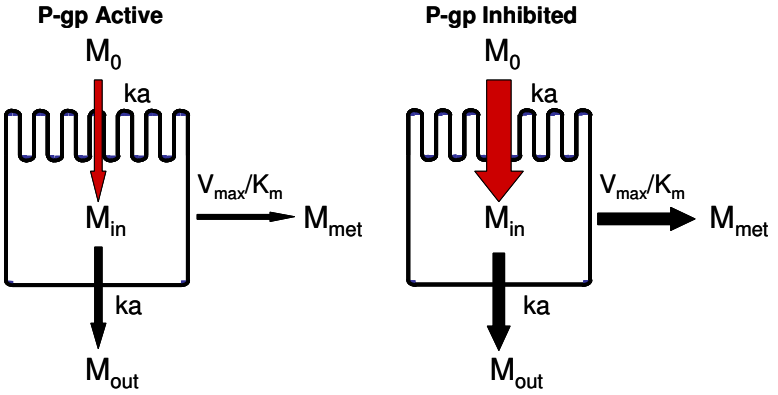

Figure 1.3. Schematic depicting ER parameters. M_0: parent dose; M_{in}: total amount of the drug that can be irreversibly cleared; M_{met}: total metabolites produced; M_{out}: amount of parent drug that reaches the basolateral chamber; AP: apical; BL: basolateral; ka: absorption rate constant

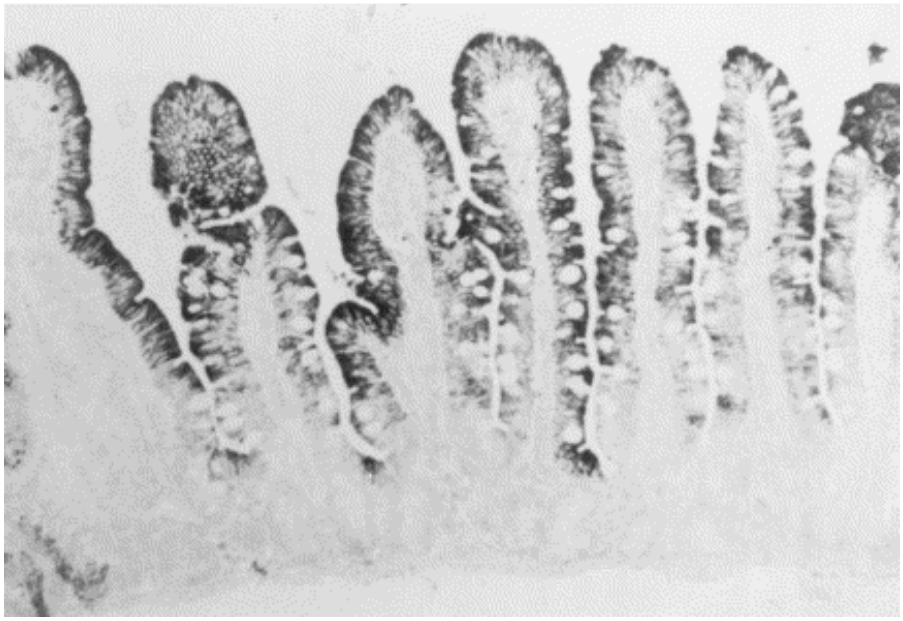

Figure 1.4. CYP3A expression in human intestinal mucosa. Watkins, P. B. (1997) *Adv Drug Deliv Rev* **27**, 161-170

CHAPTER 2: METHODS

A. CHEMICALS AND REAGENTS

Loperamide, terfenadine, testosterone, 6-β-OH-testosterone, phenacetin, dextromethorphan, dextrorphan, sodium selenite, zinc sulfate, all-trans retinoic acid, sodium hydroxide, Kreb's Bicarbonate Ringer and gentamicin were purchased from Sigma Aldrich (St. Louis, MO, USA). Metabolites of loperamide (monodemethyl- and didemethyl-loperamide) were generously provided by Janssen (Beerse, Belgium). Metabolites of terfenadine (azacyclonol and fexofenadine) were generously provided by Dr. Mary Paine. GW918 was provided by GlaxoSmithKline. Methanol, formic acid, ethyl acetate vitamin E, and scintillation fluid (Scintisafe gel) were purchased from Fisher Scientific (Pittsburgh, PA, USA). Ketamine was purchased from Veterinary Medical Supply (Zebulon, NC, USA), and xylazine from Webster Veterinary (Sterling, MA, USA). Eagle's minimum essential medium with Earle's salts and L-glutamate (MEM), Dulbecco's Modified Eagle's Medium with L-glutamine but without sodium pyruvate (DMEM), nonessential amino acids (NEAA, 100X), 0.05% trypsin-0.53 mM EDTA solution, N-Hydroxyethylpiperazine-N'-2-ethanesulfonate (HEPES, 1 M) and penicillin-streptomycin-amphotericin B solution (100X) were obtained from Gibco Laboratories (Grand Island, NY, USA). Hank's balanced salt solution (HBSS) was obtained from Mediatech, Inc. (Herndon, VA, USA). 1α, 25-dihydroxyvitamin D_3 was obtained from Biomol (Plymouth Meeting, PA, USA). Azamulin and mouse laminin were purchased from BD Biosciences (San Jose, CA, USA). [^{3}H]Digoxin and [^{3}H]mannitol were purchased from Perkin Elmer

(Waltham, MA, USA) and Moravek (Brea, CA, USA), respectively. All other reagents were of analytical grade or higher and deionized water was used in all experimental procedures. [S]-mephenytoin, diclofenac, and their authentic metabolite standards were purchased from BD Gentest (Woburn, MA, USA).

B. ANIMALS

Mice (CF-1 wild type and P-gp mutant) were purchased from Charles River Laboratories (Wilmington, MA, USA) and housed according to AAALAC requirements and protocols (numbers 04-288 and 06-303) accepted by the University of North Carolina Institutional Animal Care and Use Committee. The animal housing facility is under the supervision of the University's Campus Veterinarian, and is in compliance with public laws 89-544 and 91-579. A full-time technician in the Department of Laboratory Animal Medicine is responsible for animal husbandry in this facility. All personnel handling animals were first certified by the university Institutional Animal Care and Use Committee.

C. MATERIALS

Corning plates (12-well) with Transwell™ inserts were purchased from Fisher Scientific (Pittsburgh, PA, USA); 6-well-plates and inserts were purchased from BD Biosciences (San Jose, CA, USA). The side-by-side diffusion chamber system (Physiologic Instruments, San Diego, CA, USA) used for the animal

studies was generously loaned to our lab by GlaxoSmithKline. Mouse liver and intestinal microsomes were purchased from Xenotech. Human intestinal microsomes were generously provided by Dr. Mary Paine (School of Pharmacy, University of North Carolina, Chapel Hill, NC, USA).

D. CACO-2 CELL CULTURE

The Caco-2 cell line, clone P27.7, was obtained from Mary Paine, Ph.D. and Paul Watkins, MD (Schools of Pharmacy and Medicine, The University of North Carolina at Chapel Hill, Chapel Hill, NC, USA). Caco-2 cell monolayers were cultured according to the methods of Lee and Thakker (Lee and Thakker, 1999). Except where noted, cell culture medium consisted of 500 ml Minimum Essential Medium (MEM), 50 ml Fetal Bovine Serum (FBS), 5 ml 100X Non-Essential Amino Acids (NEAA), and 5 ml 100X Antibiotic/Antimycotic (final concentrations: 100 U/ml penicillin, 100 µg/ml streptomycin, and 0.25 µg/ml amphotericin B). Cells were grown in 75 cm^2 tissue culture (T75) flasks at 37^oC, in an atmosphere of 5% CO_2 and 90% relative humidity, and subcultured at a 1:10 ratio, using 0.05% trypsin/0.02% EDTA solution, upon reaching 90% confluency.

E. TRANSWELL® SYSTEM

For transport experiments, the polycarbonate membranes of Transwell® inserts (12 mm, 0.4 µm pore size) in 12-well plates were seeded with 60,000 cells per well (1 cm^2) during subculture from T75 flasks. Media was changed the day after seeding, and every other day thereafter. Monolayer integrity was verified by measurement of TEER using an Epithelial Tissue Voltammeter (EVOM) and an Endohm-12 Electrode (World Precision Instruments, Saratoga, FL, USA). Monolayers with TEER ≥ 250 $\Omega \cdot cm^2$ were used for experiments (passages 35-50).

For metabolic experiments, 6-well plates containing Biocoat cell culture inserts (4.2 cm^2, 1 µM pore size) were coated with murine laminin (5 $\mu g/cm^2$) and then were seeded with Caco-2 cell clone P27.7 (passages 29-42) (Schmiedlin-Ren et al., 1997) at a density of 5 X 10^5 cells/cm^2. Cultures were grown using growth medium (DMEM containing 20% heat-inactivated FBS, 0.1 mM NEAA, 50 µg/ml gentamicin, and 45 nM vitamin E) until confluence, as assessed by transepithelial electrical resistance values ≥250 $\Omega \cdot cm^2$. After that, the cells were treated for 14 days with differentiation medium (DMEM containing 5% heat-inactivated FBS, 0.1 mM NEAA, 50 µg/ml gentamicin, 45 nM vitamin E, 0.1 µM sodium selenite, and 3 µM zinc sulfate) as described by Schmeidlen-Ren et al. (Schmiedlin-Ren et al., 1997) and supplemented with 0.5 µM 1α,25-$(OH)_2$-D_3 and 0.2 µM all-*trans*-retinoic acid (Mouly et al., 2004) to induce CYP3A expression.

F. TRANSPORT STUDIES

Transport experiments were carried out using Caco-2 cell monolayers, 21-28 days post-seeding, as previously described (Lee and Thakker, 1999). Transport medium was comprised of Hank's Balanced Salt Solution (HBSS) containing 10 mM HEPES buffer and 25 mM glucose. Cell culture medium in Transwell plates was replaced with transport medium and the plates were incubated at 37°C for one hour before the experimental procedure. Membrane integrity was then assessed by TEER or by use of a paracellular marker (lucifer yellow or mannitol). After warming dosing solutions, transport medium was replaced with dosing solution in the donor compartment, and with fresh warmed transport medium in the acceptor compartment. Plates were maintained at 37°C throughout the experiment. Samples were collected from the receiver compartment at appropriate timepoints. At the final timepoint, the inserts were removed rapidly from the wells and inverted to end the incubation.

G. UPTAKE STUDIES

After a 30 minute preincubation, 0.5 ml of transport buffer containing 25 µM terfenadine was added to the donor compartment and incubated for 1 minute, after which cells were rinsed three times with ice-cold buffer. Then cell monolayers were lysed in 1% Triton X-100, extracted into ethyl acetate (2 X 1 ml), evaporated, and reconstituted in mobile phase for analysis.

H. EFFLUX STUDIES

In order to preload the intracellular space with terfenadine, 25 µM terfenadine was added to both apical and basolateral compartments and incubated for 1 hour. The cell monolayers were washed 3 times with ice-cold buffer. Then fresh warmed buffer was added and samples were collected after one minute of efflux, which is within the linear range of efflux for terfenadine. Cell monolayers were also extracted and analyzed for terfenadine content as described above.

I. METABOLIC STUDIES

To induce CYP3A expression, Caco-2 cell monolayers were grown on laminin-coated inserts in cell culture dishes, and treated with 0.5 µM 1α,25-$(OH)_2$-D_3 for 2 weeks postconfluence, as verified by TEER ≥ 250 $\Omega \cdot cm^2$ (Schmiedlin-Ren et al., 1997; Mouly et al., 2004). Transport studies were then conducted as described above. At the last timepoint, samples were collected from the donor and receiver compartments. Cell monolayers were washed and harvested by scraping into 500 µl of homogenization buffer (100 mM potassium phosphate, 0.25 M sucrose, and 1 mM EDTA, pH 7.4). CYP3A-specific metabolites were identified for each substrate, and metabolite formation over time was characterized by quantification of parent remaining and metabolite formed in all three compartments (donor, cellular and receiver). Terfenadine and its metabolites were extracted from the lysates using a validated extraction procedure. Briefly, samples were disrupted with a sonic dismembrator for 15

seconds and then vortexed with 1 ml ethyl acetate, then centrifuged and the supernatant removed. The samples were then alkalinized with 50 µl 1 N sodium hydroxide and extracted with an additional 1 ml ethyl acetate. The supernatants were combined, evaporated, and reconstituted in mobile phase.

J. DIFFUSION CHAMBER STUDIES

Male CF-1 mice were anesthetized with an IP injection of ketamine (140 mg/kg) and xylazine (15 mg/kg). At the time of sacrifice, the intestines were removed and immediately flushed with 10 ml ice-cold Krebs Bicarbonate Ringer (KBR). Three portions of jejunum (~1 inch long) were retained for the analysis. Each section was cut longitudinally and then mounted between the two halves of a diffusion chamber insert and held in place by eight small pins (Figure 2.1). The inserts were placed in ice-cold KBR until mounted between the chambers. The entire procedure was carried out as quickly as possible, on ice.

Inserts were mounted between two side-by-side diffusion chambers. KBR (3 ml) was added to each chamber and bubbled with oxygen/carbon dioxide gas to maintain viability (Johnson et al., 2002). After an equilibration period of 30 minutes, the TEER was measured, the buffer in the receiver side was replaced with fresh warmed KBR, and the buffer in the donor side was replaced with warmed dosing solution. Samples were removed from the chambers at the appropriate timepoints and replaced with fresh KBR. At the end of the

experiment, the tissues were removed and homogenized for 30 seconds with a sonic dismembrator in 200 µL of KBR, then extracted with ethyl acetate as described for cell monolayers above.

K. MICROSOME ASSAYS

Mouse and human intestinal microsomes, total protein concentration 10 mg/ml and 7.6 mg/ml, respectively, were used to determine the intrinsic kinetic parameters for each of these species. Reactions were carried out in 200 µl 200 mM phosphate buffer containing 3 mM $MgCl_2$ and 0.1 mg microsomes. Reactions were initiated with 2 mM NADPH and were terminated after 30 minutes by addition of ice-cold methanol. Inhibitor concentration was 3 µM for both ketoconazole and quinidine and was 5 µM for azamulin. A cassette dosing method was used to determine the activities of CYP enzymes in mouse and human intestinal microsomes, as previously described (Yanni et al., 2004).

L. ANALYSIS OF TERFENADINE AND LOPERAMIDE AND THEIR METABOLITES

Terfenadine and its two metabolites, fexofenadine and azacyclonol, and loperamide and its two metabolites, monodemethyl-loperamide and didemethyl-loperamide, were quantified using LC-MS/MS (LC10-ADVP quaternary pumps (Shimadzu, Kyoto, Japan), CTC-PAL autosampler (LEAP Technologies, Carrboro, NC, Sciex API-4000 triple-quadropole mass spectrometer (Applied Biosystems, Foster City, CA).

Mobile phases of 0.1% formic acid in water and 0.1% formic acid in methanol were used with a 5-95% methanol linear gradient. The column used was a Phenomenex Synergy Polar RP, 30 X 2 mm, with 5 µm particle size phenyl-ether linked stationary phase. A flow rate of 0.8 mL/min and injection volume of 15 µL were utilized. Samples were ionized using APCI and ions were monitored at the following transitions: 472/436 for terfenadine, 503/466 for fexofenadine, 268/143 for azacyclonol, 477/266 for loperamide, 463/252 for monodemethyl loperamide, and 449/238 for didemethyl loperamide. Standards were available for each of the metabolites, allowing accurate quantification. Standard curves were analyzed at the beginning and end of the run for sample quantification. Cetirizine was used as an internal standard. Retention times and peak shapes were monitored throughout the run.

M. Analysis of Testosterone and 6-β-hydroxytestosterone

Testosterone and its metabolite were quantified using HPLC (HP1100, Agilent Technologies, Santa Clara, CA) with UV detection at 242 nm. Water and methanol were used as mobile phases, with a linear gradient from 40 to 75% methanol. The column used was an Agilent Zorbax Eclipse XDB-C8, 4.6 X 150 mm, with 5 µm particle size packing. A flow rate of 0.8 mL/min and an injection volume of 50 µL were employed. A standard curve was analyzed for sample quantification. Five injections of an intermediate standard were analyzed for system suitability and injection reproducibility (<2.0% RSD). Retention time and peak shape were monitored throughout the run.

N. Analysis of [^{3}H]Digoxin and [^{14}C]Mannitol

Samples were combined with 10 ml scintillation fluid and analyzed using a Packard scintillation counter.

O. Pharmacokinetic Modeling

WinNonlin (Pharsight, Mountain View, CA) was used for all pharmacokinetic modeling. A Guass-Newton minimization method and a weighting scheme of 1/y were used for all modeling exercises. In addition to visual inspection, Akaike's Information Criterion was used to determine the best model fit to the data. Model

A consisted of three parent drug compartments, plus one pathway for metabolite formation (Figure 3.24). The model was fit to the Caco-2 cell metabolic data for terfenadine (see Chapter 3). Refer to Table 3.2 for rates used in the modeling. The metabolite formation profiles from six doses were fit simultaneously by using 24 distinct differential equations. For each dose, four equations with the following structure were used:

$$\frac{dA}{dt} = k_{BA}B - k_{AB}A$$

$$\frac{dB}{dt} = k_{AB}A + k_{CB}C - k_{BA}B - k_{BC}B - \frac{V_{\max}B}{K_m + B}$$

$$\frac{dC}{dt} = k_{BC}B - k_{CB}C$$

$$\frac{dD}{dt} = \frac{V_{\max}B}{K_m + B}$$

Where V_{max} is the maximum rate of metabolite formation, K_m is the concentration of substrate at which half of maximum velocity is achieved, and k constants represent the various first-order rate constants for movement of mass between compartments, e.g., k_{AB} represents the rate of drug movement from compartment A to compartment B. Simulations were then carried out to determine the effect of P-gp efflux (k_{BA}) on metabolic rate (dD/dt).

CYP3A expression is known to be highest in proximal intestine, while P-gp expression increases distally (Figure 4.2). To simulate different expression levels of CYP3A, V_{max} was systematically altered while the other parameters

were held constant. To determine the effect of changes in P-gp expression, the function k_{BA}*B was replaced with a saturable component, yielding:

$$\frac{J_{\max} B}{K_{mpgp} + B}$$

Where J_{max} represents the maximum rate of efflux and K_{mpgp} represents the concentration at which half of J_{max} is attained. Using these modified equations, the effect of changing J_{max} was investigated, while K_{mpgp} and all other parameters were held constant. A matrix of simulations consisting of various combinations of V_{max} and J_{max} values was generated in this manner.

To evaluate the parameters that are used to describe the relationship between P-gp activity and metabolic rate, a set of simulations were carried out by altering J_{max} and observing the effect on % metabolized and extraction ratio. The extraction ratio (ER) was calculated in two different ways. The first was based on the methods of Fisher et al. (Fisher et al., 1999):

$$ER = \frac{\sum \mathrm{M}_{\mathrm{metabolites}}}{\sum \mathrm{M}_{\mathrm{metabolites}} + \mathrm{M}_{\mathrm{out}}}$$

where $M_{metabolites}$ is the cumulative mass of all metabolites from all compartments at time *t* and M_{out} is the parent compound appearing in the receiver compartment at time *t*. The second equation was derived from Benet et al. (Benet et al., 2004); they modified the ER definition to include the amount of intracellular parent drug

(M_{parent}) in the denominator of the above equation to produce the following equation:

$$ER = \frac{\sum M_{metabolites}}{\sum M_{metabolites} + M_{out} + M_{parent}(\text{at time } t)}$$

Both methods of calculating ER were used to compare the effect of P-gp efflux on these parameters and also on percent of dose metabolized (metabolites formed/dose).

A second PK model was also designed (Model B, Figure 3.30) which incorporated an extra compartment for P-gp between the apical and cellular compartments. Since data were not available for this compartment, the rate constants k_{AB}, k_{BC} and k_{CB} were assumed to be equal. Simulations were then carried out as described above to determine the effect of changes in P-gp efflux (k_{BA}) on the CYP3A-mediated metabolism of dual substrates.

P. DATA ANALYSIS

All samples were prepared in triplicate. The permeability (P_{app}) of substrates across cell monolayers was calculated as follows:

$$P_{app} = \frac{dQ/dt}{A*C} \qquad \text{Equation 1}$$

where dQ/dt represents the mass transported per time, A is the area of the membrane, and C is the initial concentration of drug in the donor compartment. This equation assumes sink conditions (Karlsson and Artursson, 1991).

For the metabolic studies, a Michaelis-Menten model (Equation 2) was fit to the data:

$$V = \frac{V_{\max} * C}{K_m + C} \qquad \text{Equation 2}$$

where V represents the rate of metabolism, V_{max} is the maximum rate observed, K_m is the concentration at which half of the maximum velocity is achieved, and C is the dosing concentration. All metabolic data were fit using WinNonlin software (Pharsight, Mountain View, CA).

The overall difference between strains or treatments was determined using two-way analysis of variance. To estimate the difference in kinetic parameters (V_{max} and K_m), the data for the two strains or treatments were fit simultaneously using nonlinear regression analysis. The null hypotheses of H_0: $Km_1 = Km_2$ and H_0: $Vmax_1 = Vmax_2$ were then tested.

Q. REFERENCES

Benet LZ, Cummins CL and Wu CY (2004) Unmasking the dynamic interplay between efflux transporters and metabolic enzymes. *Int J Pharm* **277**:3-9.

Fisher JM, Wrighton SA, Watkins PB, Schmiedlin-Ren P, Calamia JC, Shen DD, Kunze KL and Thummel KE (1999) First-pass midazolam metabolism catalyzed by 1alpha,25-dihydroxy vitamin D3-modified Caco-2 cell monolayers. *J Pharmacol Exp Ther* **289**:1134-1142.

Johnson BM, Charman WN and Porter CJ (2002) An in vitro examination of the impact of polyethylene glycol 400, Pluronic P85, and vitamin E d-alpha-tocopheryl polyethylene glycol 1000 succinate on P-glycoprotein efflux and enterocyte-based metabolism in excised rat intestine. *AAPS PharmSci* **4**:E40.

Karlsson A and Artursson P (1991) A method for the determination of cellular permeability coefficients and aqueous boundary layer thickness in monolayers of intestinal epithelial (Caco-2) cells grown in permeable filter chambers. *Int J Pharm* **71**:55-64.

Lee K and Thakker DR (1999) Saturable transport of H2-antagonists ranitidine and famotidine across Caco-2 cell monolayers. *J Pharm Sci* **88**:680-687.

Mouly SJ, Paine MF and Watkins PB (2004) Contributions of CYP3A4, P-glycoprotein, and serum protein binding to the intestinal first-pass extraction of saquinavir. *J Pharmacol Exp Ther* **308**:941-948.

Schmiedlin-Ren P, Thummel KE, Fisher JM, Paine MF, Lown KS and Watkins PB (1997) Expression of enzymatically active CYP3A4 by Caco-2 cells grown on extracellular matrix-coated permeable supports in the presence of 1alpha,25-dihydroxyvitamin D3, in *Mol Pharmacol* pp 741-754.

Yanni SB, Thiel P, Haroldsen P and Samara E (2004) High Throughput Evaluation of Clinical Drug Interaction using LC-MS/MS. *ISSX Conference* **ASBT #582**.

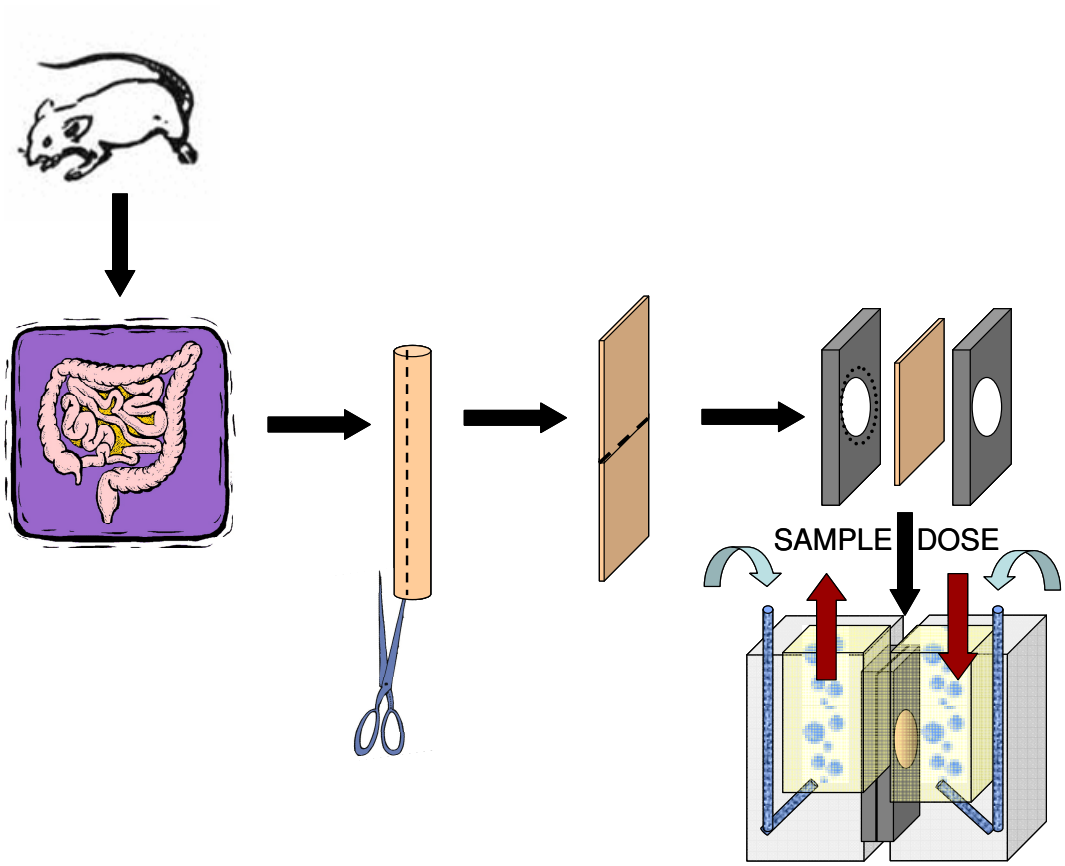

Figure 2.1. Side-by-side diffusion chamber schematic: mouse jejunum is flushed, cut longitudinally, and placed in a holder between two chambers, which are oxygenated to maintain viability.

CHAPTER 3: RESULTS

A. MODEL VALIDATION

A.1. Caco-2 Cell Model

A.1.a. Functional Activity of P-gp

In order to validate the Caco-2 cell system and demonstrate P-gp efflux activity, the permeability of the model P-gp substrate [^{3}H]digoxin (10 µM) was characterized over 90 minutes. As shown in Figure 3.1, the permeability of [^{3}H]digoxin in the basolateral-to-apical (B-to-A) direction was approximately 8-fold higher than that in the A-to-B direction. In the presence of P-gp inhibitor GW918 (1 µM), this polarity was abolished: B-to-A and A-to-B permeabilities were equal. These results established that the Caco-2 cells used in this study have functional P-gp and that it can be completely inhibited by 1 µM GW918.

A.1.b. Functional Activity of CYP3A

A CYP3A-expressing Caco-2 cell system was implemented by treatment of Caco-2 cells with 1α,25-dihydroxyvitamin D_3 for 14 days (Schmeidlen-Ren et al., 1997). In order to verify the activity of CYP3A in the Caco-2 cell system, the CYP3A-specific activity (6-β-hydroxylase activity) of the cells toward testosterone (250 µM) was measured over 120 minutes. CYP3A activity was shown to be reproducibly induced in the cells (Figure 3.2). Although P-gp is also somewhat

induced by this treatment, the effect is not likely to be significant since chemical modulation of P-gp is used in these studies rather than comparison of metabolism in induced and uninduced cells.

A.2. Mouse Intestinal Tissue Model

To validate the side-by-side diffusion model system, the permeability of the P-gp probe substrate [^{3}H]digoxin was measured over 90 minutes to demonstrate P-gp function. As seen in Figure 3.3, B-to-A permeability was approximately 3-fold higher than A-to-B permeability in the wild-type mouse, while in the P-gp deficient mouse, the B-to-A and A-to-B permeabilities were similar. These results showed that the side-by-side diffusion model, in which intestinal tissue from P-gp competent and P-gp deficient mouse is mounted in an Ussing type chamber, can be used to investigate the effect of P-gp on intestinal transport of compounds. The permeability of the paracellular marker [^{14}C]mannitol was also measured to determine the paracellular leakiness of the system. As shown in Figure 3.4, [^{14}C]mannitol permeability was about 35 ± 12 nm/sec, which is about 10-fold higher than that normally observed in the Caco-2 cell system but is similar to previously reported values for rodent intestine (Stephens et al., 2002). The higher paracellular permeability of the diffusion chamber model compared to the Caco-2 cell model may account for the lower polarity of digoxin transport in this system.

Since genetic knockout of a protein sometimes results in compensatory upregulation of a different pathway, studies were performed to compare CYP3A expression and activity in the P-gp-competent and –deficient mouse strains. No difference in intestinal metabolic activity toward the CYP3A probe substrate testosterone was observed over 90 minutes (Figure 3.5). Since testosterone is not a substrate for P-gp, this result provides evidence that CYP3A expression is not altered in the P-gp knock-out mouse model. In addition, no difference was observed in intestinal CYP3A expression by Western blot (data not shown).

B. LOPERAMIDE – INTESTINAL TRANSPORT AND METABOLISM

B.1. Transport and Metabolism in the Caco-2 Cell Model

The dual P-gp/CYP3A substrate loperamide was chosen to study the interaction between P-gp and CYP3A in the intestine. Loperamide is a lipophilic compound with excellent permeability across intestinal epithelium; however, its absorptive transport is significantly affected by P-gp (see Figure 3.6). Using the approach established by Troutman and Thakker (Troutman and Thakker, 2003), it was estimated that P-gp attenuated loperamide's absorptive permeability by approximately 60%. This provides an adequate dynamic range for P-gp-mediated attenuation of absorptive transport for the purpose of studying its effect on CYP3A-mediated metabolism. The transport of loperamide (0.25 µM) across Caco-2 cell monolayers was characterized over 60 minutes in the A-to-B and B-

to-A directions; the P-gp inhibitor GW918 was used to assess the effect of P-gp on loperamide transport in both directions. The B-to-A permeability of loperamide was about 6-fold higher than the A-to-B permeability; however, in the presence of GW918 (1 μM), this polarity was abolished (Figure 3.6), indicating that P-gp is likely to be the transporter responsible for the polarity.

For the metabolism studies, two CYP3A-specific metabolites of loperamide (monodemethyl- and didemethyl-loperamide, Figure 3.7) were quantified by LC-MS/MS. The metabolism of loperamide was studied during its absorptive transport across Caco-2 cells that were induced to express functional CYP3A by treatment with 1α, 25-dihydroxyvitamin D_3. This treatment has been shown to modestly elevate P-gp expression levels, but no effect was seen on the permeability of model P-gp substrates (Korjamo et al., 2005). In order to determine the linear range of time for metabolite formation, an initial study was conducted in which metabolites in the receiver compartment were quantified at three time points (30, 60, and 90 minutes) after a 20 μM dose of loperamide. Loperamide metabolism was found to be linear up to 90 minutes (Figure 3.8).

Next, studies were conducted over a range of loperamide dosing concentrations from 1 to 75 μM (bounded by the detection limit of metabolites and solubility of loperamide) in the presence and absence of the P-gp inhibitor GW918. Metabolites of loperamide appearing in the apical, basolateral and cellular compartments over 90 minutes were quantified by LC-MS/MS. A higher

rate of metabolism was observed in the presence of 1 µM GW918 at every dosing concentration up to and including 40 µM (Figure 3.9). Simultaneously fitting the profiles using nonlinear regression with a dummy variable determining the differences between V_{max} and K_m values for the two treatments showed a statistically significant two-fold increase in the apparent K_m value due to P-gp efflux. Presumably, P-gp efflux affected the apparent K_m for metabolism (Table 3.1) by effectively decreasing steady-state intracellular concentrations of the parent drug. No difference was seen in the V_{max} values using this statistical method, although the V_{max} may not be estimated accurately due to the large variability observed at the 75 µM dose (presumably, due to the solubility limit). The metabolic profiles were also analyzed using two-way analysis of variance (ANOVA). This statistical method tests the null hypothesis that the overall rate versus concentration profiles are not different. A statistical difference between the profiles was found using this method.

B.2. Transport and Metabolism in the Mouse Intestine – Diffusion Chamber Model

The next set of experiments involved the use of side-by-side diffusion chambers to compare the metabolic activity of fresh intestinal tissues from P-gp-competent and P-gp-deficient mice. A dosing range of 0.5 to 150 µM of loperamide was used. Three mice were utilized for each dosing concentration and three sections of jejunum were used from each mouse. At dosing

concentrations below 100 μM, intestinal tissues from P-gp-deficient mice metabolized loperamide at a higher rate than the tissues from P-gp-competent mice, causing a rightward shift in the metabolic rate versus concentration profile for the P-gp competent mice, relative to the profile for P-gp-deficient mice (Figure 3.10). When a Michaelis-Menten nonlinear function (Equation 2) was fit to the data, it was revealed that CYP3A in the P-gp-competent mouse intestinal tissue metabolized loperamide with a significantly (5-fold) higher apparent K_m than that for P-gp-deficient mouse intestinal tissue, although CYP3A from both tissues exhibited similar V_{max} values (Table 3.1), indicating that there is no intrinsic difference in CYP3A-mediated metabolism of loperamide between the two strains. The profiles for the two strains of mice were also shown to be significantly different using two-way ANOVA.

B.3. Metabolism by Intestinal Microsomes

In order to derive the intrinsic metabolic parameters for loperamide, the metabolism of loperamide was compared in mouse and human intestinal microsomes (Figure 3.11). The CYP3A-mediated metabolism was similar in the two species. The K_m values were nearly identical, while the V_{max} for mouse intestinal microsomes was about 4-fold higher than that for human (Table 3.1).

C. TERFENADINE – INTESTINAL TRANSPORT AND METABOLISM

C.1. Transport and Metabolism in the Caco-2 Cell Model

A second P-gp/CYP3A dual substrate, terfenadine, was selected for further study of the P-gp/CYP3A interaction in intestine. Terfenadine's absorptive transport is attenuated to a lesser extent (40%, AQ value 0.4) by P-gp than that of loperamide (60%, AQ value 0.6). Thus, studies were conducted to determine whether two P-gp substrates whose absorptive transport is attenuated by P-gp to a different extent are affected differently with respect to their CYP3A-mediated metabolism. Terfenadine was chosen as a second P-gp/CYP3A dual substrate because the physico-chemical and permeability properties of terfenadine are similar to that of loperamide - both are lipophilic, poorly soluble, and have high permeability across intestinal epithelium – and yet P-gp-mediated attenuation of its absorptive transport was significantly lower than that of loperamide. First, the transport of terfenadine across Caco-2 cell monolayers was characterized in the A-to-B and B-to-A directions, and also in the presence and absence of the P-gp inhibitor GW918. As shown in Figure 3.12, the apparent permeability in the B-to-A direction was approximately 8-fold higher than in the A-to-B direction under control conditions. The absorptive permeability was significantly enhanced (~3 fold) in the presence of P-gp inhibitor GW918, suggesting that absorptive transport of terfenadine is reduced by P-gp. However, the B-to-A permeability remained significantly greater than the A-to-B permeability even in the absence

of P-gp (and presumably BCRP) activity (GW918 at 1 μM concentration completely inhibits P-gp and BCRP). This trend was observed at several dosing concentrations (Figure 3.13) and suggests that an additional AP efflux transporter may be involved in terfenadine's transport across Caco-2 cell monolayers. It appears that the factors affecting the permeability are more complex for terfenadine than for loperamide.

Next, the metabolism of terfenadine was studied during its absorptive transport across Caco-2 cells that were induced to express functional CYP3A by treatment with 1α, 25-dihydroxyvitamin D_3. CYP3A-specific metabolites of terfenadine (fexofenadine and azacyclonol) (Figure 3.14) appearing in the apical, basolateral and cellular compartments were quantified by LC-MS/MS (Figure 3.15). Studies were conducted over a range of dosing concentrations (1 to 50 μM, bounded by the detection limit of metabolites and cellular toxicity of terfenadine) in the presence and absence of the P-gp inhibitor GW918. As shown in Figure 3.15, the difference between the rates of metabolite production in GW918 treated and untreated cells was not significant; this was concluded using either simultaneous curve fitting or two-way ANOVA. This is in contrast with the results obtained for loperamide, whose CYP3A-mediated metabolism was reduced by P-gp (Figure 3.9).

The metabolic pathways of terfenadine are represented in Figure 3.14. Interestingly fexofenadine, one of the metabolites of terfenadine, is a better

substrate of P-gp than its parent compound (AQ for fexofenadine is 0.97, compared to 0.43 for terfenadine). As shown in Figure 3.16, fexofenadine exhibited over a 30-fold higher permeability in the B-to-A direction than in the A-to-B direction. In the presence of P-gp inhibitor GW918, the absorptive permeability of fexofenadine increased and the secretory permeability decreased, yielding nearly equal values. Consistent with its status as a P-gp substrate, fexofenadine was primarily effluxed to the apical compartment when it was formed within the cells after an apical dose of terfenadine; however, in the presence of GW918, fexofenadine was primarily found in the basolateral compartment (Figure 3.17), implying the presence of a basolateral efflux mechanism that does not appear to compete effectively with P-gp but directs the efflux of fexofenadine predominantly to the basolateral compartment when P-gp is inhibited. The distribution of the other metabolite of terfenadine, azacyclonol, remained unchanged in the presence of GW918 (Figure 3.17). The relative distribution of fexofenadine into the apical and basolateral compartments was also examined in the presence of MK571 (25 μM), an inhibitor of MRP (multidrug-resistance associated protein) transporters. The distribution remained unchanged with respect to the control, although the metabolic rate seemed to decrease slightly (Figure 3.18). However, when combined with GW918, MK571 reduced, but did not eliminate, the polarity of fexofenadine efflux toward the basolateral side; this suggested that fexofenadine efflux across the basolateral membrane is mediated, at least in part, by one or more MRP family transporter(s).

C.2. Transport and Metabolism in the Mouse Intestine - Diffusion Chamber Model

In the diffusion chamber model, a dosing range of 0.2 to 50 µM was used for terfenadine. For dosing concentrations up to 25 µM, intestinal tissues from P-gp-deficient mice metabolized terfenadine at a higher rate than the tissues from P-gp-competent mice, causing a rightward shift in the metabolic rate versus concentration profile, relative to the profile for P-gp-deficient mice (Figure 3.19). When a simple Michaelis-Menten model (Equation 2) was fitted to the data, it was revealed that CYP3A in the P-gp-competent mouse intestinal tissue metabolized terfenadine with about a four-fold higher apparent K_m than that observed for P-gp-deficient mouse intestinal tissue, with CYP3A from both tissues exhibiting similar V_{max} values (Table 3.1). The overall profiles were also found to be statistically different using two-way ANOVA.

C.3. Metabolism by Intestinal Microsomes

The intrinsic kinetic parameters were determined for terfenadine metabolism by human intestinal microsomes (Figure 3.20) and mouse intestinal microsomes (Figure 3.21). Although the apparent K_m values for metabolism of terfenadine during absorptive transport across Caco-2 cell monolayers and across fresh mouse intestinal tissue from P-gp competent mice were similar, the K_m for its

metabolism by human intestinal microsomes was 24-fold higher than that obtained with mouse (P-gp competent) intestinal microsomes; the results are summarized in Table 3.1. These results suggested that different CYPs may metabolize terfenadine in the mouse vs. human intestine. Hence, CYP-selective inhibitors were used to determine the contribution of CYP3A (and possibly other CYP enzymes) to the intestinal metabolism of terfenadine. Interestingly, terfenadine metabolism by mouse intestinal tissue was inhibited only partially by ketoconazole (3 μM), a compound that is expected to inhibit CYP3A completely at this concentration (Figure 3.22). Since terfenadine is known to be metabolized by CYP2D6 in human liver (Jones et al., 1998), the contribution of this CYP in its metabolism by microsomes from mouse and human intestinal tissue was assessed by using CYP2D inhibitor, quinidine (3 μM). The results in Figure 3.22 show that CYP3A and CYP2D each contribute approximately 60% of the total oxidative metabolism of terfenadine. Clearly, this implies that one of the inhibitors, likely ketoconazole, is inhibiting the second CYP to some extent. Hence, another CYP3A-specific inhibitor, azamulin, was used to determine the contribution of CYP3A to terfenadine metabolism. Azamulin (5 μM) was only able to inhibit terfenadine metabolism by 41% in mouse intestinal microsomes; thus it appears that CYP3A and CYP2D contribute ~40% and 60% of the total oxidative metabolism of terfenadine in mouse intestine. In order to help understand the significant contribution of CYP2D to the mouse intestinal metabolism of terfenadine, activities of five major CYP isoforms, CYP1A1, CYP2D6, CYP2C9, CYP2C19 and CYP3A4, in the human intestine were

compared to the orthologous activities in the mouse intestine using a cassette dosing method (Yanni et al., 2004). As shown in Figure 3.23, most of the activities were similar in the mouse and human intestinal microsomes except for the activity of CYP2D (formation of dextrorphan from dextromethorphan), which was approximately 25-fold higher in mouse intestinal microsomes. This result is consistent with the inhibition profile observed for terfenadine in mouse intestinal microsomes, which shows that CYP2D plays a greater role than CYP3A in the metabolism of terfenadine.

D. PHARMACOKINETIC MODELING OF P-GP/CYP3A INTERACTIONS DURING TRANSPORT OF DUAL SUBSTRATES

The rate of apical uptake, as well as the basolateral efflux rate, was determined for terfenadine in Caco-2 cell monolayers. The results are shown in Table 3.2. In addition, the intrinsic K_m for terfenadine metabolism was determined using human intestinal microsomes. A simple Michaelis-Menten model was fit to the microsome data and the V_{max} and K_m were determined using WinNonlin. However, for the PK modeling exercises, the V_{max} for metabolism determined from Caco-2 cells was used in order to more accurately reflect the expression level of CYP3A in the Caco-2 cell system.

The basic model that describes translocation of compounds, with dual substrate activity for efflux transporters and metabolic enzymes, across intestinal epithelium is shown in Figure 3.24. Model A consists of three compartments,

and incorporates the following assumptions: the function describing metabolism is saturable; uptake into the cell across apical and basolateral membranes and efflux across the basolateral membrane is via passive diffusion; efflux across the apical membrane, mediated by P-gp, occurs at concentrations that are not likely to saturate P-gp; P-gp and CYP3A, although in different membrane compartments (apical membrane and endoplasmic reticulum, respectively), are assumed to be acting on the same cytosolic concentration of their dual substrates. Model A adequately described terfenadine efflux-metabolism interactions during absorptive transport across Caco-2 cell monolayers (Figure 3.25). In order to predict the effect of P-gp efflux on metabolic rate, a series of profiles were simulated at different values of the P-gp efflux rate constant, k_{BA}. As P-gp efflux rate increased, metabolite formation rate proportionally decreased (Figure 3.26).

As shown in Figure 3.27, P-gp expression increases in the distal regions of intestine, while CYP3A expression decreases (Liu et al., 2006). When the effect of varying expression levels of P-gp and CYP3A was investigated through simulations, metabolism was found to decrease with increasing P-gp expression or decreasing CYP3A expression (Figure 3.28). Interestingly, at high P-gp expression (J_{max}), changes in V_{max} (related to expression of CYP3A) had less of an effect on the rate of metabolism, suggesting that high expression of P-gp could buffer the metabolic changes due to differential expression of metabolic enzymes.

Several different parameters have been used by different groups to quantify the effect of P-gp efflux on CYP3A metabolism. Therefore, a simulation exercise was carried out to determine the sensitivity of these parameters to changes in P-gp efflux without changes in metabolic parameters. While the percent of dose metabolized decreased slightly with an increase in P-gp efflux activity, the ER increased significantly, regardless of the method of calculation used (Figure 3.29).

Although Model A was able to adequately describe the Caco-2 cell data for terfenadine, it is recognized that this model is oversimplified and therefore may not be entirely representative of the *in vivo* situation. Particularly, the assumption that P-gp and CYP3A act on the same (cytosolic) concentration of substrate may not be accurate. Therefore, a secondary model (Model B, Figure 3.30) was developed which does not rely on this assumption. The model incorporates a fourth "P-gp" compartment between the apical and cellular chambers. However, the addition of the fourth compartment precludes fitting the model to experimental data, since no data is available for the additional compartment. Therefore, an additional assumption was made: that the passive diffusion constants in and out of the "P-gp" compartment are equal; that is, $k_{AB} = k_{BC} = k_{CB}$.

Using Model B, the effects of changes in P-gp efflux activity (k_{BA}) on metabolism of dual substrates were simulated. As shown in Figure 3.31, the

amount of metabolites produced over time decreased with increased P-gp activity. This is similar to the result produced by Model A, except that with Model B increased P-gp activity seemed to lead to an increased lag time for CYP3A-mediated metabolism. These simulations are consistent with those performed using the previous model and are in agreement with the experimental results.

E. REFERENCES

Jones BC, Hyland R, Ackland M, Tyman CA and Smith DA (1998) Interaction of terfenadine and its primary metabolites with cytochrome P450 2D6. *Drug Metab Dispos* **26**:875-882.

Korjamo T, Honkakoski P, Toppinen MR, Niva S, Reinisalo M, Palmgren JJ and Monkkonen J (2005) Absorption properties and P-glycoprotein activity of modified Caco-2 cell lines. *Eur J Pharm Sci* **26**:266-279.

Liu S, Tam D, Chen X and Pang KS (2006) P-glycoprotein and an unstirred water layer barring digoxin absorption in the vascularly perfused rat small intestine preparation: induction studies with pregnenolone-16alpha-carbonitrile. *Drug Metab Dispos* **34**:1468-1479.

Stephens RH, O'Neill CA, Bennett J, Humphrey M, Henry B, Rowland M and Warhurst G (2002) Resolution of P-glycoprotein and non-P-glycoprotein effects on drug permeability using intestinal tissues from mdr1a (-/-) mice. *Br J Pharmacol* **135**:2038-2046.

Troutman MD and Thakker DR (2003) Novel experimental parameters to quantify the modulation of absorptive and secretory transport of compounds by P-glycoprotein in cell culture models of intestinal epithelium, in *Pharm Res* pp 1210-1224.

Yanni SB, Thiel P, Haroldsen P and Samara E (2004) High Throughput Evaluation of Clinical Drug Interaction using LC-MS/MS. *ISSX Conference* **ASBT #582**.

Table 3.1. Kinetic parameters of metabolism of terfenadine and loperamide for CYP3A-expressing Caco-2 cells with or without P-gp inhibitor GW918; for P-gp competent and P-gp deficient mouse intestine; and for mouse and human intestinal microsomes.

Parameter	Caco-2 No GW918	Caco-2 GW918	WT Mouse	KO Mouse	MIM	HIM
LOP V_{max}	0.80 ± 0.11	0.76 ± 0.06	31 ± 2.1	30 ± 3.2	102 ± 4.0	25 ± 2.0
LOP K_m	18 ± 4.0	8.6 ± 1.6	22 ± 4.8	4.5 ± 2.4	0.93 ± 0.18	0.94 ± 0.26
TF V_{max}	0.5 ± 0.1	0.6 ± 0.0	21 ± 5.6	18 ± 2.9	36 ± 2.4	67 ± 9.7
TF K_m	9.6 ± 2.6	12 ± 2.2	14 ± 5.5	4.0 ± 2.4	0.9 ± 0.2	24 ± 7.1

V_{max} = pmol/min/cm^2 for Caco-2 and mouse, pmol/min/mg for microsomes; K_m = µM; WT = LOP = loperamide; TF = terfenadine; WT = P-gp competent mouse; KO = P-gp deficient mouse; MIM = mouse intestinal microsomes; HIM = human intestinal microsomes. Mean ± SD

Table 3.2. Parameters used in fitting the PK model to terfenadine data.

Parameter	Value	
Apical uptake	0.18	ml/min
Basolateral efflux	0.0035	ml/min
V_{max}	2.1	pmoles/min
K_m	23.9	pmoles/ml
Apical efflux	119	ml/min

All parameters were experimentally derived besides the apical efflux rate, which was fitted using the model (CV = 1.2%). Apical uptake and basolateral efflux determined over 1 minute. V_{max} derived from Caco-2 metabolic data; K_m derived from human intestinal microsomes.

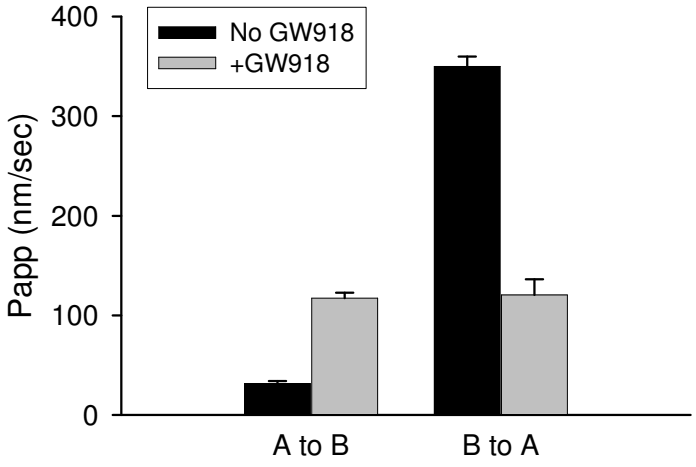

Figure 3.1. Digoxin permeability over 90 minutes in Caco-2 after a 10 µM dose.
N=3 ± SD. Black bars = control, gray bars = GW918 (1 µM) treatment. Treated and untreated wells were found to be significantly different using student's t-test ($p<0.05$). Likewise, A to B permeability was statistically different than B to A permeability in the absence of inhibitor.

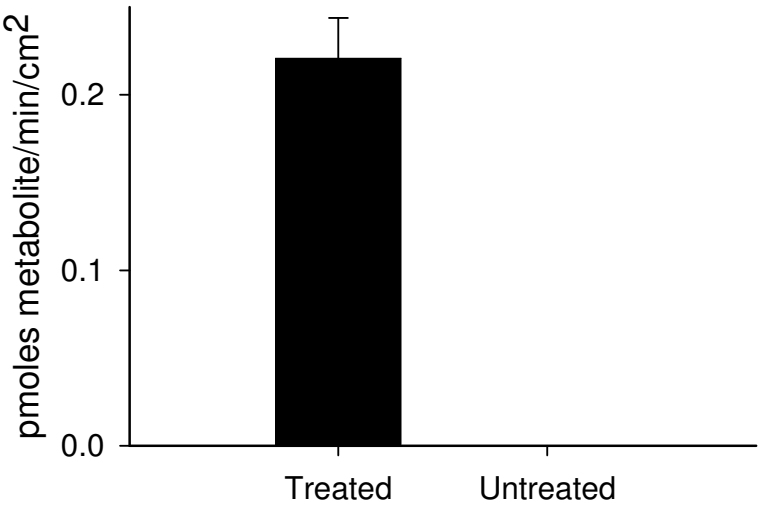

Figure 3.2. Formation of 6-β-OH-testosterone over 120 minutes from a 250 µM dose of testosterone in Caco-2 cells treated with 0.5 µM of 1α, 25-dihydroxyvitamin D_3 for 14 days versus untreated cells. Metabolites were not detectable in the untreated cells. N=5; errors bars denote standard deviation.

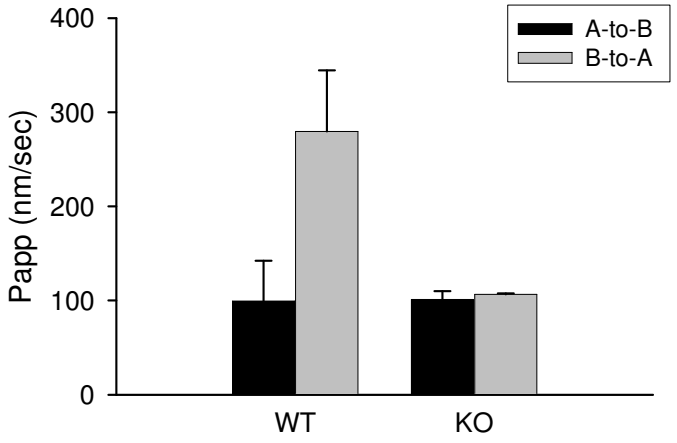

Figure 3.3. Digoxin permeability over 90 minutes across mouse intestine in Ussing chamber after a 10 µM dose. N=3; error bars = SD; WT = P-gp competent mouse; KO = P-gp deficient mouse. A-to-B permeability is significantly different (student's t-test, $p<0.05$) than B-to-A permeability in the WT only.

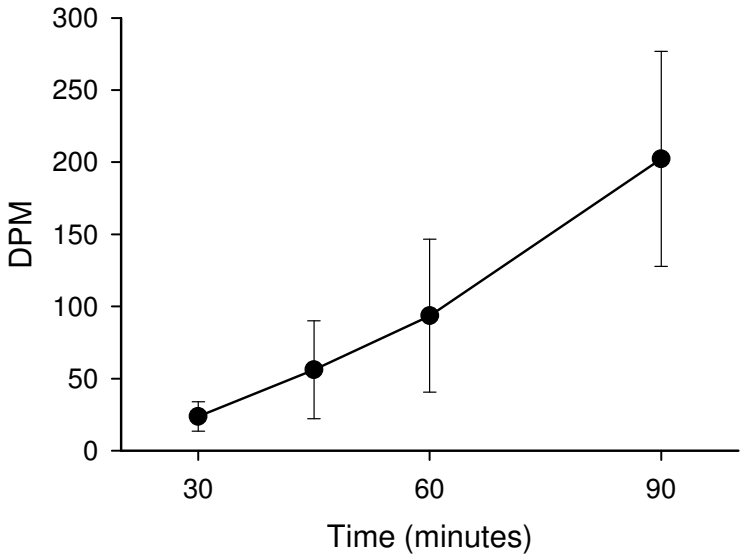

Figure 3.4. Mannitol absorptive transport across mouse intestinal tissue after a 5 µM dose.
Permeability = 35 ± 12 nm/sec. n=3; error bars = SD; DPM = disintegrations per minute.

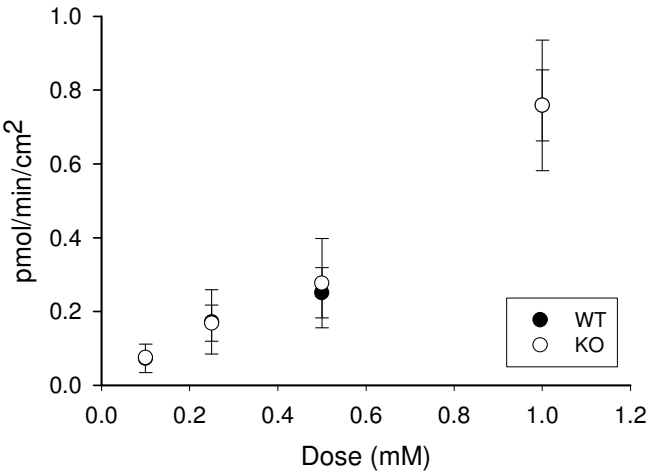

Figure 3.5. CYP3A activity (testosterone 6-β-hydroxylation) in P-gp-competent (WT) and P-gp-deficient (KO) mouse intestine over 90 minutes.
Error bars denote standard deviation. No significant difference was seen at any concentration level.

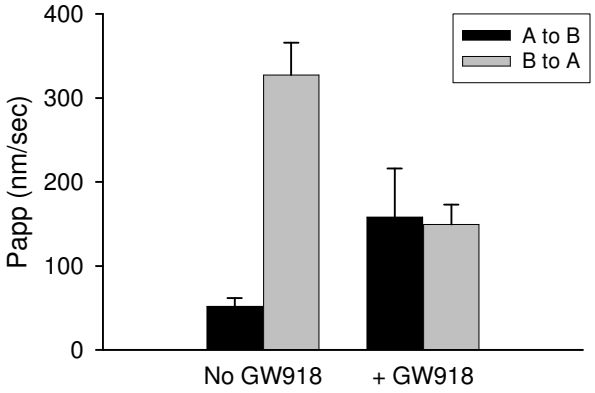

Figure 3.6. Absorptive and secretory transport of loperamide (0.25 µM dose) across Caco-2 cell monolayers in the presence versus absence of P-gp inhibitor GW918 (1 µM) over 60 minutes.
n=3, error bars denote standard deviation. A significant difference was seen between treated and untreated wells for both directions. In the untreated wells, a signficiant difference was observed in the A-to-B versus B-to-A directions (student's t-test, $p<0.05$).

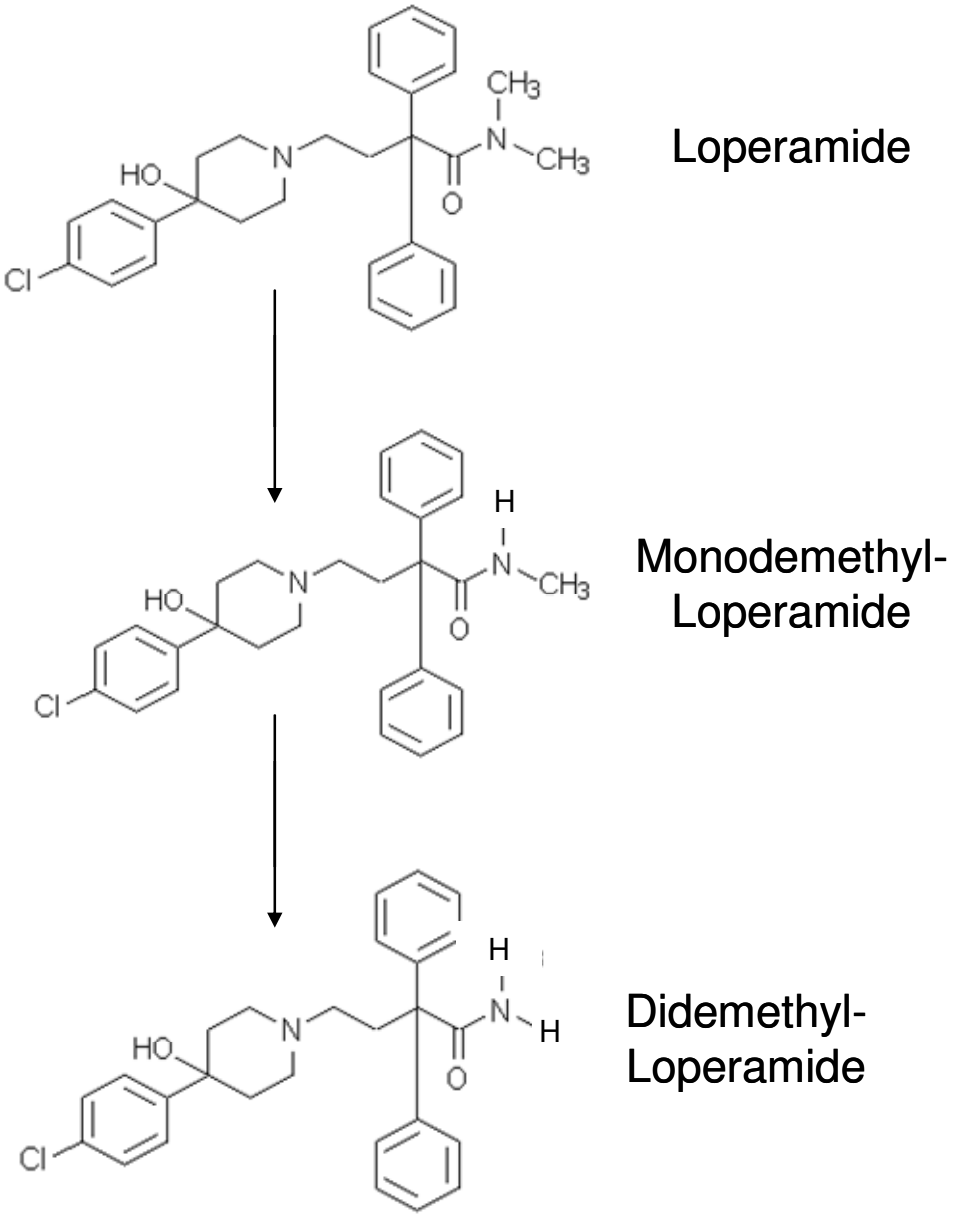

Figure 3.7. Structure of loperamide and its CYP3A metabolites, monodemethyl- and didemethyl-loperamide.

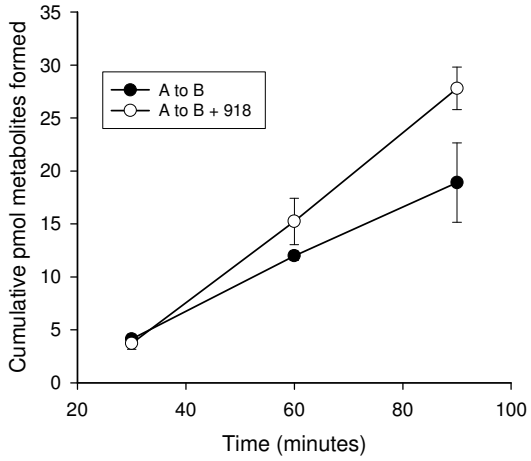

Figure 3.8. Linearity of loperamide metabolite formation during absorptive transport across Caco-2 cell monolayers.
Dose = 20 µM, n=3, error bars = standard deviation. A statistically significant difference was observed between treated and untreated wells at the 60 and 90 minute timepoints ($p<0.05$, student's t-test).

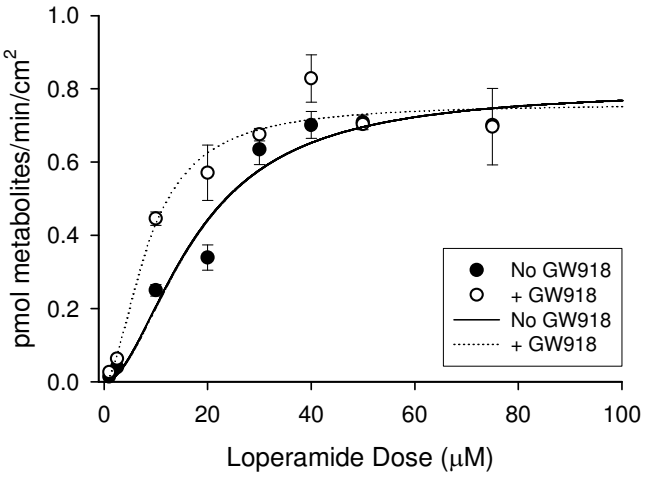

Figure 3.9. Loperamide metabolism during absorptive transport across Caco-2 cell monolayers.
n=3; error bars denote standard deviation. Profiles are statistically different (two-way ANOVA). Lines represent the fit of the model to the data.

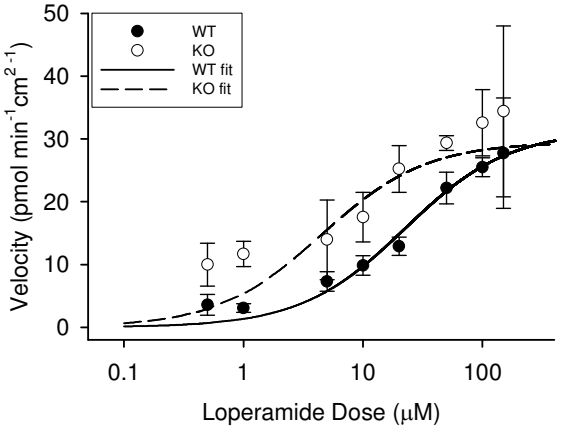

Figure 3.10. Loperamide metabolism by fresh intestinal tissue from P-gp competent (WT) and P-gp deficient (KO) mice.
n=3; error bars denote standard deviation. Profiles are statistically different (two-way ANOVA). Lines represent the fit of the model to the data.

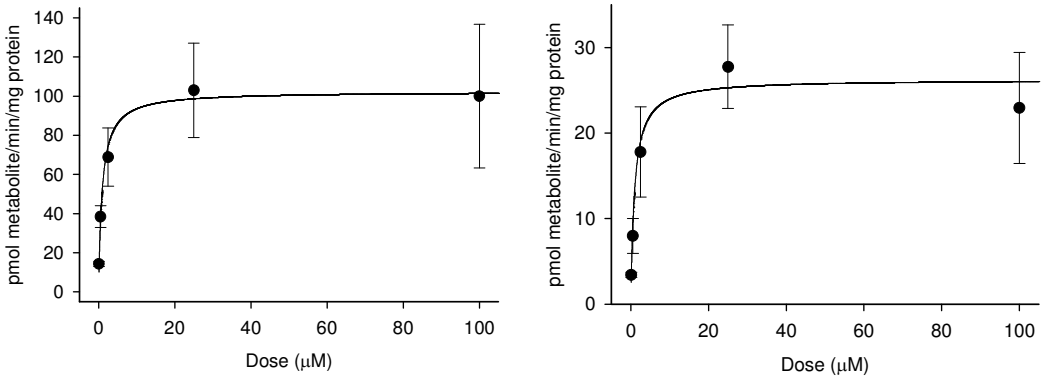

Figure 3.11. Metabolism of loperamide in mouse and human intestinal microsomes over 10 minutes.
n=3; error bars denote standard deviation. Lines represent the fit of the Michaelis-Menten model to the data.

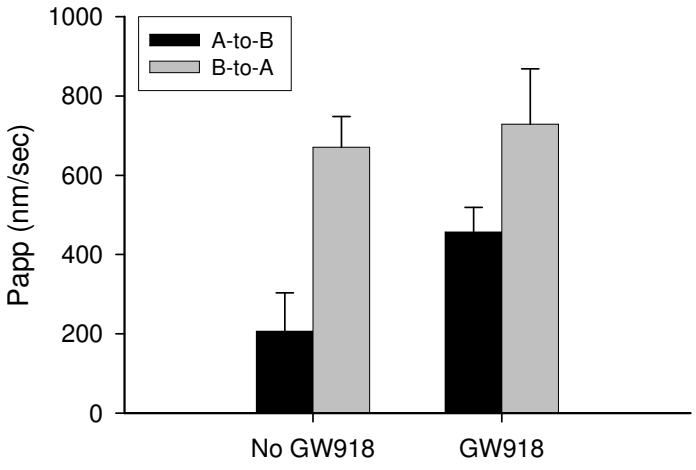

Figure 3.12. Permeability of terfenadine (20 µM dose) across Caco-2 cell monolayers in the absence (left) or presence (right) of 1 µM P-gp inhibitor GW918.
Black bars represent apical to basolateral permeability; gray bars, basolateral to apical permeability. Mean of 2 experiments with 3 wells/experiment. Error bars represent standard deviation. A statistically significant difference was observed between A-to-B and B-to-A permeability for both the treated and untreated conditions. A significant difference between treated and untreated wells was observed in the A-to-B direction only ($p<0.05$, student's t-test).

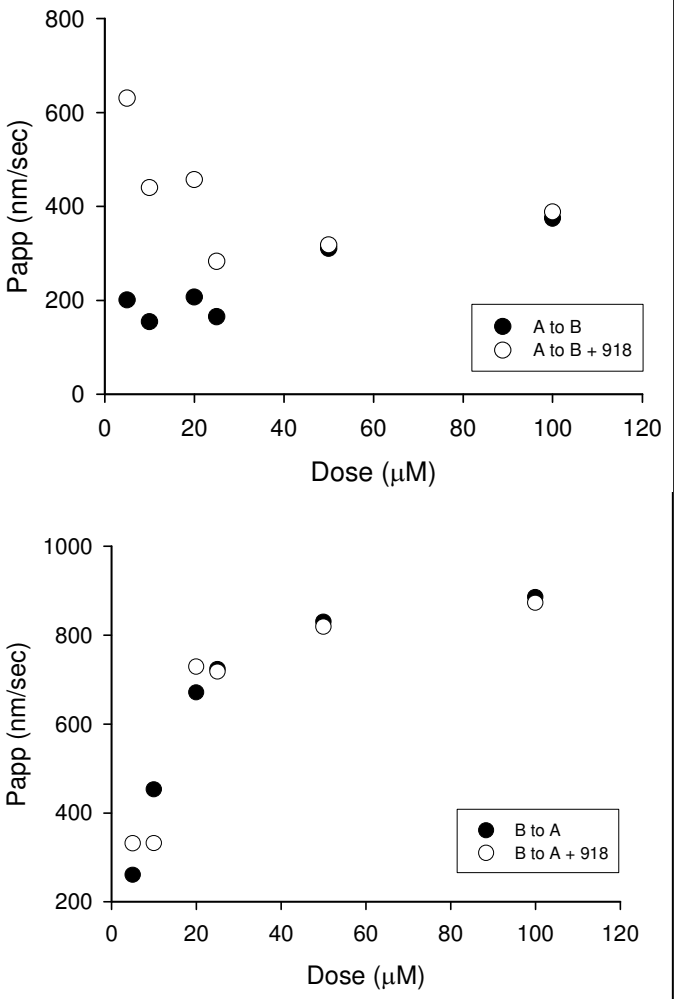

Figure 3.13. A-to-B and B-to-A permeability of terfenadine in Caco-2 cell monolayers as a function of concentration. Upper panel: apical to basolateral transport; lower panel: basolateral to apical transport.

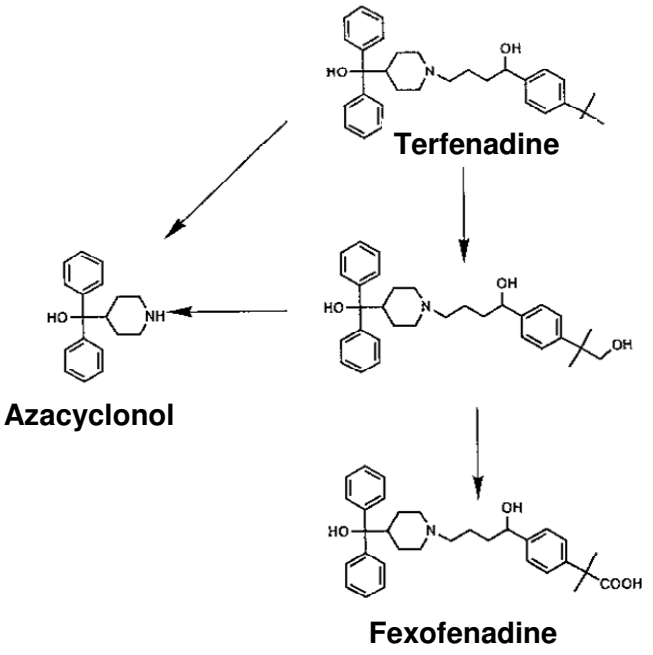

Figure 3.14. Structure of terfenadine and its metabolites formed by CYP3A.

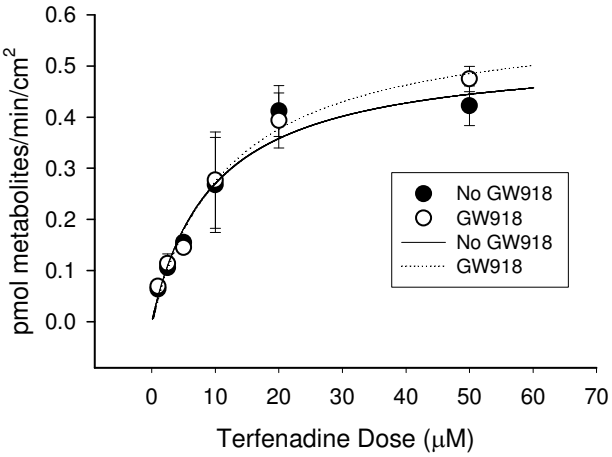

Figure 3.15. Caco-2 metabolism of terfenadine over 120 minutes at several dose levels in the presence (open circle) or absence (closed circle) of 1 μM of the P-gp inhibitor GW918. Cells showed toxicity at doses above 50 μM. n = 3; error bars = standard deviation. Lines represent the fit of the model to the data. No significant difference was found between the two profiles (two-way ANOVA).

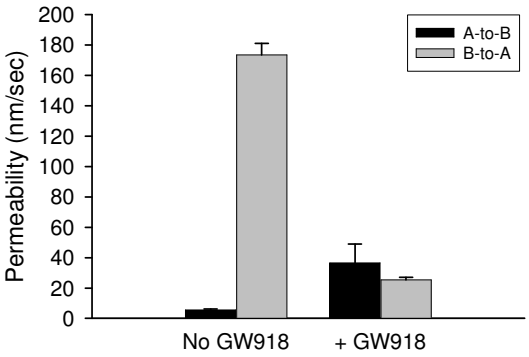

Figure 3.16. Permeability of fexofenadine (5 µM) across Caco-2 cell monolayers in the absence (left) or presence (right) of 1 µM P-gp inhibitor GW918.
Black bars represent apical to basolateral permeability; gray bars, basolateral to apical permeability. Mean of 3; error bars = standard deviation. Data from wells treated with GW918 is significantly different than control wells; A-to-B permeability was significantly different than B-to-A permeability in the untreated wells only (student's t-test, $p<0.05$).

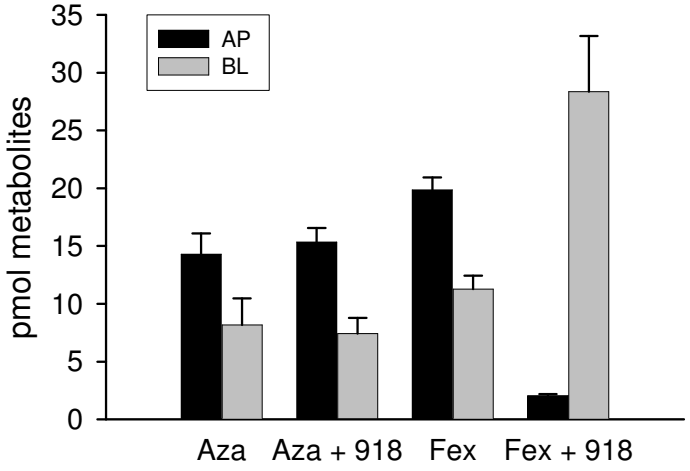

Figure 3.17. Distribution of metabolites of terfenadine after a 20 µM apical dose in Caco-2 cells. N=3; error bars = SD. Aza = azacyclonol; Fex = Fexofenadine; 918 = GW918; black bars = apical chamber; gray bars = basolateral chamber. Amounts in apical and basolateral chamber are statistically different for all conditions ($p<0.05$, student's t-test).

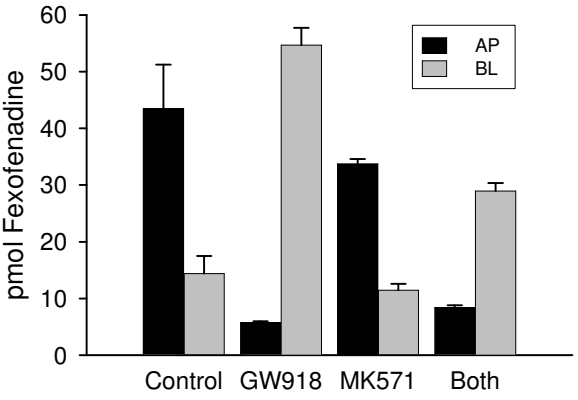

Figure 3.18. Fexofenadine distribution in induced Caco-2 cells in the absence or presence of inhibitors of P-gp (GW918) and MRP (MK571).
N=3; error bars = SD; black bars = apical compartment; gray bars = basolateral compartment. Amounts in apical and basolateral chamber are statistically different for all conditions ($p<0.05$, student's t-test).

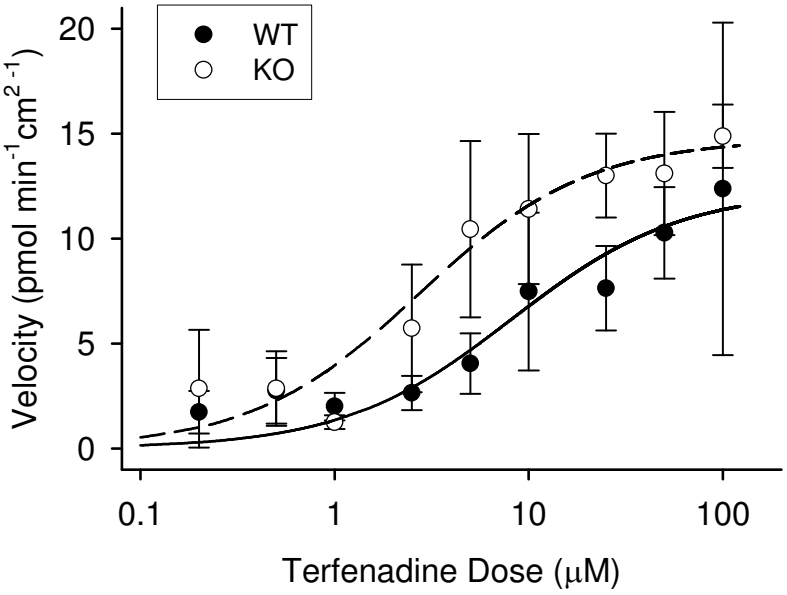

Figure 3.19. Terfenadine metabolism in P-gp-competent (WT, solid circles) and P-gp-deficient (KO, open circles) mouse intestine.
Solid and dotted lines represent the fit of the model to the data for P-gp-competent and P-gp-deficient mice, respectively. N = 3; error bars denote standard deviation. Profiles were found to be statistically different (two-way ANOVA).

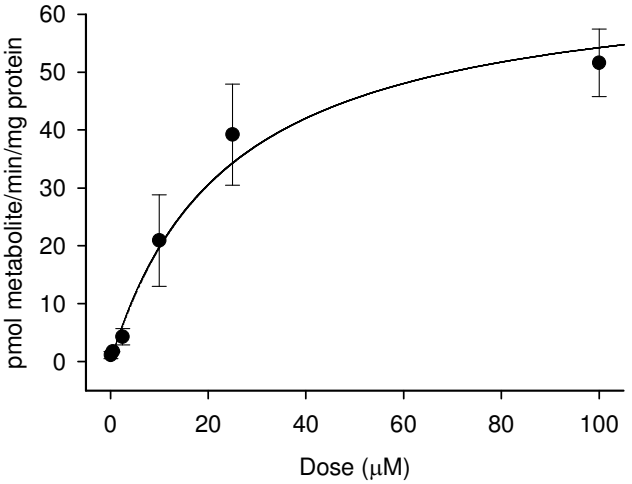

Figure 3.20. Terfenadine metabolism by human intestinal microsomes.
N=3; error bars = SD. Line represents the fit of a simple Michaelis-Menten model to the data.

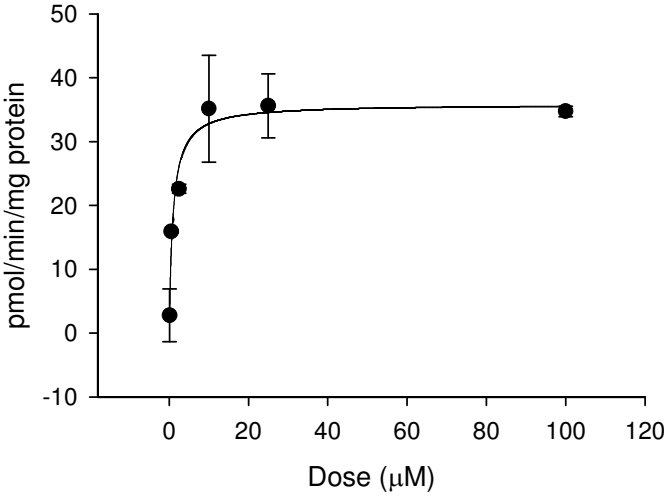

Figure 3.21. Terfenadine metabolism by mouse intestinal microsomes.
N=3; error bars = SD. Lines represent the fit of a simple Michaelis-Menten model to the data.

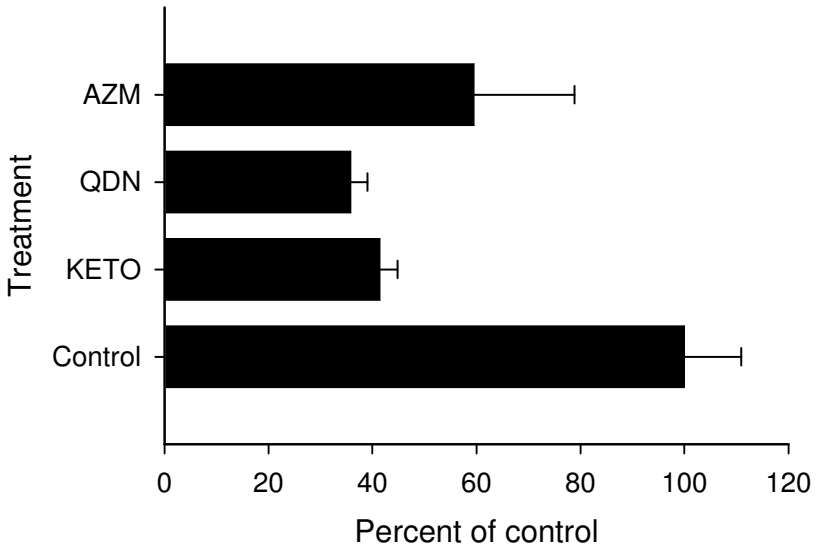

Figure 3.22. Terfenadine metabolite formation and inhibition in mouse intestinal microsomes.
N=3; error bars = SD. AZM = azamulin, 5 µM; QDN = quinidine, 3 µM; KETO = ketoconazole, 3 µM. Incubation time = 10 minutes. All treatments showed a statistically significant decrease relative to control ($p<0.05$, student's t-test).

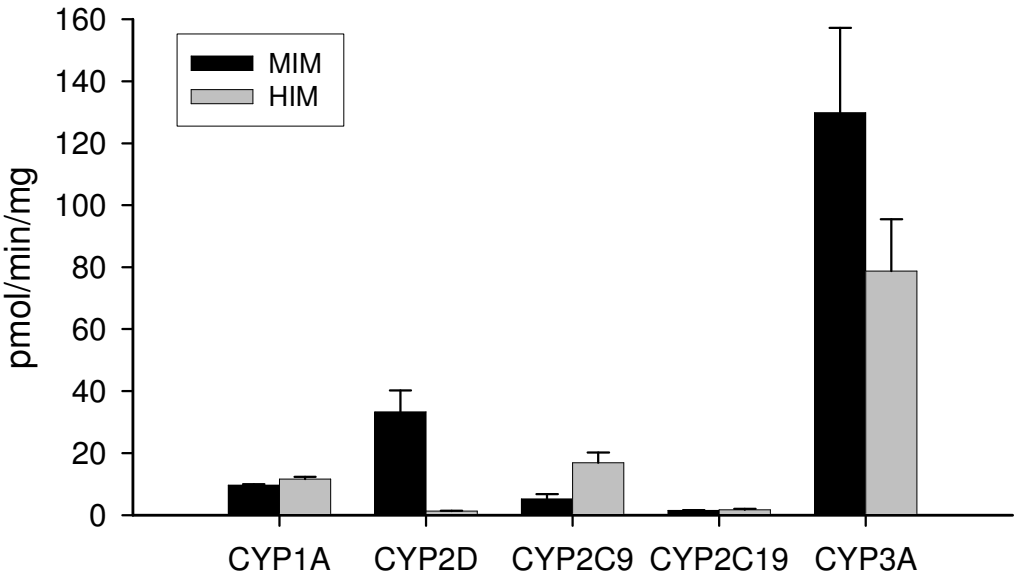

Figure 3.23. Metabolic activity of mouse intestinal microsomes (MIM) and human intestinal microsomes (HIM) toward P450 probe substrates: CYP1A2, phenacetin; CYP2D6, dextromethorphan; CYP2C9, diclofenac; CYP2C19, S-mephenytoin; CYP3A4, testosterone. N=3; error bars = SD. MIM = black bars; HIM = gray bars. (Only human isoforms listed.) Statistical differences were shown between mouse and human intestinal microsomal activity for all isoforms listed besides CYP1A and CYP2C19 ($p<0.05$, student's t-test).

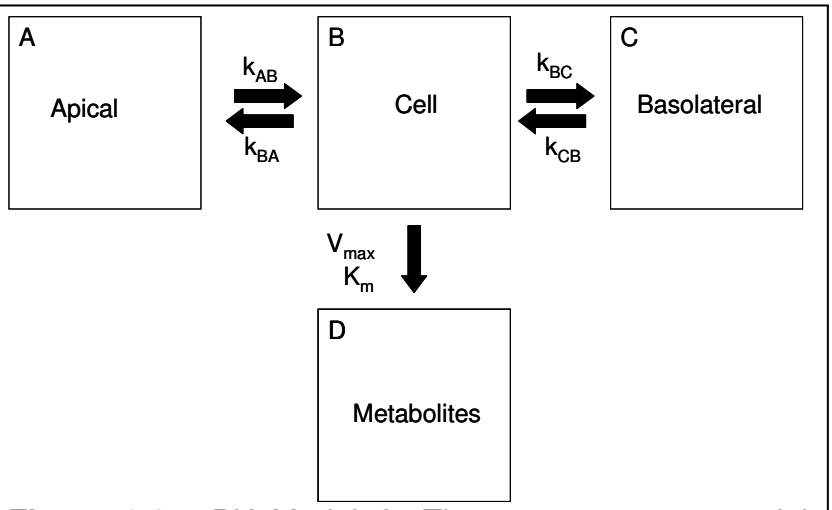

Figure 3.24. PK Model A. Three-compartment model describes the interplay between P-gp-efflux and CYP3A-mediated metabolism of dual substrates in the intestine. k values represent first-order rate constants for compound movement between compartments; V_{max} is the maximum rate of velocity achieved; K_m is the concentration at which half of maximum metabolic velocity is achieved.

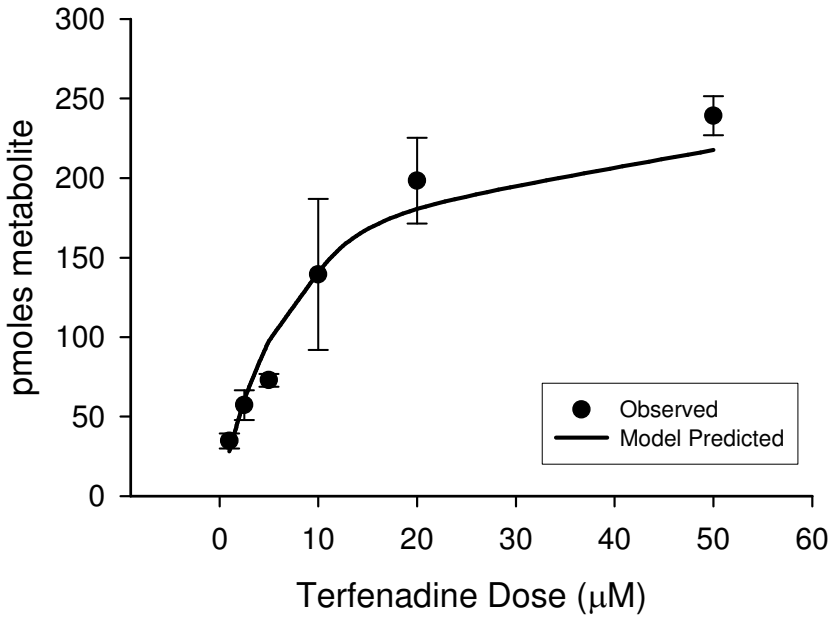

Figure 3.25. Line represents the fit of PK Model A to terfenadine Caco-2 data. N=3; error bars = SD.

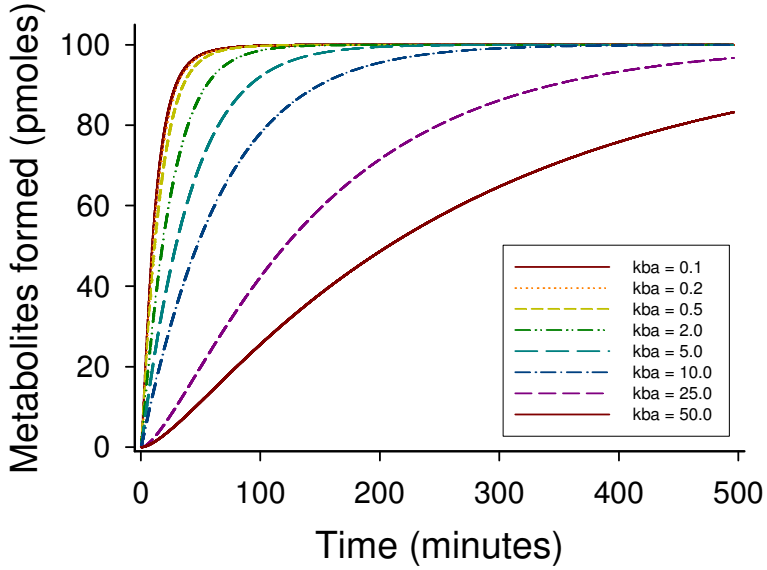

Figure 3.26. Simulation of the effect of increased P-gp efflux on amount of metabolites formed over time using Model A. kba represents the first-order rate constant for P-gp efflux.

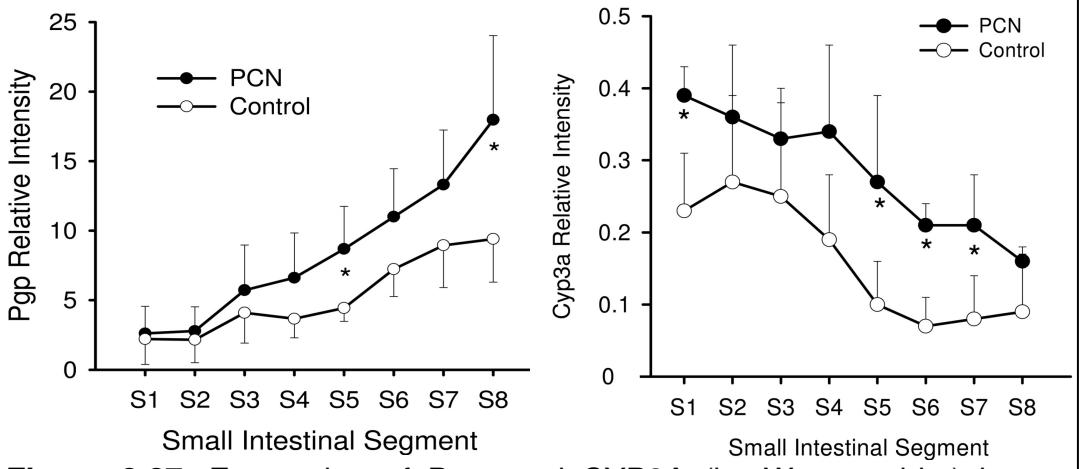

Figure 3.27. Expression of P-gp and CYP3A (by Western blot) in rat intestine. PCN = pregnenolone 16α–carbonitrile (inducer). S1 = duodenum; S2-S7 = jejunum; S8 = ileum. Liu et al., 2006

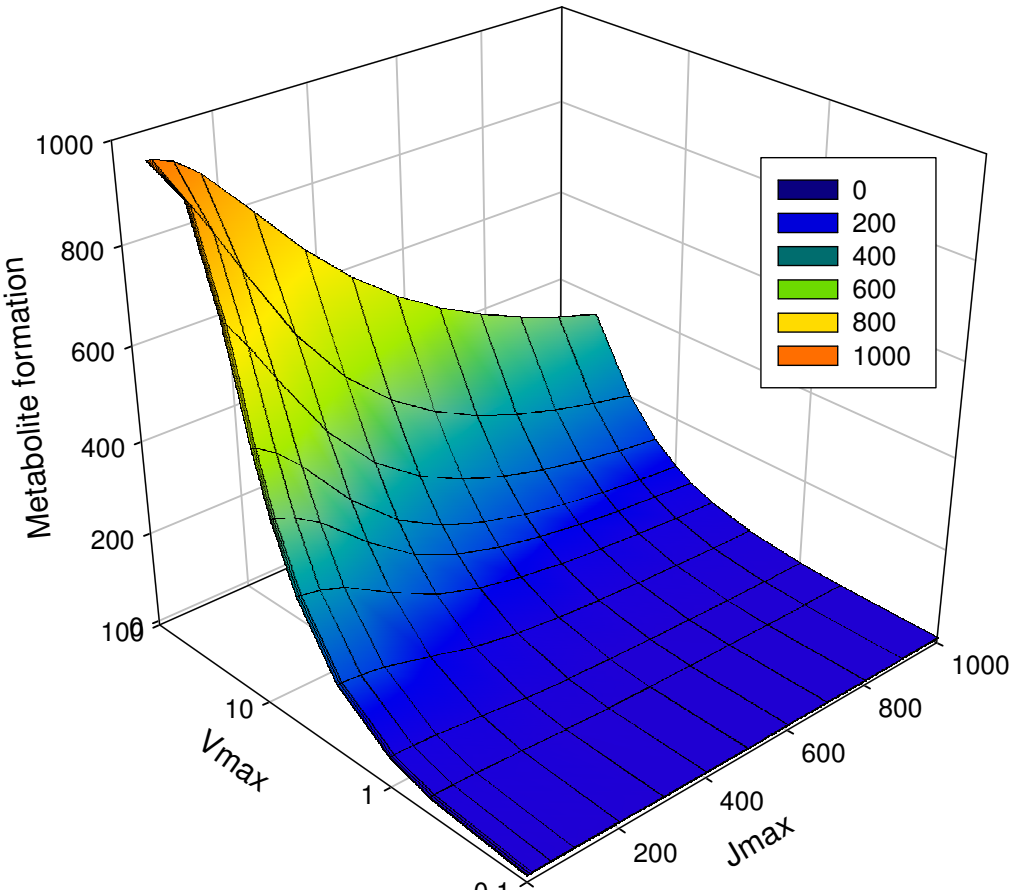

Figure 3.28. Simulations (using Model A) examining the effect of changes in P-gp and CYP3A expression throughout the intestine.

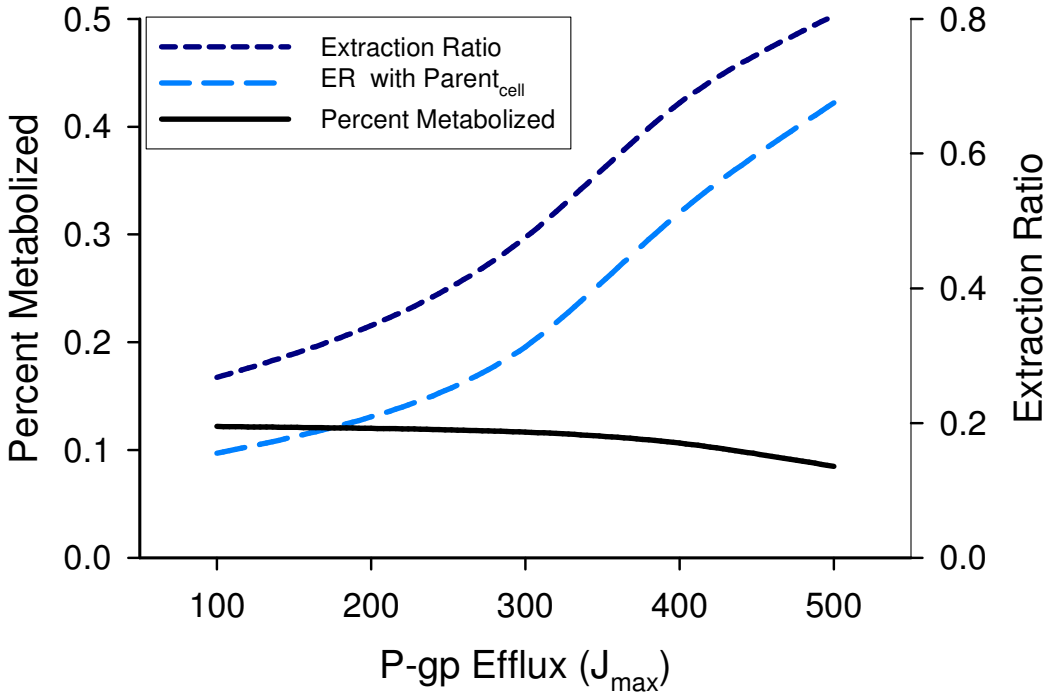

Figure 3.29. Comparison of the effect of changes in P-gp efflux activity on parameters used to quantify the interaction between P-gp and CYP3A in intestine. Model A was used for simulations.

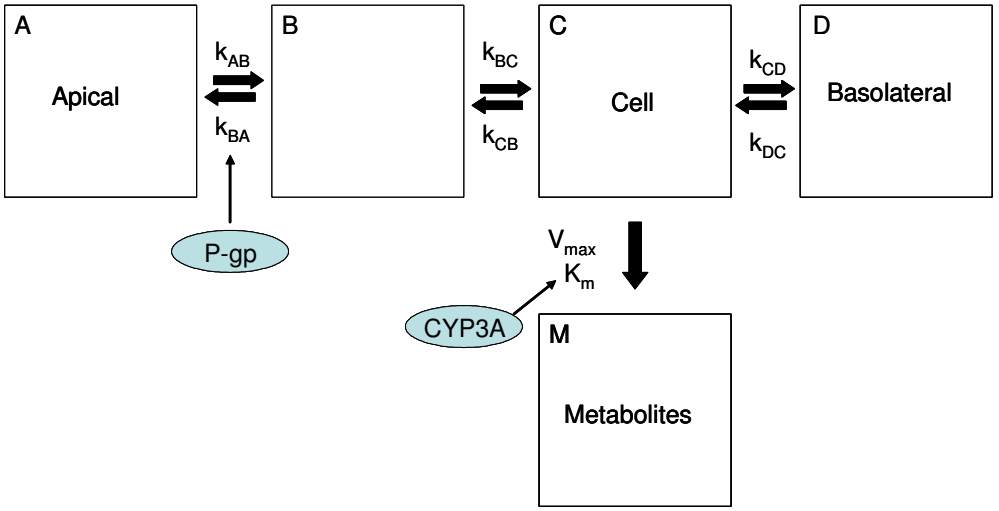

Figure 3.30. PK Model B. Four-compartment pharmacokinetic model describing the interaction between P-gp efflux and CYP3A-mediated metabolism of dual substrates in the intestine.

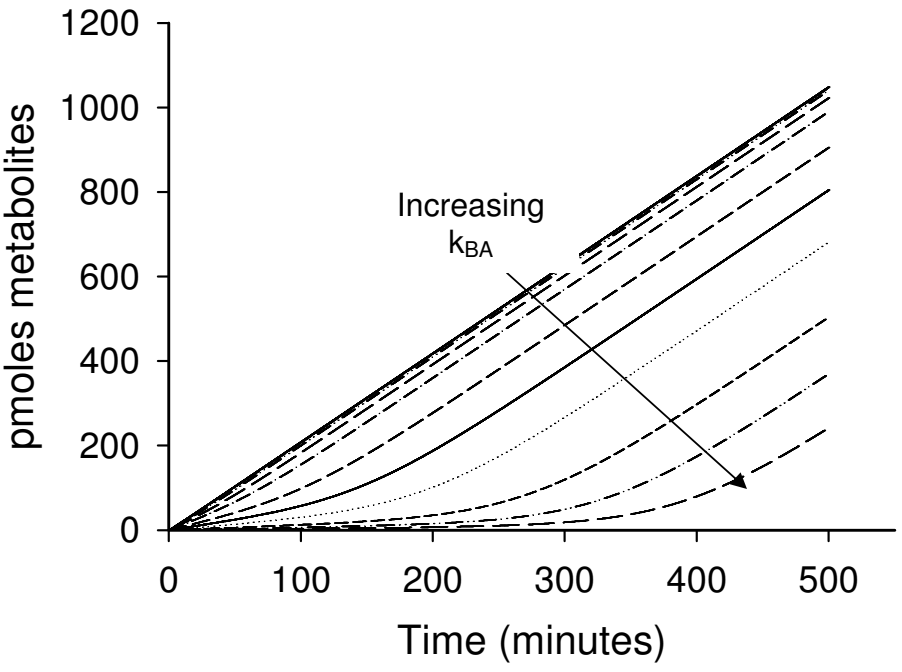

Figure 3.31. Simulation of the effect of increased P-gp efflux on amount of metabolites formed over time using Model B. kba represents the first-order rate constant for P-gp efflux.

CHAPTER 4: DISCUSSION AND CONCLUSIONS

A. INTRODUCTION

The CYP subfamily most commonly involved in drug-drug interactions is CYP3A because of its wide substrate specificity (Bu, 2006) and large interindividual and intraindividual variation in hepatic (Shimada et al., 1994) and intestinal (Paine et al., 1997) expression. While hepatic CYP3A has been implicated in drug-drug interactions for many years (Kristensen, 1976), the pioneering work by Watkins et al. (Watkins et al., 1991) demonstrated that CYP3A is also expressed in the intestinal epithelium and that it plays a significant role in drug-drug interactions. Generally, the expression of CYP3A is highest in upper small intestine and decreases distally (Paine et al., 1997). During absorption of an orally administered drug, a significant percentage of the dose could be metabolized by CYP3A, both in the intestine and in the liver, before the drug reaches the systemic circulation. This so called “first-pass metabolism” reduces the availability of the administered dose (exposure) of the drug to the systemic circulation. Thus, intestinal CYP3A could contribute significantly to drug-drug interactions when two or more CYP3A substrates are co-administered orally.

The efflux transporter P-gp (and the related transporter BCRP), expressed in the apical membrane of enterocytes, is recognized as another important biochemical barrier that can influence the rate and extent of absorption of orally administered drugs. P-gp efflux is now recognized as a cause of intestinal drug-drug interactions (Endres et al., 2006). Due to the large overlap in substrate specificity between CYP3A

and P-gp, some drug interactions previously attributed to CYP3A have been shown to be at least partially due intestinal P-gp, which can be a rate-limiting factor in absorption (Lown et al., 1997). The pharmaceutical industry has therefore begun to implement *in vitro* assays to detect interaction of drug candidates with P-gp (Polli et al., 2001).

Although metabolism and efflux are often separately assessed using *in vitro* models, these processes may not occur independently *in vivo*. The concept that P-gp-mediated efflux of a compound may influence its metabolism if the compound is also a substrate for a metabolic enzyme in the intestinal epithelium has evolved over the past few years (Johnson et al., 2003b; Tam et al., 2003; Cummins et al., 2004). This interaction could be important for many compounds, as there is significant overlap in the specificities of P-gp and CYP3A.

B. PROJECT STRATEGY

While the potential for interaction between P-gp and CYP3A in intestine is well recognized, there is little consensus regarding the nature of the interaction or its implications for drug delivery. There is some evidence that P-gp efflux could increase the extent of CYP3A-mediated metabolism in the intestine. Most of the work done to date has used *in vitro* models (e.g., Caco-2) to reach this conclusion (Cummins et al., 2002; Cummins, et al., 2004). However, other groups have used pharmacokinetic modeling to show that P-gp efflux is unlikely to enhance the rate or

extent of metabolism since metabolic and efflux processes compete with each other (Tam et al., 2003; Johnson et al., 2003). Therefore, more work is needed in this area to bridge the gap between the theory and experimental *in vitro* results.

In this work, the question of P-gp/CYP3A interactions was addressed in a unique fashion. Two *in vitro* models, an immortalized cell line and fresh intestinal tissue from a preclinical model, were used to examine the mechanism behind the P-gp/CYP3A interaction. Comparison of data from the two model systems allowed for enhanced data interpretation and model evaluation. While cell lines have frequently been used to study this phenomenon, previous studies have not addressed the concentration-dependence of the interaction. Therefore, in this work, a large range of dosing concentrations was used in order to more closely examine the effect of concentration and to attempt to extrapolate the results to *in vivo* predictions. Pharmacokinetic modeling was used to analyze the results and to extend them to hypothetical *in vivo* situations.

B.I. Caco-2 Cell Model

One model that has recently been developed to address the interaction between efflux transporters and drug metabolizing enzymes in intestine is the CYP3A-expressing Caco-2 cell model. Caco-2 is an immortalized cell line that is derived from human colon carcinoma cells. This cell line is already widely used for assessment of compound permeability and susceptibility to P-gp efflux. It has very

low constitutive CYP activity, but it has been adapted to express CYP3A. One method of inducing CYP3A expression is treatment with 1α, 25-dihydroxyvitamin D_3 (Schmiedlin-Ren et al., 2001; Mouly et al., 2004). Other groups have used Caco-2 cells transfected with the CYP3A gene (Raeissi et al., 1999; Cummins et al., 2004). Both methods produce Caco-2 cells that express functional CYP3A as well as levels of P-gp that are comparable to levels in the human intestine. P-gp is expressed on the apical membrane, while CYP3A is expressed in the endoplasmic reticulum. This system allows for *in vitro* study of both efflux and metabolism, as well as their effects on each other.

While such cellular models are generally good for acquiring mechanistic information due to their simplicity, there are also certain limitations associated with their use. One problem with these assays is their reliance on chemical inhibitors to modulate P-gp activity, since most of the available inhibitors of transporters have nonspecific effects (Achira et al., 1999). For example, the P-gp inhibitor GW918 has also been shown to inhibit BCRP (Hyafil et al., 1993; Allen et al., 1999); it has also been implied that GW918 inhibits a basolateral excretion mechanism in rat hepatocytes (Hoffmaster et al., 2004). A key limitation of using a human-derived *in vitro* model, such as Caco-2 cells, to elucidate cellular disposition of drugs is that it requires well-designed clinical studies to assess whether those findings would be valid in a clinical setting. While this is the ultimate objective of mechanistic *in vitro* studies, when there is lack of correspondence between the *in vitro* and clinical results, it is difficult to dissect what specific feature of the *in vitro* model needs to be

refined. In contrast, an *in vitro* model based on a preclinical species, e.g. mouse or rat, would allow iterative evaluation of the predictions of the *in vitro* model model in an appropriately designed *in vivo* model until the predictions of the *in vitro* model have been validated in the *in vivo* system. Refinement of the working *in vitro* model with input from a preclinically-derived *in vitro/ex vivo* model can provide better extrapolation to the clinic.

In this work, the Caco-2 cell model was used, in tandem with a secondary (preclinical *ex vivo*) model, in order to produce results that could be examined in the context of the current literature and also to facilitate data interpretation. While use of a chemical inhibitor was necessary to modulate P-gp activity in the Caco-2 cell model, appropriate controls were added to look for nonspecific effects. For example, the effect of GW918 on the metabolism of testosterone, a CYP3A probe substrate that is not a substrate of P-gp, was determined in order to ensure that GW918 does not inhibit CYP3A directly. In combination with a second model in which P-gp activity was modulated by genetic, rather than chemical, approaches, the results from the Caco-2 cell model were easier to evaluate, interpret and extrapolate to the clinical setting.

.

B.II. Diffusion Chamber Model

The P-gp-deficient mouse is a relevant model for studying the effect of P-gp efflux on metabolism. Since this model expresses no functional P-gp, the intestinal CYP3A-mediated metabolism of dual substrates can be compared between this strain and the P-gp competent strain to determine the effect of P-gp efflux on metabolism. However, using *in vivo* experiments to examine intestinal metabolism is very difficult in this small animal, since the portal vein or mesenteric artery must be cannulated in order to avoid the confounding effects of drug metabolism and transport in the liver. Therefore, fresh mouse intestinal tissue mounted in side-by-side diffusion (Ussing) chambers (Figure 2.1) provides a new *ex vivo* method for examining the metabolism/efflux interaction in a system that is closer to physiological conditions than cell lines. Since intestinal tissues remain metabolically active for at least 3 hours in Ussing chamber (van de Kerkhof et al., 2006), a sufficient amount of metabolites can be generated for LC-MS/MS detection using this model. Another important advantage of this system is that the results can be directly related to *in vivo* results in the same species (Collett et al., 2005). Information derived from this *in vitro-in vivo* correlation can then be used to further refine current *in vitro* models to more accurately reflect the *in vivo* situation.

There are some caveats to using the diffusion chamber model. First of all, unlike the Caco-2 cell system, this method is labor-intensive and therefore not amenable to high-throughput. Also, intestinal tissue in the side-by-side diffusion chamber system generally has about 10-fold higher paracellular permeability (assessed using mannitol) than the Caco-2 cell model. This may be due to the stretching of the

intestinal tissue, which could expose not only the villus tips, but also the crypt surface area for absorption. The villus tips have small pores (radius, <6 Å) while the less developed cells in the crypts have larger pores (50-60 Å) (Fihn et al., 2000). Due to the increased permeability, P-gp appears to have a decreased effect in Ussing chamber (Gotoh et al., 2005). These limitations must be kept in mind when using this model.

Species differences must also be recognized when using an animal model. The predominant CYP3A isoforms expressed in mouse intestine are CYP3A11, CYP3A13, CYP3A25 and CYP3A41. CYP3A13 has the highest expression; in duodenum, its expression even exceeds that in the liver (Martignoni et al., 2006). In addition to CYP3A, activities of CYP2E, CYP2D and CYP2C have been demonstrated in mouse intestinal microsomes (Emoto et al., 2000). Although the enzymes expressed in mouse generally mirror those in human intestine, it must be kept in mind that the expression patterns and substrate specificities of these enzymes can differ substantially between species.

Using two different models to examine the CYP3A/P-gp interaction allowed evaluation of each model relative to the other. Although the Caco-2 cell model exhibited a larger “P-gp effect” (efflux ratio) than the mouse model, it turned out to be less sensitive to the effect of P-gp on metabolism. Use of two different models also allowed closer examination of species differences between mouse and human. As discussed below, the results were not entirely consistent between the models

and the differences observed may be due to species differences, the properties of the compounds studied, and the sensitivity of the models themselves. However, the differences between models contributed to a better understanding of the interactions between P-gp and CYP3A.

B.III. Compounds

The Biopharmaceutical Classification System (BCS) was designed to help the FDA determine under what circumstances *in vitro* permeability studies could be used in lieu of clinical bioavailability studies to demonstrate bioequivalence for immediate-release dosage forms. This system categorizes drugs into four classes based on their solubility and permeability values (Amidon et al., 1995). Class I drugs (e.g., acetaminophen) have high solubility and high permeability; Class II drugs (e.g., indinavir) also have high permeability, but have low solubility; Class III drugs (e.g., atenolol) have low permeability and high solubility and Class IV drugs (e.g., furosemide), have low permeability and low solubility. Benet proposed that this classification of compounds based on their permeability and solubility also differentiates these compounds with respect to their likely interactions with uptake/efflux transporters, and even metabolic enzymes (Wu and Benet, 2005). Class I drugs are expected to enter the cells readily via passive diffusion, and could easily saturate efflux transporters and metabolic enzymes; thus, their absorption is not likely to be affected by efflux transporters or first-pass metabolism. Class II drugs enter the cells via passive diffusion, but might not achieve high membrane or

intracellular concentrations because of their low solubility. Hence, these compounds are often affected by efflux transporters, and are subject to first-pass metabolism. Class III and IV compounds, with their low permeability, are likely to be absorbed via absorptive transporters and are less likely to be affected by first-pass metabolism.

Two compounds, terfenadine and loperamide, were used in this work to study the interaction between P-gp and CYP3A. These compounds, besides being dual substrates for P-gp and CYP3A, belong to BCS Class II (high permeability, low solubility), and therefore efflux and metabolism in the intestine play a significant role in their absorption. Further, because of their high (passive) permeability, absorptive transporters are unlikely complicate interpretation of their transport behavior. In addition to their permeability and solubility properties, an important parameter that was used for their selection as test compounds was the sensitivity of their absorptive transport to P-gp-mediated efflux, as measured by the parameter AQ (Troutman and Thakker, 2003). AQ represents the degree to which the absorptive permeability of a compound is affected by P-gp efflux. The AQ value of loperamide is 0.6 and the AQ of terfenadine is 0.4; therefore, P-gp attenuates loperamide's absorptive transport by 60%, and terfenadine's transport by 40%. While compounds with greater separation of AQ values would have provided greater dynamic range to study the effect of P-gp on metabolism, compounds with their AQ values at extreme ends of the (0-1) range might have posed analytical challenges with respect to the measurement of the substrate and/or metabolites. Hence, for the first study of this kind, it was decided to use two compounds with medium but distinctly different extents of P-gp-mediated

attenuation in their absorptive transport. During the course of the project, it became clear that the metabolism of terfenadine is also different than loperamide metabolism in that terfenadine, but not loperamide, is metabolized by other enzymes besides CYP3A in mouse. Using compounds with different properties, such as AQ and the Michaelis-Menten parameters V_{max} and K_m, allowed for examination of the effect of these factors on the CYP3A/P-gp interaction.

Designing these studies required not only careful selection of compounds but also selection of appropriate dosing concentrations. One problem with assays that assess transporter/metabolism interplay is that they are generally conducted at only one dosing concentration (Cummins et al., 2002), which makes extrapolation to prediction of *in vivo* outcomes more difficult. Since both P-gp and CYP3A are saturable, the interaction between the proteins would be expected to be concentration-dependent. Therefore, all of the Caco-2 cell and diffusion chamber studies reported here were carried out over a broad range of substrate concentrations in order to determine the effect of concentration on experimental outcome. However, the range was limited at the lower end by the detection limit of the metabolites and at the upper end by both cellular toxicity and solubility of the compound. The compounds used were sparingly soluble in aqueous solution, so the maximum concentration used was about 100 µM. At the highest dosing concentrations, a larger standard deviation was observed for the metabolic data. This variability probably reflects the instability of the solution system (precipitation/crystallization) rather than variability in the interactions of the

compounds with their target proteins. While this variability imposed limitations on establishing clear statistical significance to the results obtained at the upper end of the concentration range, it added value by allowing the observation of the interactions between P-gp and CYP3A over a wide range of substrate concentrations.

C. Discussion of Results

C.I. Studies with the Caco-2 Cell Model

For both loperamide, there was a significant difference (two-way ANOVA) in the metabolic profiles in the presence and absence of P-gp inhibition. The metabolic rate increased when P-gp was inhibited by GW918. The increase in metabolic rate was relatively small at low concentrations, but became quite significant (>2-fold) in the 10-20 µM concentration range; this increase in metabolic rate was presumably caused by an increase in steady-state intracellular concentrations in the absence of P-gp. At concentrations approaching 40 µM, the rate of metabolism appeared to plateau, and at the same time the increase in metabolism due to inhibition of P-gp declined. This resulted in a two-fold higher apparent K_m in the presence of efflux. Nonlinear regression analysis showed this difference to be statistically significant, while there was no statistical difference in V_{max}, although the ability to accurately determine the V_{max} was limited due to increased variability at high dosing concentrations (presumably reflecting instability of compound in solution due to the

proximity to the solubility limit). These results clearly illustrate the value of examining the interactions between P-gp and CYP3A over a wide concentration range. Whether this interaction will be significant for loperamide in a clinical setting may depend on the dose; if the dose achieves cellular/membrane concentrations of 20-40 μM, the interactions could be significant.

A commonly used parameter for quantifying the transport/metabolism interaction in intestine is the ER (Equation 1). As shown in Figure 4.1, despite the higher rate of metabolism in the presence of P-gp inhibitor, the ER for loperamide decreased (30% for the 20 μM dose). This is because the amount of metabolite formed is normalized to the amount of parent crossing the cell monolayer, which always increases with P-gp inhibition regardless of changes in metabolic rate. Clearly extraction ratio, as it has been defined (Cummins et al., 2002), is not an ideal descriptor for quantifying the effect of P-gp on the rate or extent of metabolism of a compound. If it were used as such, it would indicate that metabolism of loperamide decreased when P-gp was inhibited, a conclusion that is contrary to the observed results. The reason why the use of ER as a parameter to describe the effect of P-gp on metabolism could be misleading is that the effect of P-gp on the permeability of the parent is embedded in the definition. Since the permeability of the parent is decreased by P-gp, the increase in metabolism is masked, and often this leads to the false conclusion that inhibition of P-gp results in a decrease in metabolism and therefore that P-gp causes an increase in metabolism. Therefore, it is inappropriate

to use the ER to interpret these results, since this would lead to erroneous conclusions.

Similar to the result for loperamide, the calculated ER values for terfenadine decreased in the presence of inhibitor; however, dissimilar to loperamide, the rates of metabolism were unchanged. There could be several reasons why the results observed for terfenadine in the Caco-2 cell model are different from those seen for loperamide. First of all, the difference in AQ between the two compounds (terfenadine AQ = 0.4; loperamide AQ = 0.6) suggests that the absorption of loperamide is affected more by P-gp efflux than is the absorption of terfenadine. That is, P-gp decreases the absorption of terfenadine and loperamide by 40% and 60%, respectively. Therefore, P-gp would be expected to have more of an effect on intracellular concentrations of loperamide than terfenadine, and therefore more of an effect on metabolism. Secondly, terfenadine (and also its metabolite fexofenadine) appears to be affected by other (possibly MRP family) transporters besides P-gp in the Caco-2 cell system. Therefore, treatment with P-gp inhibitor may not have been able to fully inhibit efflux of the compound. More importantly, based on the intrinsic metabolic parameters measured in human intestinal microsomes, the intrinsic metabolic clearance (V_{max}/K_m) of loperamide is about 10-fold higher than that for terfenadine in human. In addition, the expression of CYP3A in Caco-2 cells as a result of the 1α,25-dihydroxyvitamin D_3 treatment is rather modest, leading to lower intrinsic metabolic clearance. As illustrated in Figure 3.28, the effect of P-gp on metabolism would be expected to be dampened at lower intrinsic clearance values.

A combination of these factors is likely to be responsible for the lack of P-gp effect on CYP3A-mediated metabolism of terfenadine in the Caco-2 cell system.

C.II. Mouse Intestinal Model Results

Unlike the results seen in the Caco-2 cell model, in mouse intestine a statistical difference (using two-way ANOVA) in overall metabolic rate in the presence versus absence of P-gp efflux was seen for both terfenadine and loperamide. At low dosing concentrations, the rates of metabolism were not distinguishable between the strains due to the variability of the assay. However, in the dosing range near the K_m value for metabolism, the rates of metabolism were 2-3 fold higher in the absence of P-gp efflux, which supports the hypothesis that P-gp efflux decreases metabolism in the intestine (Tam et al., 2003). At higher concentrations, the effect was saturated and the metabolic rates were nearly equal for the two strains. A higher degree of variability was also observed in this region of the profile (near the solubility limit) due to instability of these compounds in aqueous solutions.

Based on studies using intestinal microsomes, the intrinsic metabolic clearances of loperamide and terfenadine are more similar in mouse than in Caco-2 cells, so Figure 3.28 would predict similar results for the two compounds. Indeed, a decrease in metabolic rate in the presence of P-gp efflux was observed for both compounds in the mouse model. When the curves were simultaneously fit for the

two strains of mice, the apparent K_m values were higher in the P-gp competent mice (about 5-fold higher for loperamide and 4-fold higher for terfenadine). These results imply that, while the intrinsic metabolic parameters are the same between the two strains of mice, the apparent K_m is inflated in the P-gp competent mice because the intracellular concentrations are reduced in the presence of P-gp efflux. Therefore, at intestinal concentrations close to the K_m, a higher dose of terfenadine would be required in the P-gp competent mouse to produce an equivalent concentration of drug at the enzyme site and the corresponding amount of metabolites.

For loperamide, the increase in K_m due to P-gp efflux was about 5-fold. This is much higher than the 2-fold increase seen in the Caco-2 cell system. This implies that the mouse model is more sensitive to the effect of P-gp efflux on metabolism than the Caco-2 cell model. This may be partly due to the higher intrinsic metabolic clearances of the tissues relative to the cell system. Since terfenadine showed a much higher metabolic clearance in mouse tissue relative to the Caco-2 cell model, this could further help to explain the different effects observed for terfenadine in the two models.

Differences in the results from the two model systems for terfenadine led to more mechanistic studies examining species differences in terfenadine metabolism. Studies using intestinal microsomes from mouse and human showed differences in the extent of metabolism (per mg protein) of probe substrates for several CYP enzymes. CYP3A activity was about 1.5-fold higher in mouse than in human, while

CYP2C9 activity was 3-fold higher in human than the activity of the analogous enzyme in mouse. The largest difference in activity was observed for CYP2D: the activity was about 25-fold higher in mouse than in human intestinal microsomes. Besides differences in metabolic capacity, other species differences between mouse and human were revealed through these experiments. While the metabolism of loperamide was similar in the two species, the K_m values for terfenadine varied substantially between species (Table 3.1). Further investigation revealed that terfenadine is metabolized primarily (~60%) by a member of the CYP2D family in mice. This may be due to the high relative level of activity of CYP2D in mouse intestine. This could help account for the different results observed between Caco-2 cells and mouse intestinal tissue for terfenadine, as terfenadine is metabolized only by CYP3A in Caco-2 cells, since this is the only isoform known to be induced by Vitamin D_3 treatment. Therefore, Caco-2 cells may have limited metabolic capacity for terfenadine relative to mouse tissue, leading to less of an effect of P-gp on metabolism in the Caco-2 cell model.

One of the key findings of this work is that concentration is an important consideration when examining the interactions between efflux and metabolism. Although a decrease in metabolism due to P-gp efflux was observed for loperamide in Caco-2 cells and mouse tissue as well as for terfenadine in mouse tissue, this effect was only seen within a narrow concentration range near the K_m value. At higher concentrations, such as those likely to be seen in the proximal intestine after oral dosing, this interplay may not have any effect on absorption. Therefore, the

anticipated concentration in the gut, relative to a drug's kinetic parameters, must be considered when determining the net effect of efflux and metabolism on a given substrate.

For example, the clinical dose prescribed for terfenadine was 60 mg. Assuming a volume of 250 ml in the gut, the calculated maximum concentration of terfenadine would be 500 µM. Therefore, terfenadine would likely be at a concentration near its solubility limit (~100 µM or higher, depending on the solubilizing effect of bile acids) in the intestine. According to the results reported here, the P-gp/CYP3A interaction would most likely be insignificant for terfenadine in intestine, since the process would always be saturated. Conversely, for loperamide, we may expect to see the interaction *in vivo*. The clinical dose of loperamide is only 2-4 mg, resulting in a predicted maximum concentration of only 33 µM *in vivo*. At this concentration level, the *in vitro* model presented here predicts an interaction between P-gp and CYP3A resulting in a decrease in metabolic rate. It should be kept in mind, however, that this crude method of calculating gut concentrations of compounds may not accurately reflect the concentration of the physiological microenvironment near the transporter or enzyme. Factors such as the unstirred water layer and mucous secretion may also influence the effective concentrations in the microenvironment.

When assessing this interaction for a given compound, the following three questions should be asked: 1) Is the compound a good substrate for P-gp? This

can be assessed *in vitro* using cellular models such as MDCK-MDR1 or Caco-2 cells. AQ should be determined to assess the effect of P-gp on the compound's absorption. 2) Does the compound have high metabolic clearance in intestine (does it have a high fraction metabolized)? Intestinal microsomes would be a good model to use in answering this question. 3) Is the compound poorly soluble or will it be administered at a low dose? Low-solubility and low-dose compounds would be much more likely to exhibit an interaction between P-gp and CYP3A *in vivo*: since concentrations at the transporter would be low, the effect of P-gp would be less likely to saturate. If the answer to all of these questions is "yes", then more study of the P-gp/CYP3A interaction may be warranted for the compound. Studies such as the ones described in this work would be appropriate if performed over a large concentration range. Of the two models used, mouse model seems to provide a more sensitive test for the interaction. However, more studies should be done in this area, using compounds with wider range of AQ values and kinetic parameters for metabolism, before a definitive *in vitro-in vivo* correlation model can be developed.

Ideally, compounds with a larger range of AQ (i.e., with a range of susceptibility to P-gp efflux) would have been used for these studies. Since AQ can have a value anywhere between 0 and 1, using substrates with very low and very high AQ values would provide the maximal dynamic range for these experiments. However, since no effect of P-gp efflux on CYP3A-mediated metabolism was observed for terfenadine (AQ~0.4) in the Caco-2 cell model, this AQ value may represent a cutoff at which no effect of the P-gp/ metabolism interaction is observed. In other words, a

substrate with a very low AQ would be marginally affected by P-gp efflux, so the effect of efflux on metabolism would likely be too low to detect. Conversely, compounds with very high AQ would be difficult to use for these studies, since the permeability would be so low that very little compound would reach the cellular and basolateral chambers, and therefore very little metabolite would be produced, leading to problems with analytical detection. As a result of these limitations, the range of AQ for the compounds selected for these studies was only 0.4-0.6, yet the differences observed in the results for these two compounds imply that this range was probably sufficient to differentiate between the effects of P-gp on CYP3A-mediated metabolism for compounds of differing AQ values. For future studies, additional compounds should be analyzed with a wider range of P-gp effect on absorption, physicochemical properties (solubility, permeability), and metabolic parameters (K_m, V_{max}) to define the interactions between P-gp and CYP3A-mediated metabolism more rigorously and under wider physiological conditions.

C.III. Pharmacokinetic Modeling Results

Due to the large overlap in substrate specificity between CYP3A and P-gp, some drug interactions previously attributed to CYP3A have been shown to be caused at least partially by intestinal P-gp, which can be a rate-limiting factor in absorption (Lown et al., 1997). Although metabolism and efflux are often separately assessed using *in vitro* models, these processes probably do not occur independently *in vivo*. Therefore, complex models, or a better understanding of the implications of data

generated using current models, may be needed to evaluate the drug-drug interaction potential of a given compound.

Here, pharmacokinetic modeling was used to more fully understand the *in vitro* results obtained for terfenadine and loperamide, and also to make predictions for compounds with different properties. A simple three-compartment pharmacokinetic model (Model A) was able to adequately describe the data generated from terfenadine metabolism in the Caco-2 cell system. Simulations were then carried out using this model in order to predict the effect of P-gp efflux on CYP3A metabolism under different conditions (i.e., for compounds with differing degrees of efflux and metabolism). While the experimental studies provide data on the activity of CYP3A in the presence and absence of P-gp efflux, modeling studies can predict the effect of varying degrees of P-gp activity on metabolic rate. The model predicted a decrease in the rate of metabolism with increasing P-gp efflux.

Simulations were also performed in order to determine the effect of changing P-gp or CYP3A expression levels. Since CYP3A is known to be expressed to a greater extent in the proximal intestine, while P-gp expression is higher in the distal regions, the effect of P-gp on CYP3A-mediated metabolism can vary throughout the intestine. The results from these simulations indicate that the effect of P-gp on metabolism would be expected to decrease in the distal areas of intestine as CYP3A expression decreases and P-gp expression increases.

Another finding revealed by these simulations was that, since P-gp modulates the metabolism distally, a change in V_{max} (such as that observed with noncompetitive inhibition) would have less of an effect on metabolic rate in this region. That is, the percent change in metabolism due to inhibition of the enzyme would be less than expected. In other words, P-gp may be able to effectively reduce the impact of inhibition when the mechanism is not competitive. Conversely, at lower values of V_{max}, the effect of P-gp efflux on metabolism would be predicted to be reduced. This is consistent with the difference in results observed for terfenadine and loperamide in the Caco-2 cell model, as was discussed earlier. According to the model, the lower intrinsic metabolic clearance for terfenadine translates into a reduced effect of P-gp on metabolism.

Finally, the different parameters used to quantify the interaction between CYP3A and P-gp in intestine were compared. The ER, a commonly used parameter for describing the P-gp/CYP3A interaction, increased with increased P-gp efflux, even though the metabolic rate and percentage of dose metabolized remained relatively constant. If these parameters were applied to the results for terfenadine in Caco-2 cells, there would be no change in percent metabolized with P-gp inhibition, but ER would decrease. This could lead to the conclusion that P-gp efflux increases the extent of terfenadine metabolism, but this is an artifact. The results of these simulations confirm that the use of ER to determine the nature of the interaction between P-gp and CYP3A may be misleading, as has been previously suggested (Johnson et al., 2003a; Knight et al., 2006). Therefore, caution should be used in

choosing parameters to quantify this interaction. The percent of dose metabolized (or rate of metabolism) seems like a more relevant value for quantifying this interaction, since the effect of P-gp efflux on absorption is not incorporated into this parameter.

Although Model A produced some interesting results, it should be recognized that this model may be oversimplified in that it assumes P-gp and CYP3A to be acting on the same (cytosolic) compartment. However, this is the most complex model that could be developed based on the data acquired. A second, more theoretical model (Model B) was written which incorporated an additional compartment (ostensibly representing the apical membrane) for P-gp efflux. Simulations of the effect of P-gp efflux on metabolic rate were carried out using this model, and the result was similar to those obtained with Model A. An increase in P-gp efflux resulted in a predicted decrease in metabolic rate, as was observed with Model A, but it also resulted in an increased lag time for metabolism. It appears that incorporation of a separate compartment for P-gp can increase the time it takes for the substrate to reach the CYP3A enzyme.

D. LITERATURE CONTEXT FOR FINDINGS OF THIS DISSERTATION RESEARCH

Several conflicting reports have been published that articulate the interaction between P-gp and CYP3A during intestinal absorption of dual substrates using different parameters; this has caused considerable confusion regarding the effect P-

gp-mediated efflux has on CYP3A-mediated metabolism. Pharmacokinetic theory predicts that P-gp efflux would decrease intracellular concentrations of parent drug, thereby decreasing metabolite formation. In spite of this, studies done in cellular models have led some researchers to the conclusion that P-gp efflux may enhance metabolism of substrates. This theory is primarily based on the observation that P-gp inhibition decreased the extraction ratio (ER) of substrates in cellular models. The ER has been defined as follows (Fisher et al., 1999):

$$ER = \frac{\sum M_{metabolites}}{\sum M_{metabolites} + M_{out}} \qquad \text{Equation 1}$$

Where $M_{metabolites}$ = mass of metabolites in the apical, cellular, and basolateral compartments and M_{out} = mass of parent in the basolateral chamber. Some researchers also include the mass of the parent within the cell in the calculation for M_{out} (Benet et al., 2004). However, as recently noted (Knight et al., 2006), this ratio by definition decreases in the presence of a P-gp inhibitor, since the denominator increases when P-gp inhibition increases the flux and intracellular concentrations of the parent drug. Therefore, changes in this parameter may not necessarily be indicative of changes in metabolic rate since the effect of P-gp on absorption is incorporated into the ER.

For example, Hochman, et al. reported that the extent of indinavir metabolism was not affected by inhibition of P-gp with cyclosporine A in the Caco-2 cell system. However, by using the ER (normalizing the amount of metabolite produced to the

amount of parent transported), the authors concluded that inhibition of P-gp efflux decreases metabolism (Hochman et al., 2000).

Also using the Caco-2 cell system, Cummins et al. reported that the ER for the cysteine protease inhibitor K77 decreased from 0.33 to 0.14 in the presence of P-gp inhibitor (Cummins et al., 2002). These results could possibly be explained by the fact that K77 has been shown to inhibit CYP3A with an IC50 of 60 nM (Jacobsen et al., 2000). When P-gp is inhibited, intracellular concentrations of drug would increase, causing inhibition of CYP3A and confounding the effect of P-gp on metabolism. However, examination of the data shows that the amount of metabolites produced actually increased slightly, so the percentage of dose metabolized increased. The use of ER in these studies led to the conclusion that P-gp increases the extent of metabolism, when in reality the amount of metabolites formed was lower in the presence of P-gp efflux. This illustrates the point that the rate of metabolism and percent metabolized are more relevant parameters for examining transport/metabolism interactions, since use of these parameters to interpret the data would lead to the appropriate conclusion that P-gp decreased the extent of metabolism. In a subsequent study, the same group showed that the ER of sirolimus decreased 25% in the presence of P-gp inhibitor (Cummins et al., 2004). The amount of metabolites produced was not reported, so the percentage of dose metabolized cannot be estimated.

Another group used the dual substrate saquinavir to study the interaction between P-gp and CYP3A (Mouly et al., 2004). Unlike the previously described studies, this study was done at multiple dosing concentrations to examine the effect of concentration on the interaction. The authors were able to show that the ER decreased with P-gp inhibition, but also decreased with increasing dose. This illustrates the importance of differentiating the linear from nonlinear range of metabolism when performing these studies. Since P-gp inhibition increases the amount of parent drug within the cell, at certain concentrations this could lead to saturation of the enzyme and a corresponding decrease in the ER.

In order to correctly interpret these types of results, the rate of metabolism must be considered in addition to the total mass of metabolite produced. As discussed earlier, the rate of metabolism and percent of dose metabolized are more relevant parameters than ER for examining the ultimate effect of efflux on metabolism. In Chapter 3, the effects of changes in P-gp efflux on ER and percent metabolized were compared through a simulation exercise. As can be seen in Figure 3.29, ER increases with an increase in P-gp activity, while percent metabolized only slightly decreases. Clearly, use of this metric (ER) to determine the effect of efflux on metabolism would be confounded by changes in parent disposition due to efflux itself. Therefore, the rates of metabolism and the percent of dose metabolized should be used instead of ER to interpret the results of these types of studies.

One of the theories about the interaction between efflux and metabolism suggests that P-gp efflux synergistically enhances metabolism through repeated cycles of drug entering the cell, being partially metabolized, and being effluxed back into the intestinal lumen. However, this “recycling hypothesis” is inconsistent with what is known about the mechanism of P-gp efflux. Since the active site of P-gp has been localized to the apical membrane, drug molecules need not enter the cytoplasm before being subject to efflux by P-gp (Figure 4.2). In fact, many of the substrates of P-gp are lipophilic in nature and are therefore likely to accumulate in the membrane. There is also further evidence for this mechanism. The fluorescent probe fura-2 acetoxymethyl ester (a P-gp substrate) is hydrolyzed by esterases to its free acid (a non-P-gp substrate) within cells. NIH-3T3 mouse fibroblasts expressing P-gp trapped less of the free acid than cells without P-gp, suggesting that the ester was able to be effluxed from the membrane before reaching the esterases within the cell (Homolya et al., 1993). Similarly, the Calcein-AM assay for P-gp activity (Figure 4.3) relies on the concept that hydrolyzed fluorescent compound is trapped in the cells to a lesser extent in the presence of P-gp efflux (Polli et al., 2001). If the compound were being “recycled” in and out of the cell, it would be more extensively converted to its hydrolyzed form, which is not a P-gp substrate.

Proponents of the theory that P-gp efflux enhances metabolism also assert that P-gp increases the ER by increasing the mean residence time (MRT) of the compound, therefore providing more opportunities for metabolism. However, extensive pharmacokinetic modeling done by Tam et al. showed that, although MRT

can be increased due to P-gp efflux, the rate of metabolism was still decreased under linear conditions (Tam et al., 2003). Under nonlinear conditions, however, there is a possibility for P-gp to increase metabolic rate by "desaturating" the enzyme; that is, by bringing the rate of metabolism back into the linear range. The data presented in this dissertation support the conclusions derived from those modeling studies but also provide experimental results to support the hypothesis that P-gp efflux decreases the rate of CYP3A metabolism of dual substrates in the intestine. The use of a wide range of dosing concentrations provides further insight into the *in vivo* relevance of this important interaction.

E. FUTURE STUDIES

E.1. Terfenadine Studies

Overall, the probable involvement of other transporters and drug metabolizing enzymes in the absorption of terfenadine makes interpretation of the data more difficult. For future studies, dual substrates should be more fully characterized (to rule out the involvement of transporters besides P-gp and metabolizing enzymes besides CYP3A) before being chosen for study of the P-gp/CYP3A intestinal interaction.

Due to the complexity of its metabolism and transport, there are several additional studies that could be designed based on the work done using terfenadine.

Although the disposition and metabolism of terfenadine have been described here in some detail, several questions remain regarding its behavior *in vivo*. For example, it is not clear whether terfenadine may be affected by other transporters besides P-gp. Since its uptake into Caco-2 cells was increased by treatment with the MRP inhibitor MK571, it seems likely that other apical efflux transporters are involved, possibly transporter(s) in the MRP family. In addition, the involvement of as yet unidentified transport proteins that are subject to inhibition by MK571 cannot be ruled out. The most common model used to clearly determine which transporters are affecting the compound is the singly-transfected MDCK cell system. The permeabilities (A-to-B and B-to-A) of the compound can be measured in cells which express a single transporter and can then be compared to the permeabilities of the parent cell line. Differences in the permeabilities can then be attributed to a specific transporter. These experiments could therefore be done using MDCK cells which express MRP2 on the apical membrane to determine whether MRP2 is important in the disposition of terfenadine.

The metabolism of terfenadine by multiple P450 isoforms in intestine is another interesting area of study. Until recently, terfenadine was thought to be strictly a CYP3A substrate. However, terfenadine has clearly been shown to be a substrate for CYP2J (Patten et al., 2003). Since CYP2J was relatively recently discovered, not much is known about its role in intestinal metabolism. However, since CYP2J is expressed in intestine (Zeldin et al., 1997), it seems likely that its effect could be quite significant for some compounds. Terfenadine has also been shown to be a

substrate of CYP4F12 (Patten et al., 2003) and CYP2D6 (Jones et al., 1998). In this work, about 60% of the metabolism of terfenadine in mouse intestine was found to be mediated by CYP2D (presumably by CYP2D22, the mouse analog of CYP2D6), while the remaining 40% was mediated by CYP3A. Although terfenadine is only used as a probe substrate, since it is no longer a marketed drug due to its cardiotoxicity, it could still be important to understand its properties if it is to be used for future mechanistic studies. More importantly, since CYP2D6 is polymorphic in humans, an interaction between P-gp and CYP2D6 could have implications for drug-drug interactions involving CYP2D6 substrates. In intestine, the activity of CYP2D in human appeared to be substantially lower than that for mouse, so CYP2D6 metabolism is not likely to be important in the first-pass intestinal metabolism of most compounds in humans. However, CYP2D6 is known to be highly expressed in the brain (Miksys et al., 2002). Since many CNS drugs (such as antidepressants) are metabolized by CYP2D6, perhaps there is even a possibility for interaction between drug transporters and CYP2D6 in the brain. This would be a very interesting area for future studies.

E.2. Studies with Different Dual Substrates

Another important study that could stem from this research is the investigation of the metabolism/efflux interaction using additional substrates. It would be desirable to choose CYP3A/P-gp dual substrates with different physicochemical or kinetic properties than those already examined. In this way, the effect of additional

parameters, such as passive permeability, on the metabolism/efflux interaction could be examined. It would be optimal to test compounds with a larger range of AQ values to determine the effect of varied P-gp influence on absorptive transport on the interaction, although, as discussed earlier, using compounds at the extremes of the range may not be practical. It may also be interesting to compare substrates from BCS Classes II and III to determine which is more affected by this interaction. It has been hypothesized that compounds in Class II would be more susceptible to these interactions (Wu and Benet, 2005); it would be interesting to test this hypothesis using the model systems described here. The data presented here indicate that the types of compounds likely to be affected by this interaction would be high clearance, low solubility compounds. If compounds with different properties were tested, the understanding of which properties affect the P-gp/CYP3A interaction would be expanded. Ultimately, a model could be developed for prediction of the effect of this interaction on the disposition of new compounds.

E.3. *In vivo* Studies

Although *in vitro* data reveal important mechanistic information, they are basically derived from a static system. The same types of studies performed here could be implemented in a whole organism, since it is a more dynamic system. Therefore, the next step in testing the hypotheses presented here would studies in an appropriate *in vivo* model. This would allow determination of the *in vivo* relevance of the *in vitro* results and would facilitate development of an *in vitro/in vivo* correlation.

This data could then be used to validate and refine current in vitro models. If this information were gathered for several compounds, a model could begin to be developed for prediction of the *in vivo* effect of the P-gp/CYP3A interaction on the disposition of other compounds based on *in vitro* data alone. *In situ* intestinal perfusion using P-gp-deficient and P-gp-competent mice would reveal whether the metabolism/efflux interaction is important *in vivo*. Animals deficient in other transport proteins could also be used to study interactions between efflux and metabolism. For example, an mrp2 deficient mouse is available that could be used to study the relationship between glucuronidation and mrp2 efflux. This information would be very useful for extrapolating *in vitro* results to predictions of the effect of the interaction in humans.

A few *in situ* intestinal perfusion studies have been done in this area using rats and chemical modulation of P-gp. Cummins et al. measured the metabolism of K77 in the presence and absence of P-gp inhibitor GW918. Inhibition of P-gp caused a marked increase in the amount of metabolite produced over time, so the percentage of dose metabolized increased. While they reported a decrease in the ER with P-gp inhibition (from 0.60 to 0.49), this change was not statistically significant (Cummins et al., 2003). Another group used the dual substrate verapamil to conduct a similar study. They also reported an increase in the amount of metabolites formed in the presence of P-gp inhibitor, yet the ER decreased by 15% (Johnson et al., 2003b). In each case, the conclusions drawn depend on the method of interpretation of the data. The ER value includes the effect of P-gp inhibition (increased absorption) in

the equation and therefore cannot be used to assess the effect of P-gp efflux on metabolism alone. Instead, rate of metabolism or the percent metabolized should be used to assess the effect of transport/metabolism interplay.

Determining the clinical significance of the metabolism/efflux interaction is, of course, the ultimate goal of this work. So, could a clinical study be designed to address the hypotheses detailed here? If so, a relatively innocuous P-gp inhibitor and CYP3A/P-gp dual substrate would be needed for study in humans. As with the rodent studies, a perfusion technique would be employed, similar to that used by Lennernas, et al. (Lennernas, 1997), to compare the metabolism of a dual substrate in the presence versus absence of P-gp inhibitor. Systemic concentrations of metabolite could not be used to assess metabolism due to the confounding effects of the liver. Therefore, blood would have to be collected before it enters the liver. However, it would probably not be feasible to collect samples from the portal vein or mesenteric artery in humans, so disappearance of parent would probably have to be used as a measure of metabolism. Of course, parent disappearance is a function of absorption, efflux and metabolism, so this method may not be effective for studying the interaction between these factors.

Metabolite formation could also be measured, but only within the lumen. This is also problematic since, as shown in this work, metabolite disposition can change with P-gp inhibition. For example, we noticed that fexofenadine is primarily secreted into the apical compartment when P-gp is active, but when P-gp is inhibited,

fexofenadine localizes to the basolateral compartment. If only the apical compartment were being sampled, the decrease in fexofenadine in the presence of inhibitor may be misinterpreted as a decrease in metabolic rate due to P-gp inhibition. Since it is not possible to sample all three compartments (apical, basolateral, and tissue), designing a clinical study to examine this issue is probably not feasible at this time. Therefore, we must rely on studies in rodents and *in vitro* systems to provide information about the effect of P-gp efflux and metabolism *in vivo*.

F. SUMMARY

The interplay between P-gp efflux and CYP3A metabolism in intestine is an important area of research. Most studies in this area have used the Caco-2 cell model at a single dosing concentration and the results have been interpreted using ER as a measure of the effect of P-gp on the extent of metabolism. In this work, a second model has been used in addition to the Caco-2 cell model: metabolism of dual P-gp/CYP3A substrates was assessed in intestinal tissue from mice genetically deficient in P-gp and compared to that in normal mouse intestine. Combination of these two models enabled better assessment of the results from each system. Using the rates of drug metabolism as a measure of the effect of P-gp, these studies were able to show that P-gp efflux could reduce the rate of metabolism of the dual substrate loperamide in both models and for terfenadine in the mouse model.

In order to help predict the effect of the transport/metabolism interaction at expected *in vivo* concentrations, a wide range of dosing concentrations was used for these studies. This strategy revealed that the P-gp/CYP3A interaction is limited to a concentration range near the K_m of metabolism for both substrates used. Combination of these results with pharmacokinetic modeling facilitated prediction of the effect of P-gp on intestinal metabolism of these substrates at physiologically relevant drug concentrations. Further studies are planned to examine this interaction for dual P-gp/CYP3A substrates with different properties that are expected to influence the P-gp/CYP3A interplay.

G. REFERENCES

Achira M, Suzuki H, Ito K and Sugiyama Y (1999) Comparative studies to determine the selective inhibitors for P-glycoprotein and cytochrome P4503A4. *AAPS PharmSci* **1**:E18.

Allen JD, Brinkhuis RF, Wijnholds J and Schinkel AH (1999) The mouse Bcrp1/Mxr/Abcp gene: amplification and overexpression in cell lines selected for resistance to topotecan, mitoxantrone, or doxorubicin. *Cancer Res* **59**:4237-4241.

Amidon GL, Lennernas H, Shah VP and Crison JR (1995) A theoretical basis for a biopharmaceutic drug classification: the correlation of in vitro drug product dissolution and in vivo bioavailability. *Pharm Res* **12**:413-420.

Bu HZ (2006) A literature review of enzyme kinetic parameters for CYP3A4-mediated metabolic reactions of 113 drugs in human liver microsomes: structure-kinetics relationship assessment. *Curr Drug Metab* **7**:231-249.

Clarke SE (1998) In vitro assessment of human cytochrome P450. *Xenobiotica* **28**:1167-1202.

Collett A, Tanianis-Hughes J, Carlson GL, Harwood MD and Warhurst G (2005) Comparison of P-glycoprotein-mediated drug-digoxin interactions in Caco-2 with human and rodent intestine: Relevance to in vivo prediction, in *Eur J Pharm Sci*.

Cummins CL, Jacobsen W and Benet LZ (2002) Unmasking the dynamic interplay between intestinal P-glycoprotein and CYP3A4. *J Pharmacol Exp Ther* **300**:1036-1045.

Cummins CL, Jacobsen W, Christians U and Benet LZ (2004) CYP3A4-transfected Caco-2 cells as a tool for understanding biochemical absorption barriers: studies with sirolimus and midazolam. *J Pharmacol Exp Ther* **308**:143-155.

Cummins CL, Salphati L, Reid MJ and Benet LZ (2003) In vivo modulation of intestinal CYP3A metabolism by P-glycoprotein: studies using the rat single-pass intestinal perfusion model. *J Pharmacol Exp Ther* **305**:306-314.

Emoto C, Yamazaki H, Yamasaki S, Shimada N, Nakajima M and Yokoi T (2000) Characterization of cytochrome P450 enzymes involved in drug oxidations in mouse intestinal microsomes. *Xenobiotica* **30**:943-953.

Endres CJ, Hsiao P, Chung FS and Unadkat JD (2006) The role of transporters in drug interactions. *Eur J Pharm Sci* **27**:501-517.

Fihn BM, Sjoqvist A and Jodal M (2000) Permeability of the rat small intestinal epithelium along the villus-crypt axis: effects of glucose transport. *Gastroenterology* **119**:1029-1036.

Fisher JM, Wrighton SA, Watkins PB, Schmiedlin-Ren P, Calamia JC, Shen DD, Kunze KL and Thummel KE (1999) First-pass midazolam metabolism catalyzed by 1alpha,25-dihydroxy vitamin D3-modified Caco-2 cell monolayers, in *J Pharmacol Exp Ther* pp 1134-1142.

Gotoh Y, Kamada N and Momose D (2005) The advantages of the Ussing chamber in drug absorption studies. *J Biomol Screen* **10**:517-523.

Hochman JH, Chiba M, Nishime J, Yamazaki M and Lin JH (2000) Influence of P-glycoprotein on the transport and metabolism of indinavir in Caco-2 cells expressing cytochrome P-450 3A4. *J Pharmacol Exp Ther* **292**:310-318.

Hoffmaster KA, Zamek-Gliszczynski MJ, Pollack GM and Brouwer KL (2004) Hepatobiliary Disposition of the Metabolically Stable Opioid Peptide [D-penicillamine2,5]enkephalin (DPDPE): Pharmacokinetic Consequences of the Interplay Between Multiple Transport Systems. *J Pharmacol Exp Ther*.

Homolya L, Hollo Z, Germann UA, Pastan I, Gottesman MM and Sarkadi B (1993) Fluorescent cellular indicators are extruded by the multidrug resistance protein. *J Biol Chem* **268**:21493-21496.

Hyafil F, Vergely C, Du Vignaud P and Grand-Perret T (1993) In vitro and in vivo reversal of multidrug resistance by GF120918, an acridonecarboxamide derivative. *Cancer Res* **53**:4595-4602.

Jacobsen W, Christians U and Benet LZ (2000) In vitro evaluation of the disposition of A novel cysteine protease inhibitor. *Drug Metab Dispos* **28**:1343-1351.

Johnson BM, Charman WN and Porter CJ (2003a) Application of compartmental modeling to an examination of in vitro intestinal permeability data: assessing the impact of tissue uptake, P-glycoprotein, and CYP3A. *Drug Metab Dispos* **31**:1151-1160.

Johnson BM, Chen W, Borchardt RT, Charman WN and Porter CJ (2003b) A kinetic evaluation of the absorption, efflux, and metabolism of verapamil in the autoperfused rat jejunum. *J.Pharmacol Exp Ther* **305**:151-158.

Jones BC, Hyland R, Ackland M, Tyman CA and Smith DA (1998) Interaction of terfenadine and its primary metabolites with cytochrome P450 2D6. *Drug Metab Dispos* **26**:875-882.

Kolars JC, Awni WM, Merion RM and Watkins PB (1991) First-pass metabolism of cyclosporin by the gut. *Lancet* **338**:1488-1490.

Knight B, Troutman M and Thakker DR (2006) Deconvoluting the effects of P-glycoprotein on intestinal CYP3A: a major challenge. *Curr Opin Pharmacol* **6**:528-532.

Kristensen MB (1976) Drug interactions and clinical pharmacokinetics. *Clin Pharmacokinet* **1**:351-372.

Lennernas H (1997) Human jejunal effective permeability and its correlation with preclinical drug absorption models. *J Pharm Pharmacol* **49**:627-638.

Lown KS, Mayo RR, Leichtman AB, Hsiao HL, Turgeon DK, Schmiedlin-Ren P, Brown MB, Guo W, Rossi SJ, Benet LZ and Watkins PB (1997) Role of intestinal P-glycoprotein (mdr1) in interpatient variation in the oral bioavailability of cyclosporine, in *Clin Pharmacol Ther* pp 248-260.

Madani S, Paine MF, Lewis L, Thummel KE and Shen DD (1999) Comparison of CYP2D6 content and metoprolol oxidation between microsomes isolated from human livers and small intestines. *Pharm Res* **16**:1199-1205.

Martignoni M, Groothuis G and de Kanter R (2006) Comparison of mouse and rat cytochrome P450-mediated metabolism in liver and intestine. *Drug Metab Dispos* **34**:1047-1054.

Miksys S, Rao Y, Hoffmann E, Mash DC and Tyndale RF (2002) Regional and cellular expression of CYP2D6 in human brain: higher levels in alcoholics. *J Neurochem* **82**:1376-1387.

Mouly SJ, Paine MF and Watkins PB (2004) Contributions of CYP3A4, P-glycoprotein, and serum protein binding to the intestinal first-pass extraction of saquinavir. *J Pharmacol Exp Ther* **308**:941-948.

Paine MF, Khalighi M, Fisher JM, Shen DD, Kunze KL, Marsh CL, Perkins JD and Thummel KE (1997) Characterization of interintestinal and intraintestinal variations in human CYP3A-dependent metabolism. *J Pharmacol Exp Ther* **283**:1552-1562.

Patten C, Gagne P, Miller V, Crespi C and Thummel K (2003) Terfenadine Hydroxylation by Recombinant CYP2J2 and 4F12. *Drug Metab Rev* **35**:121.

Polli JW, Wring SA, Humphreys JE, Huang L, Morgan JB, Webster LO and Serabjit-Singh CS (2001) Rational use of in vitro P-glycoprotein assays in drug discovery. *J Pharmacol Exp Ther* **299**:620-628.

Raeissi SD, Hidalgo IJ, Segura-Aguilar J and Artursson P (1999) Interplay between CYP3A-mediated metabolism and polarized efflux of terfenadine and its metabolites in intestinal epithelial Caco-2 (TC7) cell monolayers. *Pharm Res* **16**:625-632.

Schmiedlin-Ren P, Thummel KE, Fisher JM, Paine MF and Watkins PB (2001) Induction of CYP3A4 by 1 alpha,25-dihydroxyvitamin D3 is human cell line-specific and is unlikely to involve pregnane X receptor. *Drug Metab Dispos* **29**:1446-1453.

Shimada T, Yamazaki H, Mimura M, Inui Y and Guengerich FP (1994) Interindividual variations in human liver cytochrome P-450 enzymes involved in the oxidation of drugs, carcinogens and toxic chemicals: studies with liver microsomes of 30 Japanese and 30 Caucasians. *J Pharmacol Exp Ther* **270**:414-423.

Tam D, Sun H and Pang KS (2003) Influence of P-glycoprotein, transfer clearances, and drug binding on intestinal metabolism in Caco-2 cell monolayers or membrane preparations: a theoretical analysis. *Drug Metab Dispos* **31**:1214-1226.

van de Kerkhof EG, Ungell AL, Sjoberg AK, de Jager MH, Hilgendorf C, de Graaf IA and Groothuis GM (2006) Innovative methods to study human intestinal drug metabolism in vitro: precision-cut slices compared with ussing chamber preparations. *Drug Metab Dispos* **34**:1893-1902.

Wu CY and Benet LZ (2005) Predicting drug disposition via application of BCS: transport/absorption/ elimination interplay and development of a biopharmaceutics drug disposition classification system. *Pharm Res* **22**:11-23.

Zeldin DC, Foley J, Goldsworthy SM, Cook ME, Boyle JE, Ma J, Moomaw CR, Tomer KB, Steenbergen C and Wu S (1997) CYP2J subfamily CYPs in the gastrointestinal tract: expression, localization, and potential functional significance. *Mol Pharmacol* **51**:931-943.

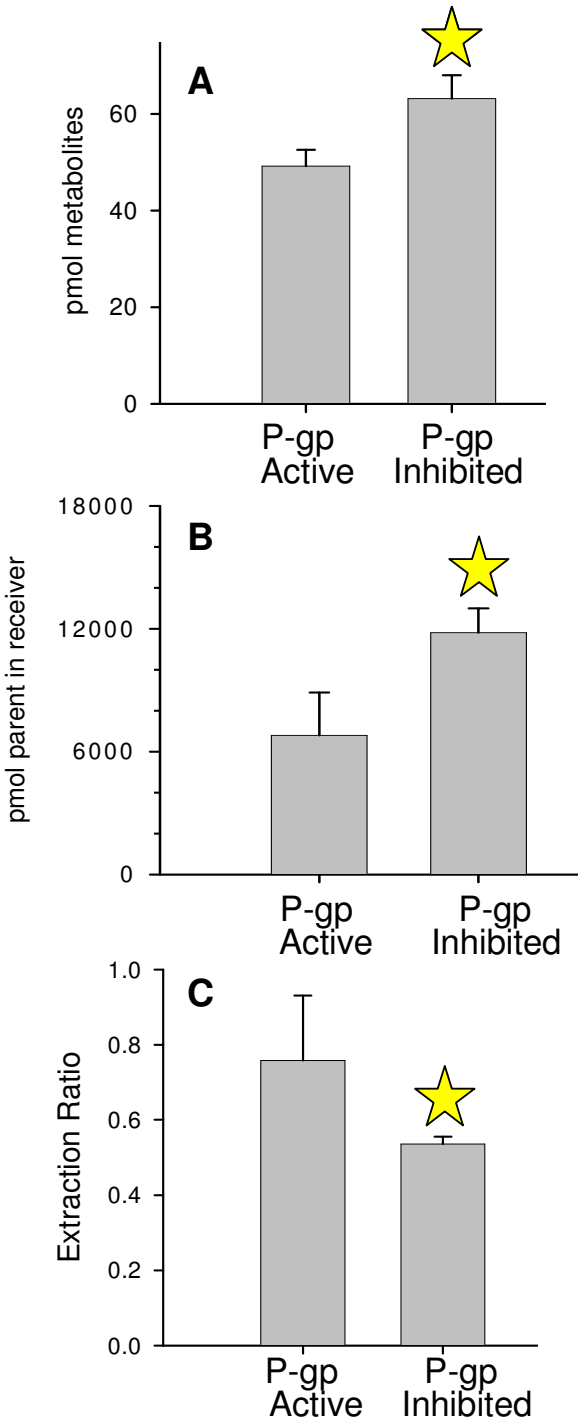

Figure 4.1. Comparison of metabolite formation (A), parent in receiver (B), and extraction ratio of loperamide (20 µM dose) (C) in Caco-2 cell monolayers.
n=3; error bars = SD. Stars indicate statistical significance (students' t-test; $p<0.05$).

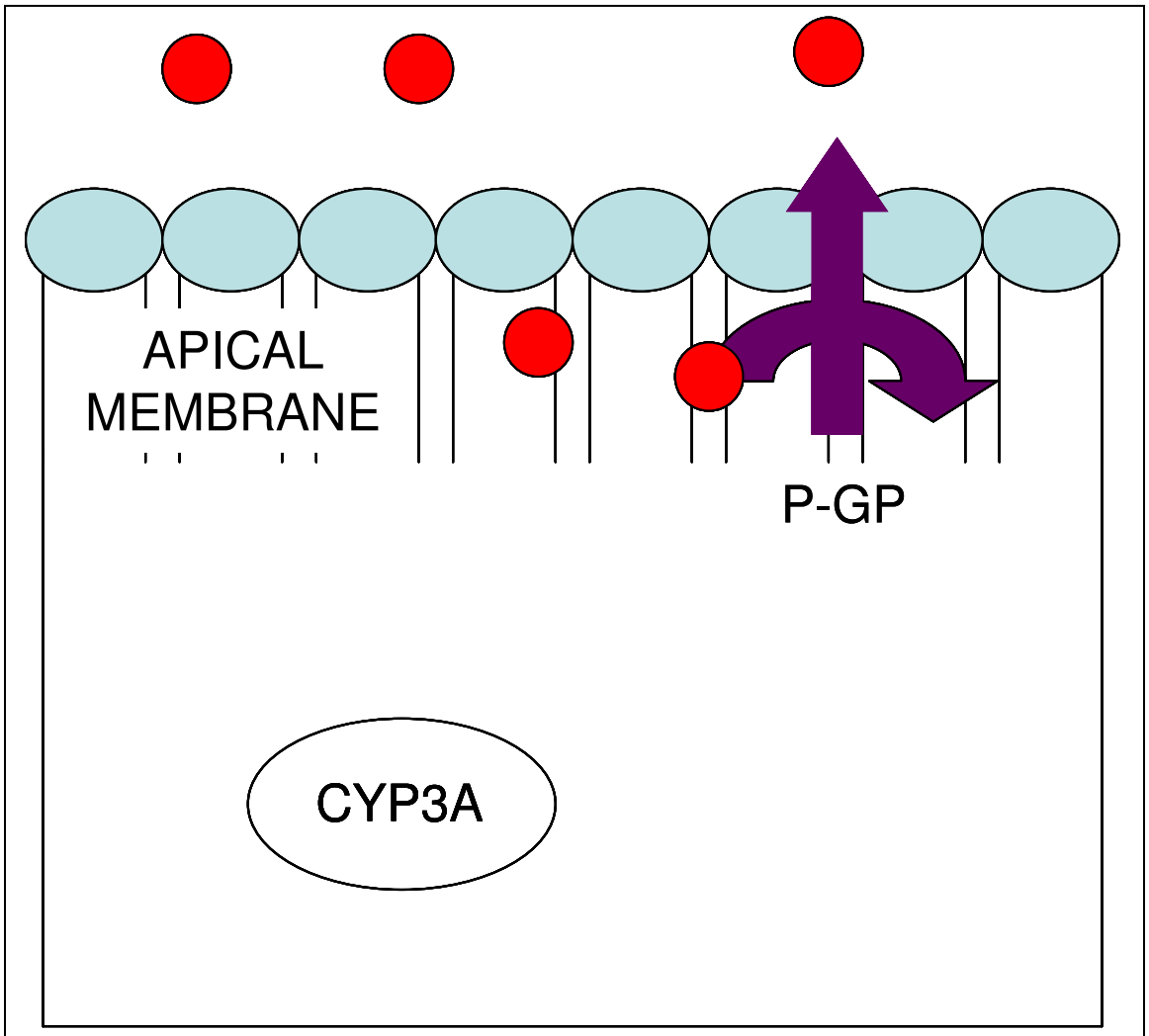

Figure 4.2. Proposed mechanism of P-gp activity: P-gp prevents drug from entering the cell by interacting with substrates within the apical membrane, while CYP3A acts inside the cell in the endoplasmic reticulum.

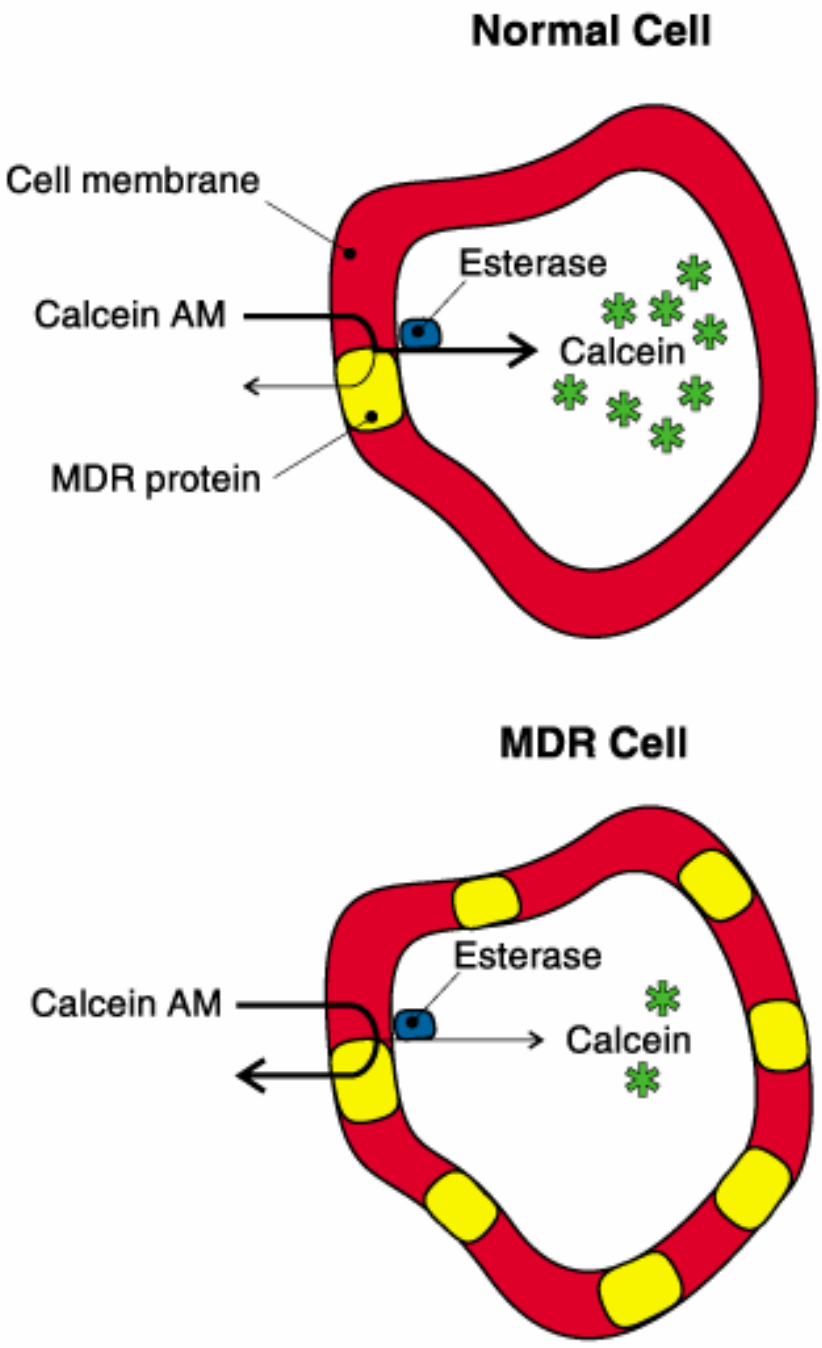

Figure 4.3. Calcein AM assay for P-gp activity. Normal cell lacks P-gp efflux; MDR cell expresses P-gp. Calcein AM is a P-gp substrate, while the esterase product calcein is not, so P-gp expressing cells accumulate less calcein, which is detected by fluorescence. (www.invitrogen.com)

Appendix I: Involvement of Multidrug Resistance-associated Proteins in Intestinal Transport of the Antiallergic Drug Fexofenadine

Xin Ming, Beverly Knight and Dhiren R. Thakker

AAPS, 2006

A. ABSTRACT

Purpose

Both apical and basolateral efflux of fexofenadine appears to be mediated by MRPs. The purpose of this study is to elucidate the role of MRPs, expressed in the apical and basolateral membranes, in the absorptive transport of fexofenadine across Caco-2 cells.

Methods

For the cellular efflux studies, Caco-2 cell monolayers were first incubated with fexofenadine on both apical and basolateral sides for 1 hour in the absence and presence of GW918 (P-gp inhibitor) and/or MK-571 (MRP inhibitor). The cells were then washed and transferred to fresh medium to measure the efflux of fexofenadine over a 2-minute period into both sides in the absence and presence of inhibitors. For the transport study, Caco-2 cell monolayers were first incubated with transport buffer with or without inhibitors for 30 minutes; the absorptive and secretory transport was performed by adding fexofenadine into the donor reservoir and measuring the transported compound in the receiver compartment. Terfenadine, the parent drug of fexofenadine, was dosed to Caco-2 cells which expressed functional CYP3A and the distribution of fexofenadine, formed inside the cells, to basolateral and apical sides was measured over 120 minutes in the presence and absence of GW918.

Results

GW918 and MK-571 stimulated the accumulation of fexofenadine into Caco-2 cells by 4 and 2-fold, respectively, when cells were exposed to fexofenadine from both apical and basolateral sides. Fexofenadine accumulated in cells was preferentially transported out of the cells across the apical membrane. When P-gp was inhibited, fexofenadine was effluxed primarily to the basolateral side. MK-571 inhibited the efflux of cellular fexofenadine across the apical and basolateral membranes by 40% and 50%, respectively. MK-571 decreased the absorptive transport rate slightly; however, it increased the secretory transport rate by 30%. When fexofenadine was formed from terfenadine metabolism in CYP3A-expressing cells, it was primarily effluxed to the apical side; however, in the presence of GW918, most of the compound was transported to the basolateral side.

Conclusions

The present study suggests that the MRP(s) and P-gp in the apical membrane may attenuate the absorptive transport by efflux of fexofenadine into GI lumen, whereas the MRP(s) in the basolateral membrane facilitates the absorption by causing egress of fexofenadine from the enterocytes to the serosal side.

B. INTRODUCTION

Both apical (AP) and basolateral (BL) efflux of fexofenadine appear to be mediated by multidrug resistant associated proteins (MRPs) in addition to the apical efflux mediated by P-glycoprotein (P-gp). The purpose of this study was to elucidate the roles of these transporters in the transport of fexofenadine in Caco-2 cells.

Intestinal absorptive transport involves entry into the enterocytes across the apical membrane from the GI lumen and exit from the cells across the basolateral membrane. Depending on their relative efficiency and capacity, an uptake transporter in the apical membrane or an efflux transporter in the BL membrane can become rate-limiting for transepithelial movement (Cheeseman, 1992). However, compared with the clear roles of apical transporters in the transcellular transport process, it is still unclear whether BL transporters play an important role in intestinal transport.

Fexofenadine has been used as a suitable probe to investigate carrier mediated transport processes due to its low passive permeability and relatively low extent of metabolism (Petri et al., 2004). In the apical membrane of enterocytes, organic anion transporting polypeptide 1A2 (OATP1A2) mediates the uptake process of fexofenadine into enterocytes (Cvetkovic et al., 1999). Fexofenadine is also a good substrate of the apical efflux transporter P-gp (Cvetkovic et al., 1999); several clinical reports have suggested that intestinal P-gp was the main site for drug-drug

interaction (Yasui-Furukori et al., 2005; Shimizu et al., 2006). However, it is still unclear whether the BL egress of fexofenadine is a transporter mediated process, and whether MRPs are involved in the intestinal transport of fexofenadine (Figure I.1).

In this study, we first studied the distribution of fexofenadine which was formed by terfenadine metabolism in CYP3A-expressing Caco-2 cells with or without inhibition of P-gp. Then, the efflux of fexofenadine after preloading was examined to evaluate the possible role of MRPs. Finally, absorptive and secretory transport were studied to assess the significance of these transporters in the transport of fexofenadine in Caco-2 cells.

C. METHODS

C.1. Cell Culture

Caco-2 cells were cultured at 37°C in MEM, supplemented with 10% FBS, 1% NEAA, 1% antibiotic-antimycotic solution in an atmosphere of 5% CO_2. Caco-2 cells were seeded at a density of 60,000 cells/cm^2 on Transwell™ filters. Medium was changed the day after seeding, and every other day thereafter. The cells were cultured for 21-25 days before use.

To induce CYP3A activity, the Caco-2 cells were seeded onto laminin-coated culture inserts at a density of 500,000 cell/cm^2. After reaching confluence, the cell cultures were maintained in DMEM including 1α,25-$(OH)_2$-D_3 (0.5 μM) for 14 days.

C.2. Accumulation and Efflux studies

Caco-2 cell monolayers were incubated for 1 hour with 100 μM fexofenadine in both AP and BL sides in the absence or presence of inhibitors. After washing both sides 3 times with cold transport buffer (HBSS containing HEPES and glucose), efflux was determined over 2 minutes in the absence or presence of inhibitors. Then monolayers were dissolved in 300 μl 1% Triton X-100 for 4 hr with shaking and the solution was extracted with 1 ml ethyl acetate. The organic phase was evaporated to dryness under nitrogen gas, and the residue was reconstituted with 200 μl 25% methanol. The samples were analyzed by LC-MS/MS with cetirizine as internal standard.

C.3. Transport Study

Caco-2 cell monolayers were incubated for 30 min with transport buffer. Transport studies were initiated by replacing the donor chamber with 10 μM fexofenadine in the absence or presence of inhibitors. The receptor chamber was sampled at selected times and analytes were quantified by LC-MS/MS.

C.4. Distribution of Fexofenadine Formed from Terfenadine

Terfenadine, the parent drug of fexofenadine, was dosed at 20 μM to Caco-2 cells which expressed functional CYP3A; the distribution of fexofenadine, formed inside the cells, to BL and AP sides was measured over 120 minutes in the presence and absence of 1 μM GW918.

C.5. Data Analysis

Data were expressed as mean ± S.D. from three measurements. Statistical significance was evaluated using unpaired *t* tests or ANOVA followed by Tukey's test for multiple comparisons. The apparent permeability coefficient was calculated according to the following equation: $$P_{app} = \frac{1}{A \times C_o} \times \frac{dQ}{dt}$$

where dQ/dt is the flux across the cell monolayers with the surface area of A. C_0 is the initial dose concentration.

D. Results and Discussion

When fexofenadine was formed from terfenadine metabolism in CYP3A-expressing cells, it was primarily effluxed to the AP side; however, in the presence of GW918 (1 μM), most of the compound appeared in the BL side (Figure I.2). These results reveal the presence of an efflux transporter for fexofenadine in the BL membrane. GW918 (1 μM) and MK-571 (25 μM) stimulated the accumulation of fexofenadine into Caco-2 cells by 4 and 2-fold, respectively, when cells were exposed from both sides (Figure I.3). These results suggest the involvement of MRP, in addition to P-gp, in fexofenadine efflux from Caco-2 cells.

MK-571 (25 μM) inhibited the efflux of cellular fexofenadine across the AP and BL membranes by 40% (Figure I.4) and 50% (Figure I.5), respectively, indicating the involvement of MRPs in both AP and BL efflux of fexofenadine from Caco-2 cells. After preloading, fexofenadine was preferentially transported out of the cells across the AP membrane by 2-fold (Figure I.4). When P-gp was inhibited, efflux to the BL side was preferred by 1.5-fold (Figure I.5).

GW918 nearly completely inhibited apical efflux, indicating the strong effect of P-gp (Figure I.4). Surprisingly, GW918 also inhibited basolateral efflux of fexofenadine (Figure I.5). This may be indirectly caused by the high intracellular concentration attained after preloading with GW918. MK-571 at 25 μM slightly decreased the absorptive transport (Figure I.6). When P-gp was inhibited, further treatment with

MK-571 decreased the transport rate by 25% (Figure I.6). MK571 alone increased the secretory transport rate by 30 % (Figure I.7).

E. CONCLUSIONS

The present study suggests that fexofenadine appears to be a substrate for MRP(s) in AP membrane and MRP(s) in BL membrane of human intestine. Based on known cellular distribution of MRPs in intestine, MRP2 and MRP3 may be the candidate transporters in AP and BL membrane, respectively.

Although MRP2 may also be a player, P-gp appears to dominate apical efflux of fexofenadine. MRP(s) in BL membrane limit secretory transport and could facilitate absorption by causing egress of fexofenadine from the enterocytes to the serosal side, but the one(s) in AP membrane may counteract the BL transporter by mediating AP egress. Specific siRNA knockdown is desired to evaluate the relative contribution of individual MRPs.

F. REFERENCES

Cheeseman C (1992) Role of intestinal basolateral membrane in absorption of nutrients. *Am J Physiol* **263**:R482-488.

Cvetkovic M, Leake B, Fromm MF, Wilkinson GR and Kim RB (1999) OATP and P-glycoprotein transporters mediate the cellular uptake and excretion of fexofenadine. *Drug Metab Dispos* **27**:866-871.

Petri N, Tannergren C, Rungstad D and Lennernas H (2004) Transport characteristics of fexofenadine in the Caco-2 cell model. *Pharm Res* **21**:1398-1404.

Shimizu M, Uno T, Sugawara K and Tateishi T (2006) Effects of itraconazole and diltiazem on the pharmacokinetics of fexofenadine, a substrate of P-glycoprotein. *Br J Clin Pharmacol* **61**:538-544.

Yasui-Furukori N, Uno T, Sugawara K and Tateishi T (2005) Different effects of three transporting inhibitors, verapamil, cimetidine, and probenecid, on fexofenadine pharmacokinetics. *Clin Pharmacol Ther* **77**:17-23.

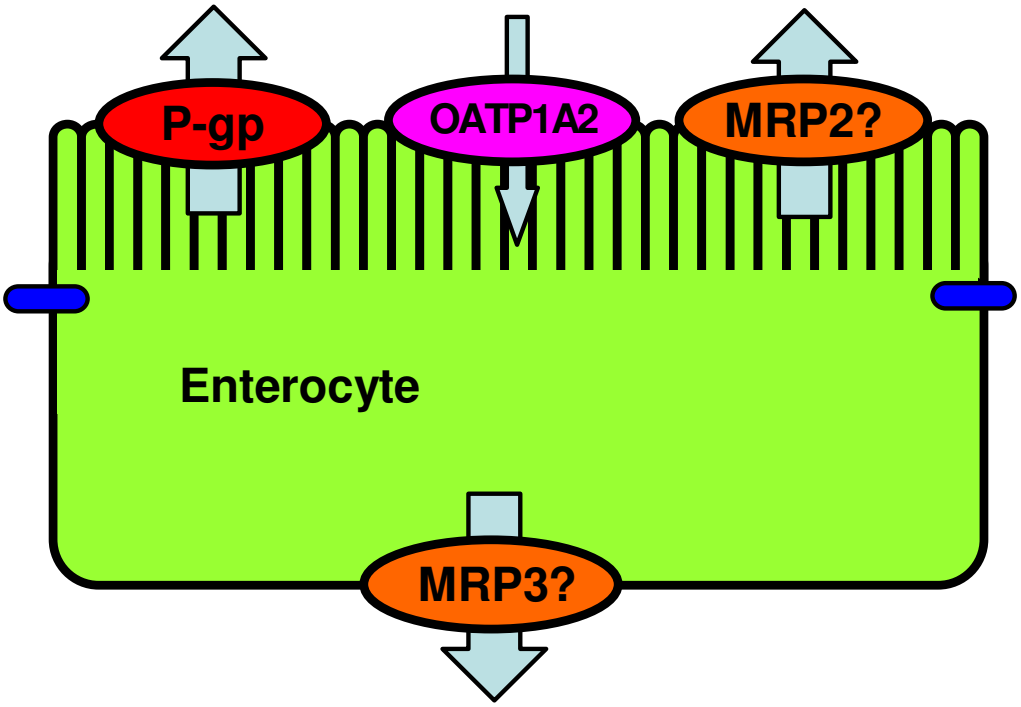

Figure I.1. Model for intestinal transport of fexofenadine

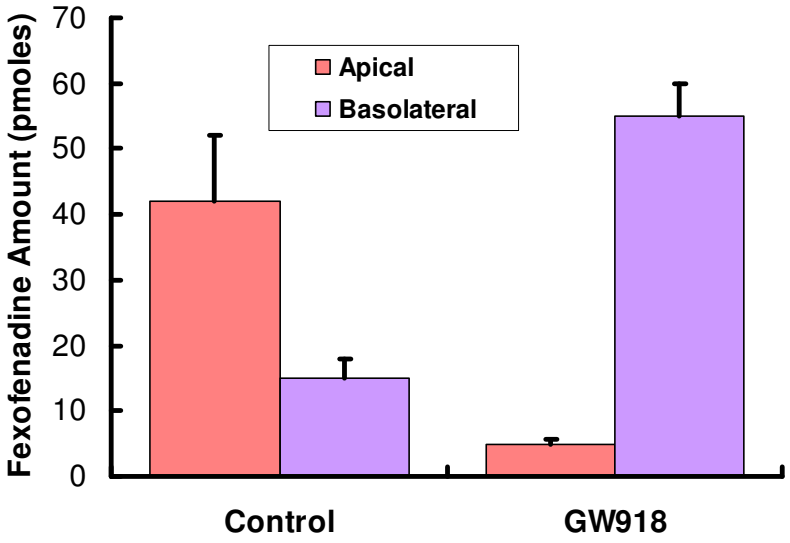

Figure I.2. Disposition of fexofenadine during absorptive transport of terfenadine across Caco-2 cells. Mean of 3 ± SD. A statistical difference was observed between appearance of fexofenadine in apical and basolateral chambers, under treated and untreated conditions ($p<0.05$, student's t-test).

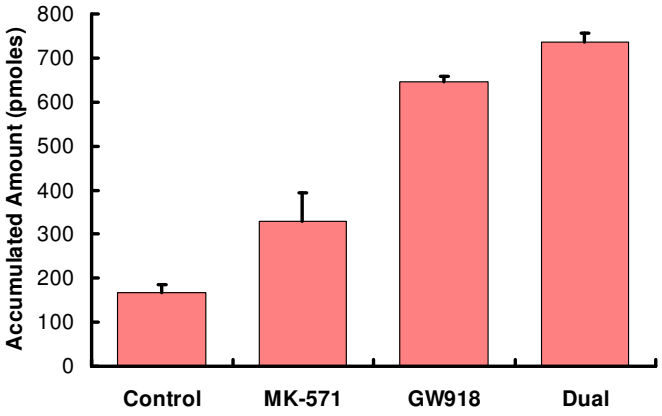

Figure I.3. Accumulation of fexofenadine after preloading in Caco-2 cells. Mean of 3 ± SD. A statistical difference was observed between all treated and untreated conditions ($p<0.05$, student's t-test).

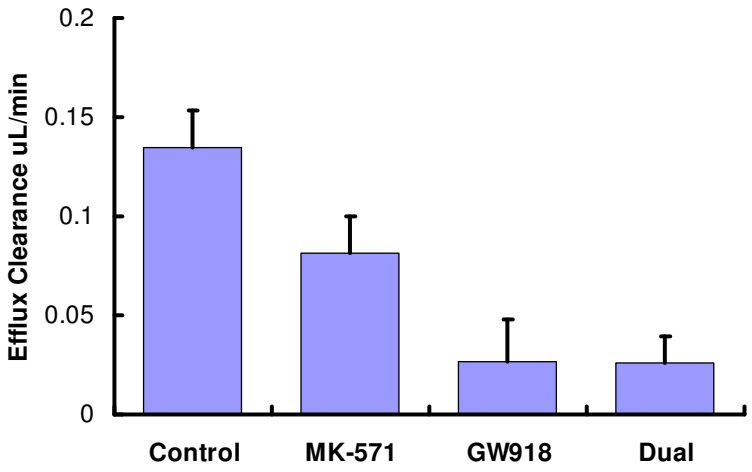

Figure I.4. AP efflux of fexofenadine in Caco-2 cells. Mean of 3 ± SD. A statistical difference was observed between all treated and untreated conditions ($p<0.05$, student's t-test).

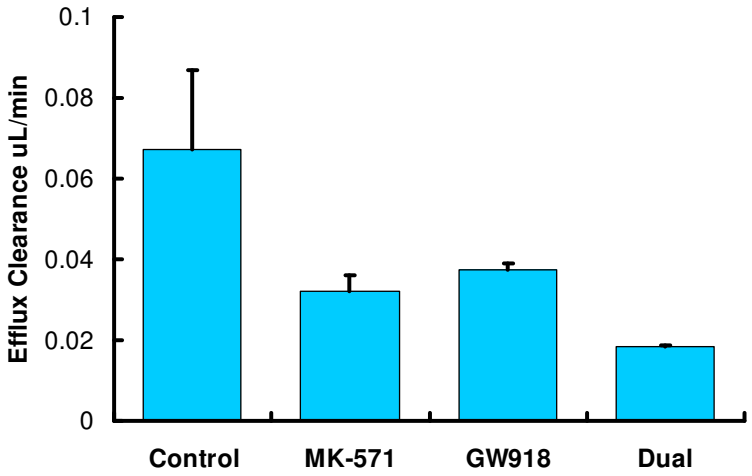

Figure I.5. BL efflux of fexofenadine in Caco-2 cells. Mean of 3 ± SD. A statistical difference was observed between all treated and untreated conditions ($p<0.05$, student's t-test).

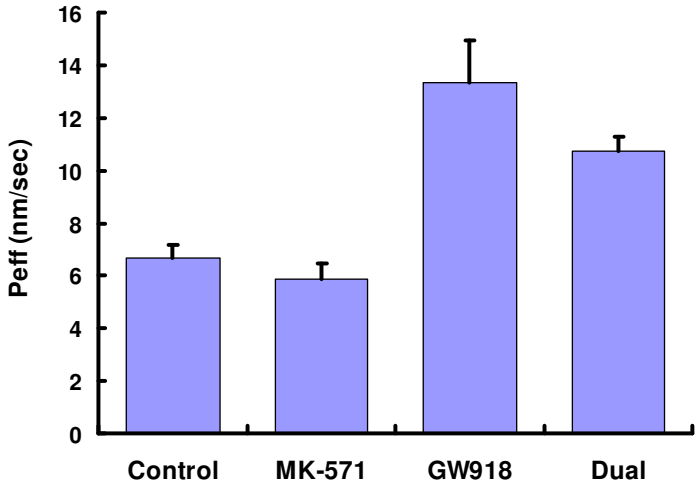

Figure I.6. Absorptive transport of fexofenadine in Caco-2 cells. Mean of 3 ± SD. A statistical difference was observed between treated and untreated conditions for GW918 and dual treatments ($p<0.05$, student's t-test).

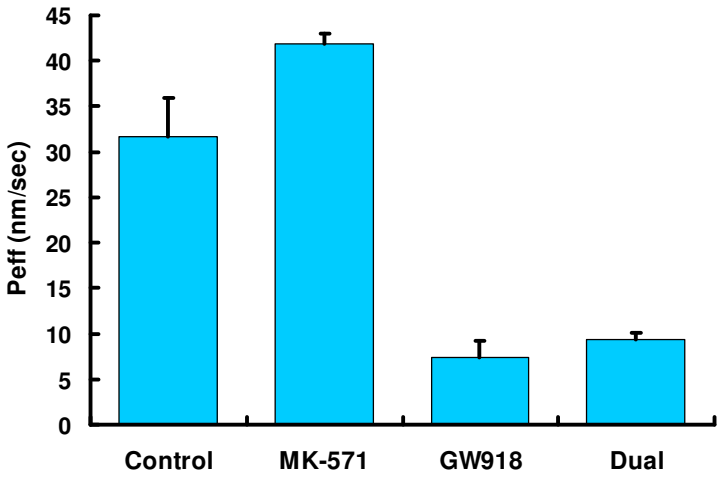

Figure I.7. Secretory transport of fexofenadine in Caco-2 cells. Mean of 3 ± SD. A statistical difference was observed between treated and untreated conditions for GW918 and dual treatments ($p<0.05$, student's t-test).

APPENDIX II: THE ROLE OF P-GLYCOPROTEIN IN ATTENUATING OPIOID RECEPTOR RESPONSE: A PHARMACOKINETIC/PHARMACODYNAMIC MODELING STUDY

Beverly M. Mowrey and Gary M. Pollack

AAPS, 2002

A. ABSTRACT

Purpose

P-glycoprotein (P-gp)-deficient mice are thirty times more sensitive to the peptidic opioid DPDPE than corresponding P-gp-competent mice. The competent mice have a 10-fold higher brain EC_{50}, which is the concentration required to produce 50% of the maximum antinociceptive response. This discrepancy cannot be explained fully by the difference in brain penetration; this implies that P-gp has other functions in the brain besides efflux at the luminal membrane of the capillary endothelium.

Methods

A mathematical modeling approach was used to assess the mechanism of the difference in EC_{50}. A pharmacokinetic/pharmacodynamic model was proposed which attributes the difference in sensitivity to pharmacokinetic processes.

Results

The model identified is consistent with in vivo results; it includes a central and peripheral compartment, plus three brain compartments. Brain EC_{50} was estimated at 0.166 µg/ml in the P-gp-competent mice, but was only 0.012 µg/ml in the P-gp-deficient mice. The model required inclusion of P-gp at sites other than endothelial cell membranes.

Conclusions

Concentration profile and antinociceptive effect data collected in DPDPE-treated P-gp-competent and -deficient mice can be characterized by a pharmacokinetic / pharmacodynamic model in which the role of P-gp in modulating receptor response

is critical. An understanding of this link between pharmacokinetics and effect could significantly change the goals of CNS drug development.

B. INTRODUCTION

Studies have shown that many opioids are P-glycoprotein (P-gp) substrates. Chen et al. showed that P-gp-deficient mice required 30-fold lower doses of the peptidic opioid (D-Penicillamine^{2,5})enkephalin (DPDPE) than P-gp-competent mice to produce equivalent antinociception(Chen and Pollack, 1998). However, the P-gp-deficient animals exhibited a brain/serum ratio of DPDPE which was only ~3-fold higher, indicating that P-gp may have additional barrier functions in the brain beyond efflux at the blood-brain barrier (BBB), consistent with reported extra-endothelial localization of P-gp in brain(Golden and Pardridge, 1999). This study was conducted to evaluate the linkage between P-gp-mediated transport and opioid pharmacodynamics.

P-glycoprotein (ABCB1 or P-gp) is a 170 KD protein that resides in the cell membranes of many tissues. It is encoded by the MDR1 gene in humans, while in mice the mdr1a and mdr1b gene products both play important roles. P-gp acts as an efflux transporter that pumps xenobiotics out of cells, deriving energy from ATP hydrolysis.

The importance of P-gp in the central nervous system (CNS) is well established. The efflux transporter is expressed in the capillary endothelial cells of the blood-brain barrier (BBB), where it restricts the entry of drugs via the transcellular route. The endothelial cells themselves considerably limit paracellular passage of molecules from the blood to the brain parenchyma due to the presence of tight junctions between cells.

One relationship that has not been adequately explored is the effect of P-gp activity on pharmacodynamic response. In particular, some data suggest that P-gp may be able to modulate the effect of substrates that are ligands for the opioid receptor(Chen and Pollack, 1998).

Most pain relieving drugs that have been developed to target this family of receptors are mu-receptor type agonists, but recently there has been an increased interest in utilizing the delta-opioid receptor as a therapeutic drug target. Some information suggests that delta-agonists have the potential to be at least as effective as mu-agonists at treating pain, but with a reduction in the side effects associated with mu-agonists, such as constipation, respiratory depression and the development of physical dependence.

Cyclization, one strategy used to improve the stability and increase the residence time of such drugs, was employed in development of the delta-opioid receptor agonist (D-penicillamine^{2,5})-enkephalin (DPDPE)(Kramer et al., 1989) (Figure II.1).

The pentapeptide (molecular weight 646 Da) exhibits enhanced metabolic stability; however, it is subject to rapid biliary excretion(Chen and Pollack, 1997). The passive permeability of DPDPE at the blood-brain barrier is quite low. It has, however, been shown to enter the brain through a saturable mechanism(Dagenais C, 2001), and is subject to active efflux by P-gp(Chen and Pollack, 1999).

A previous *in vivo* study (Chen and Pollack, 1998) compared the disposition and effect of tritium-labeled DPDPE in "P-gp knockout" mice, which lack the gene for P-gp expression (*mdr1a(-/-)*) with that in wild-type (P-gp competent) FVB mice (*mdr1a(+/+)*). Although systemic pharmacokinetics were not altered by the mutation, the lack of P-gp at the BBB increased brain penetration of [^{3}H]DPDPE 2–4 fold in the *mdr1a(-/-)* mice. As expected, knockout mice exhibited a higher response to DPDPE; i.e. a much smaller dose was required for antinociception. This was reflected in an approximately 30-fold lower ED_{50} value - the dose of drug required to elicit 50 % of the maximal response - in knockout mice. However, this reduction in ED_{50} could not be attributed to enhanced permeation of the BBB alone. Measurement of the respective brain concentrations revealed a significant difference in sensitivity, even after normalization for brain concentrations (Figure II.2). That is, the EC_{50} of brain tissue (concentration of drug in whole brain homogenate that will produce 50% of the maximal response) was approximately 10 times lower in the *mdr1a(-/-)* mice versus the *mdr1a(+/+)* mice. This interesting finding remains unexplained.

Data generated by Pollack and colleagues provided evidence against the hypothesis of a change in intrinsic receptor response or number of receptors. Since it was not possible to achieve identical brain concentrations in vivo in mdr1a(+/+) and mdr1a(-/-) mice due to the sensitivity of the knockout animals, an in vitro analysis was employed. The binding to membrane fractions of radiolabeled guanosine-5'-O-(3-[^{35}S]thio)triphosphate (abbreviated [^{35}S]GTPγS), an analog of GTP that is resistant to hydrolysis, was used as a measure of activation of G-protein coupled opioid receptors (methods described elsewhere(Selley et al., 1998)). When this analysis was performed using membrane fractions from P-gp competent and deficient mouse brains, no significant difference in response ($p>0.1$) was found between the strains.

Similarly, data were generated in the Pollack lab that ruled out differences between the P-gp competent and deficient mice in uptake or binding of [^{3}H]DPDPE to brain slices in vitro (unpublished data, Matheny and Pollack).

In the absence of a binding affinity or receptor activity alteration, the most likely mechanism for modulation of receptor response would be an alteration of drug pharmacokinetics. If this were the case, the concentration at the receptor would produce the same response, but the drug would be restricted from the receptor biophase by the transporter. This implies that P-gp could have additional roles in the CNS besides efflux at the level of the capillary endothelium. The possibility that P-glycoprotein could modulate not only the pharmacokinetics, but also the

pharmacodynamics, of opioids requires additional investigation. The aim of the investigations presented here is to examine in detail the pharmacodynamic link between P-gp transport and opioid receptor response, using a PK/PD modeling approach, and to explore possible causative mechanisms.

C. MATERIALS AND METHODS

All pharmacokinetic and pharmacodynamic modeling and simulation were performed using the program WinNonlin 4.1 (Pharsight Corp., Mountain View, CA). Although their data were not fit directly, information from the DPDPE study by Chen et al.(Chen and Pollack, 1998) was used in creating the models. The goal of the modeling was to explain the data obtained and to draw conclusions which would allow predictions to be made. Some of the parameters derived by the investigators, such as EC_{50}, gamma and volume of the central compartment were used directly, while others were used as starting points for model construction. The value of brain EC_{50} observed for the knockout mice was used to simulate the data, the goal being to find the model which would shift the brain EC_{50} to the level observed in competent mice. Response was calculated using the Hill equation:

$$E = \frac{Emax * C^{\gamma}}{EC50^{\gamma} + C^{\gamma}}$$

where E = effect, C = drug concentration and γ = sigmoidicity factor.

Since P-gp V_{max} and K_m values have not been reported for this compound, those obtained for a similar peptidic drug (DAMGO)(Oude Elferink and Zadina, 2001) were used as a starting point around which a range of values was examined. An average mouse weight of 30 g, a total brain volume of 0.0038 ml, and a brain weight of 0.35 g were assumed. Physiological volumes and scaling factors were obtained from the literature(Davies and Morris, 1993).

Nine distinct pharmacokinetic/pharmacodynamic (PK/PD) model scaffolds were constructed; the ability of each to describe the disposition and action of DPDPE in both P-gp-competent and P-gp-deficient mice, based on previously reported data(Chen and Pollack, 1998), was evaluated. Standard selection criteria were employed, and a scaffold segregating the brain into 3 compartments (one containing the effect site) was identified for further experiments. All models assumed a stationary pharmacodynamic system over the time range evaluated (200 minutes).

Factors used to compare the models included the relative levels of brain and blood concentrations and the shapes of the concentration-time curves as well as Akaike's Information Criterion. Most importantly, the effect of P-gp on the dose-response curve (EC_{50}) was examined (Figure II.3).

D. RESULTS AND DISCUSSION

A model was identified (Figure II.4) that describes the phenomenon observed by Chen et al. The 10-fold increase in brain EC_{50} of P-gp competent versus P-gp deficient mice can be accounted for by the presence of P-gp at sites other than the endothelial cell luminal membranes. The model includes a central compartment, plus a peripheral compartment to account for systemic disposition. Characterization of brain pharmacokinetics called for separation of the brain into three compartments – endothelial cells (2), parenchyma (4) and cerebrospinal fluid (3).

The differentials used in the model were as follows:

$$\textit{Initial Conditions} \; : C_1^0 = \frac{\text{Dose} * \text{Weight}}{V_1}$$

$$\frac{dC_1}{dt} = -(k_{12} * C_1) - (k_{10} * C_1) + \frac{Vmax * X_2}{(Km + X_2) * V_1} + \frac{k_{31} * X_3}{V_1} - (k_{13} * C_1) + \frac{k_{21} * X_2}{V_1} - (k_{15} * C_1) + \frac{k_{51} * X_5}{V_1}$$

$$\frac{dX_2}{dt} = \frac{k_{12} * C_1}{V_1} - (k_{24} * X_2) + (k_{42} * X_4) - \frac{2 * Vmax * X_2}{(Km + X_2)} + \frac{k_{31} * X_3}{V_1} - (k_{21} * X_2) + (k_{32CP} * X_3)$$

$$\frac{dX_3}{dt} = \frac{Vmax * X_2}{(Km + X_2)} + (k_{13} * C_1 * V_1) - (k_{31} * X_3) - (k_{32CP} * X_3)$$

$$\frac{dX_4}{dt} = (k_{24} * X_2) - (k_{42} * X_4)$$

$$\frac{dX_5}{dt} = (k_{15} * C_1 * V_1) - (k_{51} * X_5)$$

where C represents concentration, X represents mass, k values represent the first-order rate constants for compound movement between compartments, V_{max} represents the maximum rate of efflux, and K_m represents the concentration at which half of maximum efflux is achieved. As can be seen in Figure II.5, the blood concentration profiles after a 10 mg/kg dose were predicted to coincide in the two

strains of mice (P-gp competent versus deficient, respectively). Effect, however, was markedly different in magnitude and duration. The dose required to produce a 50% response (ED_{50}) was estimated to be 21 mg/kg for the wild-type, but only 0.9 mg/kg for the knockout mouse. As shown in C-D, brain concentrations were higher in the knockout mice at equivalent dosage levels. Brain EC_{50} was estimated at 0.166 µg/ml in the P-gp competent mice, but only 0.012 µg/ml in the P-gp deficient mice.

Figure II.6 shows the change in area under the effect curve (AUEC), 0 to 200 minutes, calculated using the linear trapezoidal method, with varying Vmax to Km ratios (intrinsic efflux clearance) at a fixed dose. It is clear that pharmacodynamic effect decreases rapidly with increased rates of efflux.

Sensitivity analyses were performed for the model by varying certain parameters and simulating the effect on system response. The parameter k_{12} describes the penetration of drug through the endothelial cell layer; as this parameter changes, the expected receptor response shows large changes at early time points. This underscores the importance of the tight junctions at the blood-brain barrier, which keep permeability quite low. It may also be indicative of the active uptake of DPDPE across the blood-brain barrier by a saturable mechanism, which may be a member of the organic anion transporting polypeptide (OATP) family (Dagenais C, 2001). This aspect of DPDPE disposition has not been included in the model for simplicity.

E. CONCLUSIONS

Parameter sensitivity analysis and comprehensive PK/PD simulations revealed that DPDPE pharmacodynamics were exquisitely sensitive to P-gp when the transporter was not localized only to the BBB. These results support the hypothesis that P-gp presents tertiary barriers for substrate presentation to opioid receptors in brain. Potential synergistic barrier functions of efflux transporters at multiple sites in brain should be considered in assessing the influence of such transporters on CNS pharmacodynamics.

F. REFERENCES

Chen C and Pollack GM (1997) Extensive biliary excretion of the model opioid peptide [D-PEN2,5] enkephalin in rats. *Pharm Res* **14**:345-350.

Chen C and Pollack GM (1998) Altered disposition and antinociception of [D-penicillamine(2,5)] enkephalin in mdr1a-gene-deficient mice. *J Pharmacol Exp Ther* **287**:545-552.

Chen C and Pollack GM (1999) Enhanced antinociception of the model opioid peptide [D-penicillamine] enkephalin by P-glycoprotein modulation. *Pharm Res* **16**:296-301.

Dagenais C DJaPG (2001) Uptake and efflux of the peptidic delta-opioid receptor agonist [D-Penicillamine2,5]enkephalin at the murine blood-brain barrier by in situ perfusion. *Neuroscience Letters* **301**:155-158.

Davies B and Morris T (1993) Physiological parameters in laboratory animals and humans. *Pharm Res* **10**:1093-1095.

Golden PL and Pardridge WM (1999) P-Glycoprotein on astrocyte foot processes of unfixed isolated human brain capillaries. *Brain Res* **819**:143-146.

Kramer TH, Shook JE, Kazmierski W, Ayres EA, Wire WS, Hruby VJ and Burks TF (1989) Novel peptidic mu opioid antagonists: pharmacologic characterization in vitro and in vivo. *Journal of Pharmacology & Experimental Therapeutics* **249**:544-551.

Oude Elferink RP and Zadina J (2001) MDR1 P-glycoprotein transports endogenous opioid peptides. *Peptides* **22**:2015-2020.

Selley D, Liu Q and Childers S (1998) Signal transduction correlates of mu opioid agonist intrinsic efficacy: receptor-stimulated [35S]GTPgS binding in mMOR-CHO cells and rat thalamus. *The Journal of Pharmacology and Experimental Therapeutics* **285**:496-505.

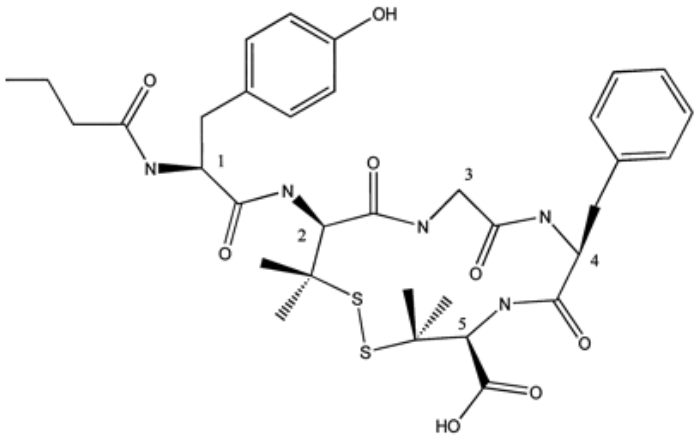

Figure II.1. Structure of DPDPE

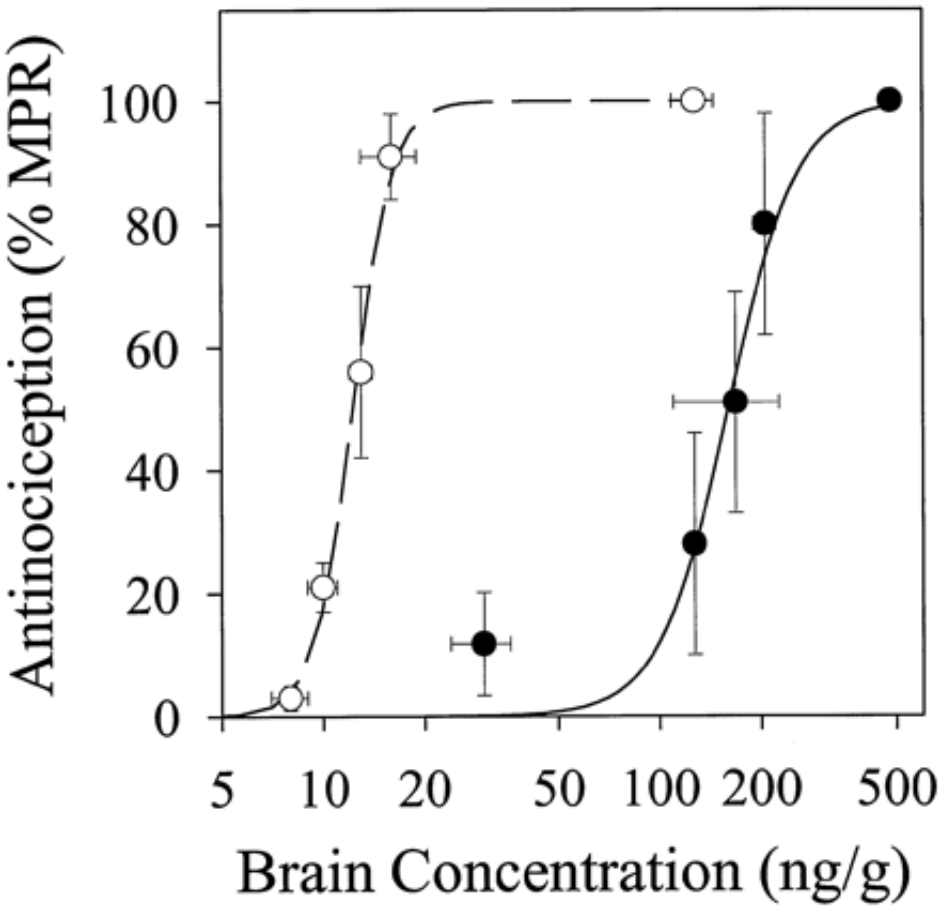

Figure II.2. Brain concentration vs. effect profiles for P-gp deficient (open circles) and P-gp competent (closed circles) mice. Chen and Pollack, 1998

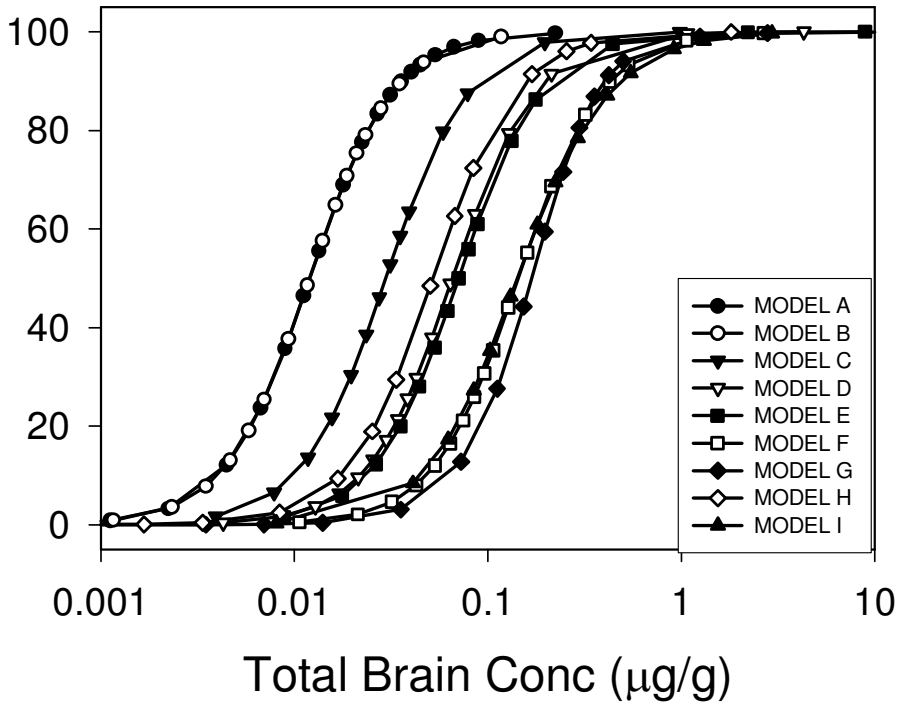

Figure II.3. Simulated brain concentration vs. effect profiles for nine PK/PD models.

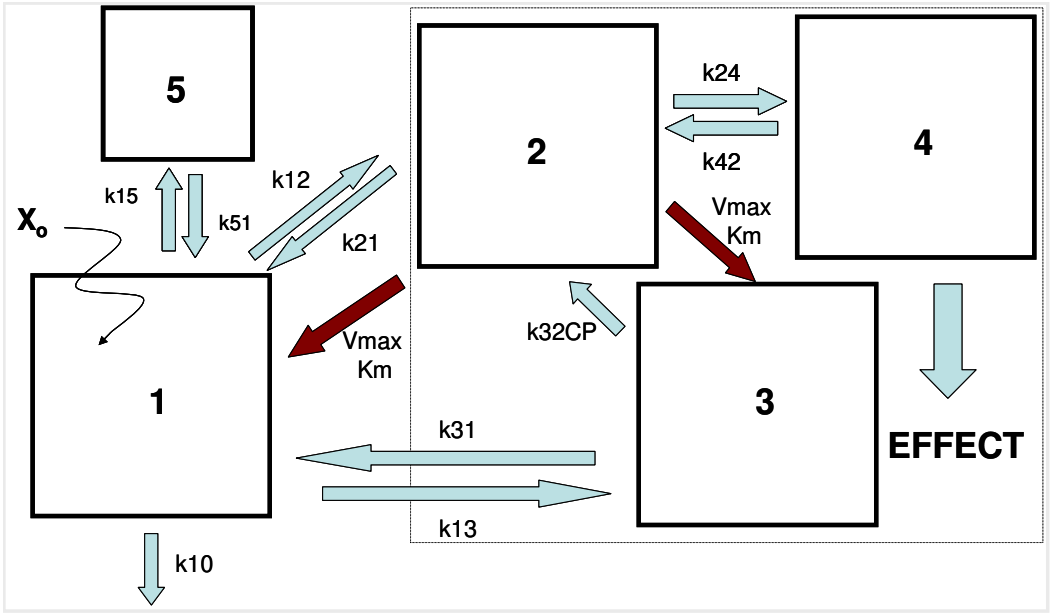

Figure II.4. The model used to simulate PK/PD data. Note: C represents concentration, X represents mass, k values represent the first-order rate constants for compound movement between compartments, V_{max} represents the maximum rate of efflux, and K_m represents the concentration at which half of maximum efflux is achieved.

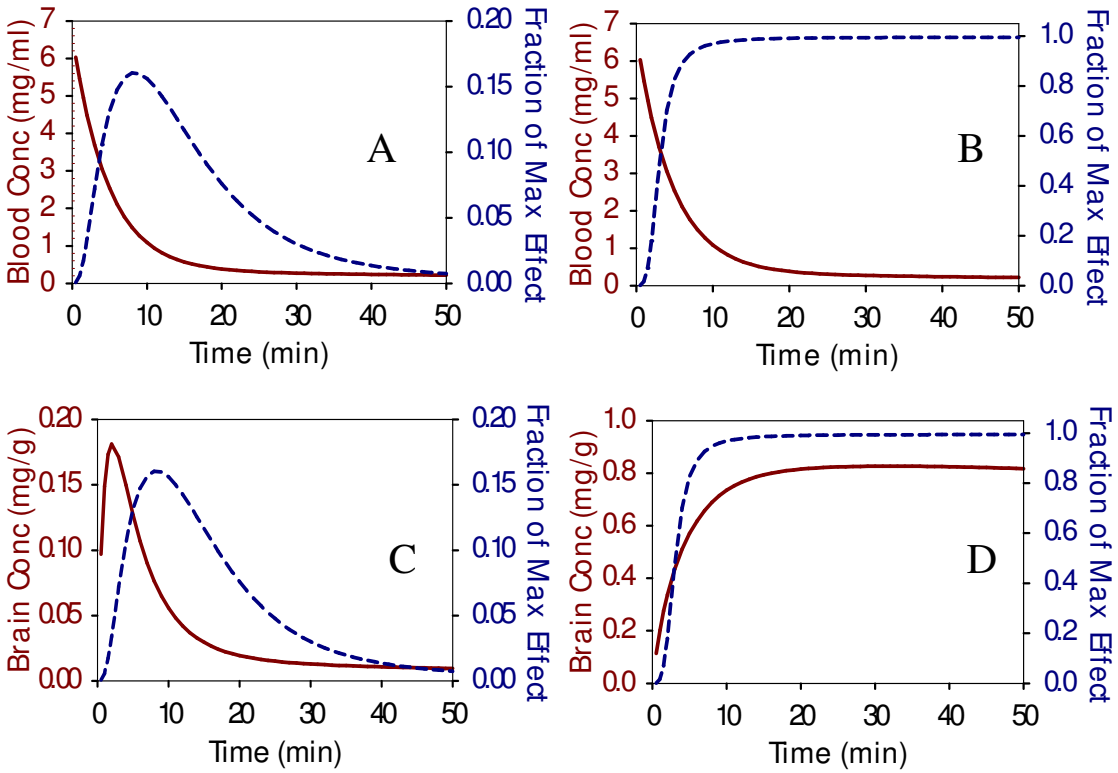

Figure II.5. Predicted blood and brain concentration-response profiles generated from the selected model. Panels A and C portray the data from the P-gp competent mice, and panels B and D show the data from the P-gp deficient mice.

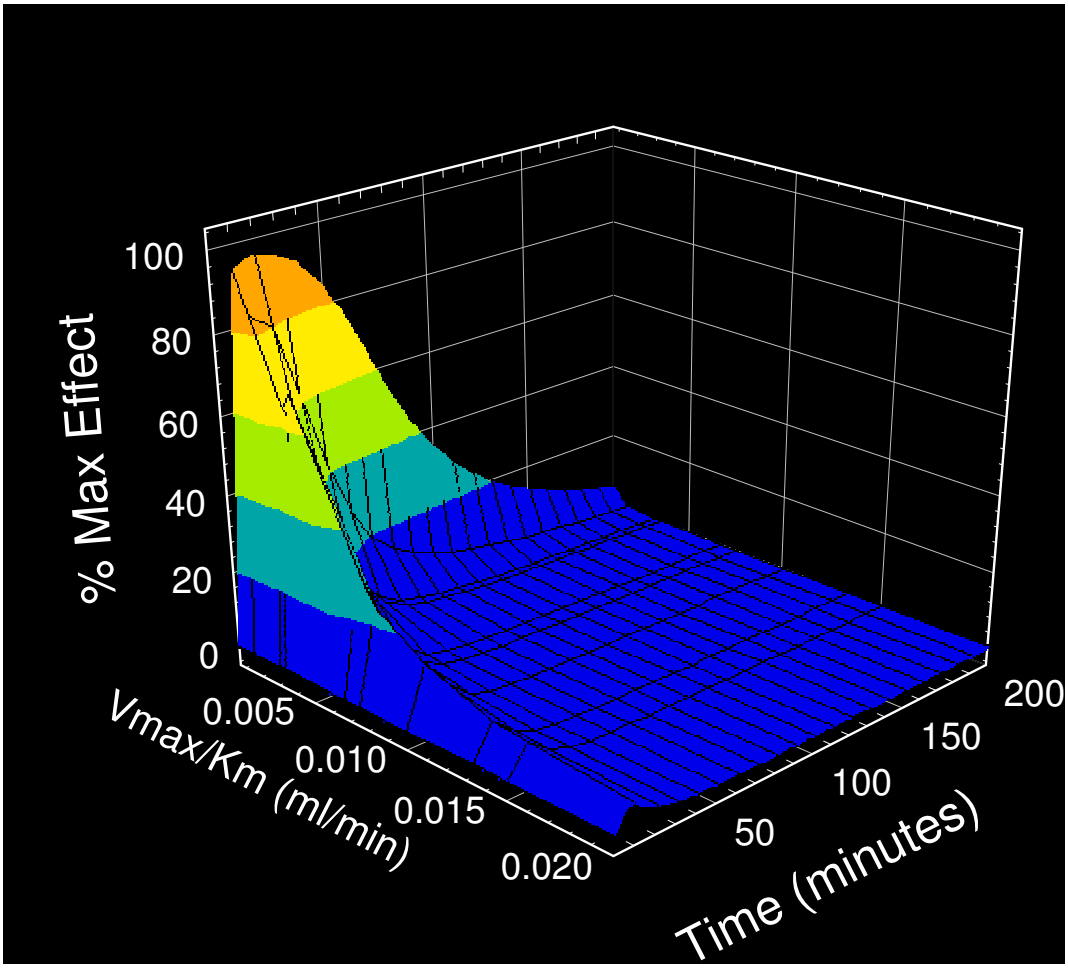

Figure II.6. The effect of changes in intrinsic efflux rate (Vmax/Km) on pharmacodynamic response.

APPENDIX III: MECHANISMS OF DISTRIBUTION OF ANTINEOPLASTIC AGENTS IN DRUG-SENSITIVE AND DRUG-RESISTANT CELL LINES

Beverly M. Knight and Jeffrey Krise

A. ABSTRACT

Purpose

The aims of this project were to develop methods of quantifying antineoplastic drugs in isolated nuclei in order to understand drug distribution mechanisms in drug resistant and drug sensitive cell lines.

Methods

A sucrose gradient method was developed for isolation of nuclei from disrupted cells. Acetonitrile was used to extract the drug from the nuclei. HPLC methods were developed for each compound. In addition, fluorescence microscopy was used to visualize the distribution of compounds within intact drug sensitive and drug resistant cell lines.

Results and Discussion

Nuclear fractionation, extraction, and HPLC quantification methods were successfully developed for several compounds. CEM-C1 (drug resistant) nuclei accrued slightly less drug than their untransformed counterparts (CEM). Similarly, there was a striking reduction in the HL60R (drug resistant) cell nuclei compared to the corresponding drug sensitive cells (HL60S) due to development of drug resistance mechanisms. Camptothecin and daunorubicin appeared to accumulate in punctate cellular compartments in the drug-resistant cell line when examined by fluorescence microscopy.

Conclusions

Drug resistance mechanisms in HL60R and CEM-C1 cell lines involve redistribution of compound within the cell away from the nucleus (site of action).

B. INTRODUCTION

Understanding the distribution of drugs within cells is an important goal in drug delivery. Drug targets are often located within the nucleus (e.g., for gene delivery) or other organelles. Elucidating the factors which determine the intracellular localization of a compound would allow better design of drugs that target specific compartments. These factors include binding specificity as well as physicochemical parameters such as pKa and lipid partitioning. For example, weakly basic drugs have been shown to accumulate in lysosomes and other acidic organelles due to the ion trapping phenomenon (Hurwitz et al., 1997) (de Duve et al., 1974) (Chou et al., 2001). In addition, hydrophobic cationic compounds accumulate in the mitochondria due to the net negative membrane potential of these organelles (Hatefi, 1985).

The properties of specific cell types can also determine intracellular distribution. For example, the lipid composition of the membranes as well as the expression of membrane-bound proteins may differ between cell types. The changes associated with development of multidrug resistance in cells are particularly interesting. Multidrug resistance (MDR) occurs when cells are chronically exposed to certain drugs, including many anticancer agents. While it is known that drug efflux transporters are overexpressed in multidrug resistant cells, many other changes that are less understood are associated with this transformation (Larsen et al., 2000). These adaptive changes may influence the intracellular distribution of compounds such that the drugs can no longer reach their targets (e.g., nucleus).

In order to study the intracellular distribution of therapeutic agents, as well as changes in distribution associated with development of multidrug resistance, methods must be available to separate the different components of the cell. Most of the studies done in this area involve visualization of drug distribution by fluorescence microscopy. However, isolation of individual organelle types would allow accurate quantification of drug levels in these compartments. In this study, a cell fractionation approach (Duvvuri et al., 2004), coupled with HPLC with fluorescence detection, has been used in an effort to better understand intracellular drug distribution.

C. MATERIALS AND METHODS

The HPLC system consisted of a Waters 600S Controller, Waters 616 Pump, Waters 474 Scanning Fluorescence Detector, Waters 717plus Autosampler and Shimadzu C-R3A Chromatopac Integrator. Tetraethylammonium acetate was purchased from Pfaltz and Bauer. Glacial acetic acid, acetonitrile and potassium hydroxide were purchased from J.T. Baker. Sucrose, sodium phosphate and potassium phosphate were purchased from Mallinckrodt. Potassium chloride was purchased from EM Science. Sodium chloride, camptothecin, DMSO, TEA, PBS, daunorubicin and SR-101 were purchased from Sigma Aldrich. Doxorubicin was purchased from Alexis. Formic acid and ammonium formate were purchased from Fisher Scientific. RPM1 medium with L-glutamine was purchased from Gibco.

C.1. Cell Culture

CEM, CEM-C1, HL60R and HL60S cells were routinely grown in suspension in RPM1 medium with L-glutamine and split every 4-5 days. Cells were incubated at 37^{o}C at 95% humidity and 5% CO_2.

C.2. Cell Incubations

HL-60S (drug sensitive) and HL-60R (drug resistant) as well as CEM (drug sensitive) and CEM-C1 (drug resistant) cell lines were used at a concentration of 8.7 X 10^7 cells per prep. Cells were incubated with each drug for 2 hours @ 37^{o}C.

C.3. Nuclear Fractionation

The separation of intact nuclei from cells was carried out using a slightly modified version of the procedure by Duvvuri, et al. (Duvvuri et al., 2004) Briefly, 8.0 x 10^7 cells were incubated in 0.5 µM of daunorubicin for 2 hours at 37°C, pelleted, and washed twice with ice-cold PBS, pH 7.4. The cells were resuspended in 10 ml of 0.25 M sucrose in TKMC buffer (50 mM Tris, 25 mM KCl, 5 mM $MgCl_2$, pH 7.0), and homogenized in a Dounce homogenizer with a tight-fitting B pestle. Ten ml of 2.3 M sucrose in TKMC buffer containing 0.75% Triton-X 100 were added and this solution was layered on top of 2.3 M sucrose in TKMC buffer and centrifuged at 15,000 rpm in a Beckman SW28 swinging bucket rotor for 70 minutes at 4°C.

C.4. Extraction of Drug

Acetonitrile (750 µL) was added to the pelleted nuclei. The samples were then sonicated for 15 minutes and centrifuged for 10 minutes at 13,000 rpm. Next, 500 µL of supernatant were evaporated to dryness and reconstituted in 50 µL of mobile phase for analysis. The residues from the samples were reconstituted with MeOH and dilute HCl, then treated as above, to determine whether any drug was still bound to the cell DNA after extraction.

C.5. Extraction Efficiency

The following concentrations were extracted: 50 nM, 100 nM, 150 nM and 200 nM. Each preparation contained 126 X 10^6 HL-60 S cells. The separation and

extraction were carried out as previously described, except a single 1000 µl portion of ACN was used instead of two 500 µl portions of ACN: MeOH, for the extraction.

C.6. Fluorescence Microscopy

Cells were incubated with drug (camptothecin = 50 µM; daunorubicin = 1 µM) for 1 hour at 37^{o}C, then centrifuged 5 min @ 1000 rpm. Media was removed and cells were washed with 1 ml ice-cold PBS pH 7.4 and centrifuged 5 min @ 1000 rpm. PBS was removed and cells were washed with 1 ml ice-cold PBS (pH 7.4) and centrifuged 5 min @ 1000 rpm. PBS was removed and 10 µl cell mounting solution was added. The result was transferred to a microscope slide w/coverslip and sealed.

C.7. Quantitation of Camptothecin by HPLC

A HPLC method was developed to quantify Sulforhodamine-101. The method utilized a flow rate of 0.7 ml/min, an injection volume of 20 µl and a run time of 10 minutes. Fluorescence detection was employed with an excitation wavelength of 360 nm and an emission wavelength of 440 nm. Optimal wavelengths were determined by scanning the 100 nM standard. Mobile phase consisted of 675 ml TEAA buffer buffer 1.5% (pH adjusted to 5.5 with glacial acetic acid) and 225 ml acetonitrile. The column was a Waters Symmetry C18 (3.0 x 100 mm).

C.8. Quantitation of Daunorubicin and Doxorubicin by HPLC

A HPLC method was developed to quantify both daunorubicin and doxorubicin. The method utilized a flow rate of 0.3 ml/min, an injection volume of 20 µl and a run time of 10 minutes. Fluorescence detection was employed with an excitation wavelength of 470 nm and an emission wavelength of 550 nm. Optimal wavelengths were determined by scanning the 100 nM standard. The mobile phase for doxorubicin consisted of 770 ml ammonium formate buffer (pH adjusted to 3.0 with formic acid) and 230 ml acetonitrile. For daunorubicin, 900 ml of the doxorubicin mobile phase was combined with 100 ml acetonitrile. The column was an X-terra MS C_{18} (3.5µm, 2.1 x 150 mm).

C.9. Quantitation of Sulforhodamine-101 by HPLC

A HPLC method was developed to quantify Sulforhodamine-101. The method utilized a flow rate of 0.5 ml/min, an injection volume of 10 µl and a run time of 8 minutes. Fluorescence detection was employed with an excitation wavelength of 320 nm and an emission wavelength of 580 nm. Optimal wavelengths were determined by scanning the 100 nM standard. Mobile phase consisted of 1190 ml ammonium formate buffer (pH adjusted to 3.0 with formic acid) and 510 ml acetonitrile. The column was an X-terra MS C_{18} (3.5µm, 2.1 x 150 mm).

D. RESULTS

HPLC methods were successfully developed for all four compounds (camptothecin, doxorubicin, daunorubicin and SR-101). As shown in Figure III.1, the camptothecin (CPT) HPLC method worked well after several adjustments to the method, producing acceptable peak shape for CPT as well as its lactone form. The standard curve was linear up to 100 nM. Figure III.2 shows the peak shape as well as the standard curve for doxorubicin (DOX). For daunorubicin (DNR), a very similar method was used, which also produced good linearity. Figure III.3 shows the standard curve for SR-101, which also looked quite linear. For all of the methods developed, r^2 values for the standard curves were greater than or equal to 0.999.

A cell fractionation approach, using differential centrifugation, was used to separate nuclei from organelles after drug treatment. Extraction efficiency was determined for SR-101 and daunorubicin by spiking cells with compound then carrying out the fractionation. Acceptable recovery values (~50%) were obtained for both compounds (Tables III.1 and III.2).

Next, cells were incubated with either doxorubicin (for CEM and CEM-C1 cell lines) or daunorubicin (for HL60S and HL60R cell lines). The cells were washed and fractionated to isolate the nuclei. Figure III.4 compares doxorubicin accumulation in nuclei of CEM (drug-sensitive) and CEM-C1 (drug resistant) cells. CEM-C1 nuclei accrued slightly less drug than their untransformed counterparts. Similarly, Figure

III.5 compares daunorubicin accumulation in nuclei of HL60S (drug-sensitive) and HL60R (drug-resistant) cells. There was a very significant reduction in the HL60R cell line due to development of drug resistance mechanisms.

Finally, the intracellular distribution of antineoplastic drugs was examined for the CEM and CEM-C1 cell lines by fluorescence microscopy. Figure III.6 shows that camptothecin is more concentrated in intracellular organelles outside of the nucleus in the drug resistant cell line. In order to better visualize this difference we attempted to increase the camptothecin treatment concentration, but this resulted in precipitation of the compound and unclear visualization of distribution (Figure III.7).

Similar to camptothecin, daunorubicin accumulated in punctate cellular compartments in the drug-resistant cell line (Figure III.8).

E. DISCUSSION

The HPLC methods worked well for easy quantification of camptothecin, doxorubicin, daunorubicin, and sulforhodamine-101 (Figures III.1-3). The extraction method produced acceptable recovery values (Table III.1).

Drug-resistant cells (CEM-C1) accumulated slightly less doxorubicin in their nuclei than drug-sensitive cells (CEM) (Figure III.4). HL60 drug-sensitive cell nuclei accumulated significantly more daunorubicin than the corresponding drug-resistant cell nuclei ($p=0.01$) (student's t-test) (Figure III.5). The HL60R cell line appears to more effectively partition drug away from the nucleus. This method does not, however, distinguish whether drug was excluded from the cell or sequestered in a secondary compartment.

For the fluorescence microscopy, the camptothecin signal was at first weak, which made visualization difficult, although some differences can be seen in the nuclear accumulation of the sensitive (CEM) and resistant (CEM-C1) cells (Figure III.6). The experiment was repeated with a higher concentration of camptothecin (Figure III.7), but this resulted in precipitation of the compound and unclear visualization. Daunorubicin, however, clearly distributed to punctuate compartments in the drug resistant cell line.

F. CONCLUSIONS

HPLC methods were developed for camptothecin, doxorubicin and daunorubicin, and SR-101. A method of nuclear isolation and extraction of drug was validated. Daunorubicin exhibited a large difference in the amount accumulated in the nucleus between CEM and drug-resistant CEM-C1 cells, with the resistant cells accumulating significantly more compound. Doxorubicin showed the same trend in HL60R cells compared with HL60S cells, but the difference was minimal. Camptothecin and daunorubicin showed different distribution patterns in drug-resistant and drug-sensitive cells. The mechanisms of redistribution of drugs away from the nuclear target are likely to be compound- and cell line-specific.

G. REFERENCES

Chou KM, Paul Krapcho A and Hacker MP (2001) Impact of the basic amine on the biological activity and intracellular distribution of an aza-anthrapyrazole: BBR 3422. *Biochem Pharmacol* **62**:1337-1343.

de Duve C, de Barsy T, Poole B, Trouet A, Tulkens P and Van Hoof F (1974) Commentary. Lysosomotropic agents. *Biochem Pharmacol* **23**:2495-2531.

Duvvuri M, Feng W, Mathis A and Krise JP (2004) A cell fractionation approach for the quantitative analysis of subcellular drug disposition. *Pharm Res* **21**:26-32.

Hatefi Y (1985) The mitochondrial electron transport and oxidative phosphorylation system. *Annu Rev Biochem* **54**:1015-1069.

Hurwitz SJ, Terashima M, Mizunuma N and Slapak CA (1997) Vesicular anthracycline accumulation in doxorubicin-selected U-937 cells: participation of lysosomes. *Blood* **89**:3745-3754.

Larsen AK, Escargueil AE and Skladanowski A (2000) Resistance mechanisms associated with altered intracellular distribution of anticancer agents. *Pharmacol Ther* **85**:217-229.

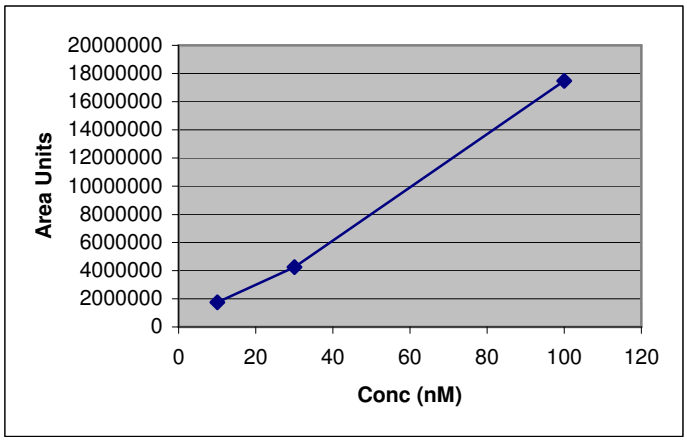

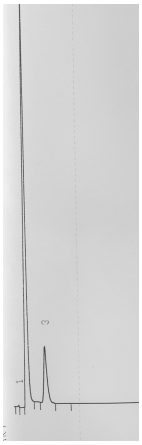

CPT + lactone

Figure III.1. Standard curve and representative chromatogram for camptothecin (CPT)

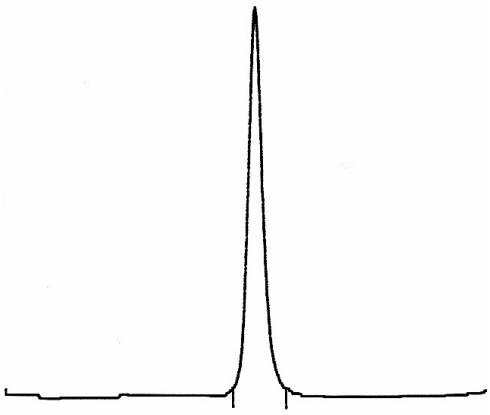

A

B

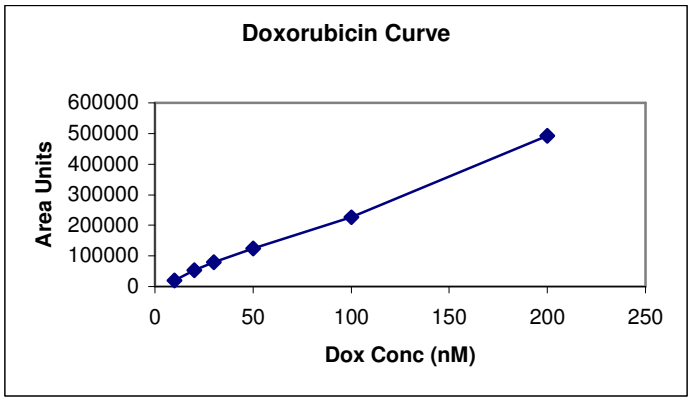

C

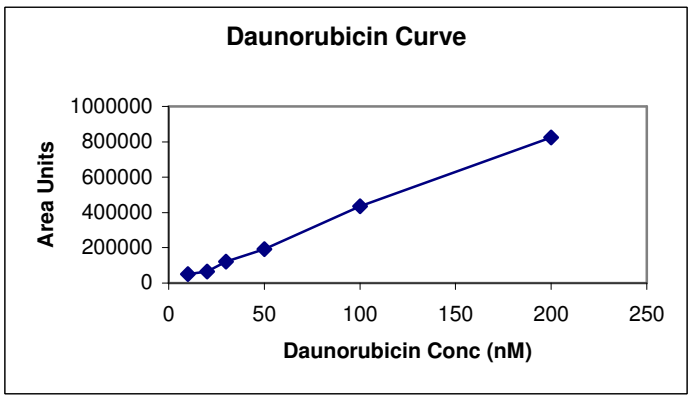

Figure III.2. A) Doxorubicin representative chromatogram; B) doxorubicin and C) daunorubicin standard curves.

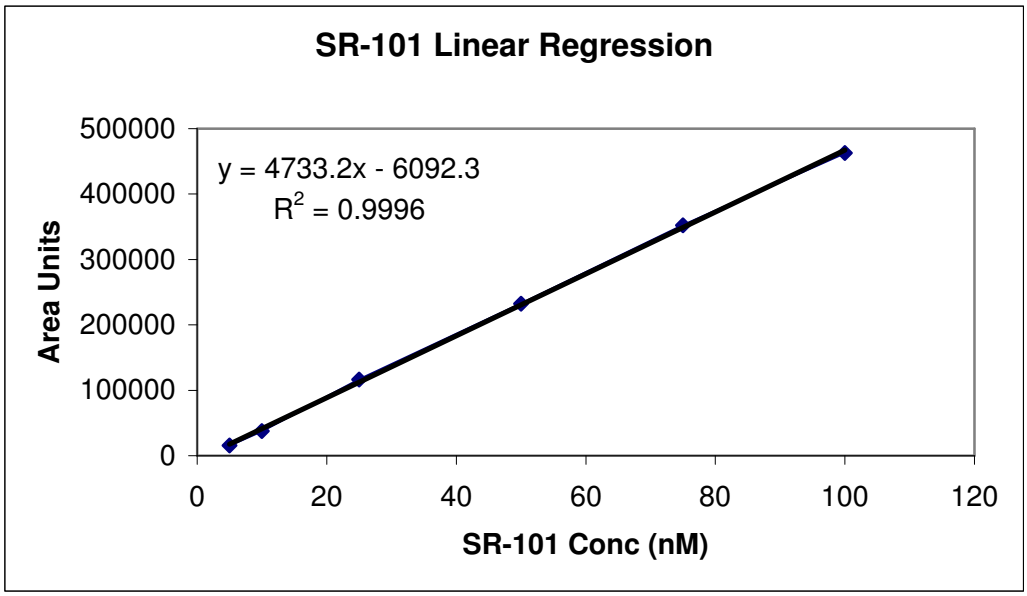

Figure III.3. Standard curve for SR-101.

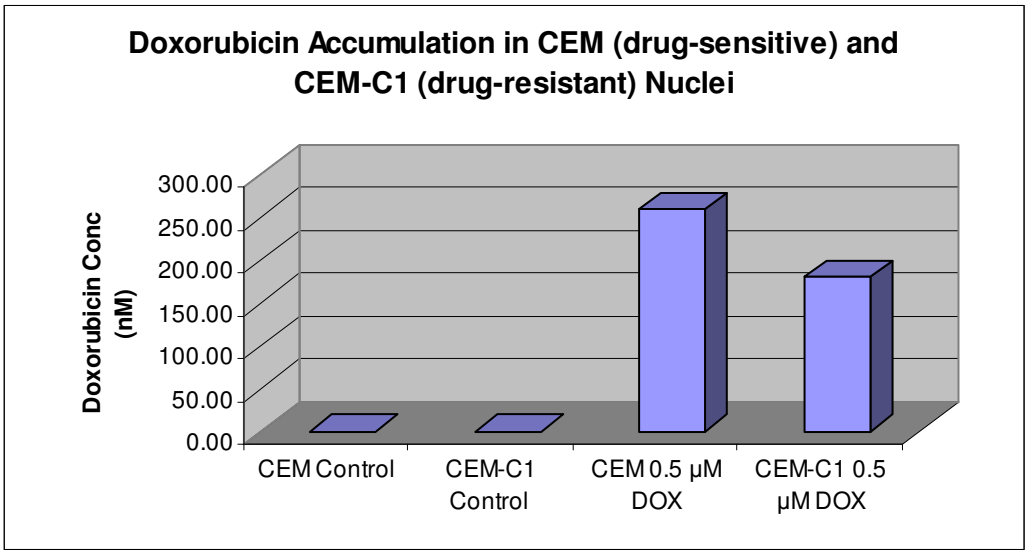

Figure III.4. Accumulation of doxorubicin in nuclei of CEM and CEM-C1 cells. A significant difference was seen between drug accumulation in drug-sensitive and drug-resistant cell nuclei ($p<0.05$, student's t-test).

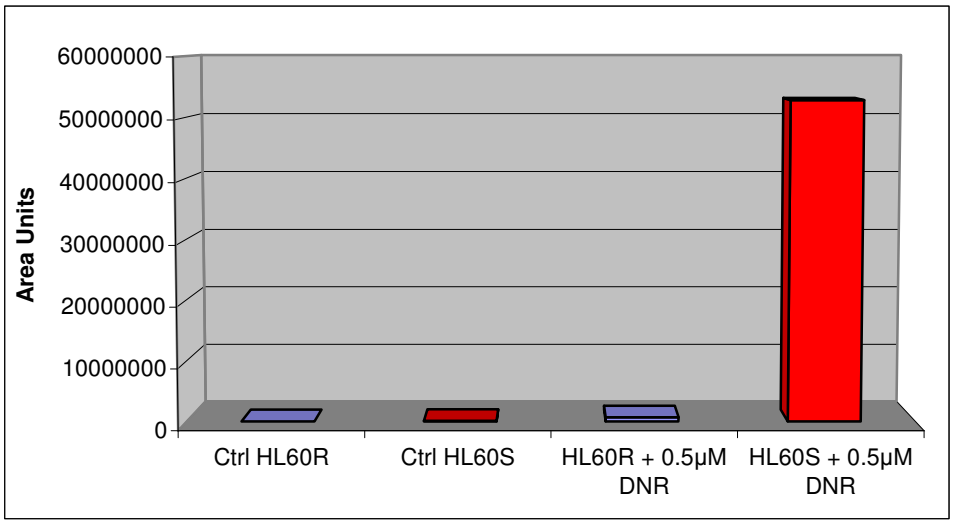

Figure III.5. Accumulation of daunorubicin in HL60R and HL60S cell nuclei. A significant difference was seen between drug accumulation in drug-sensitive and drug-resistant cell nuclei ($p<0.05$, student's t-test).

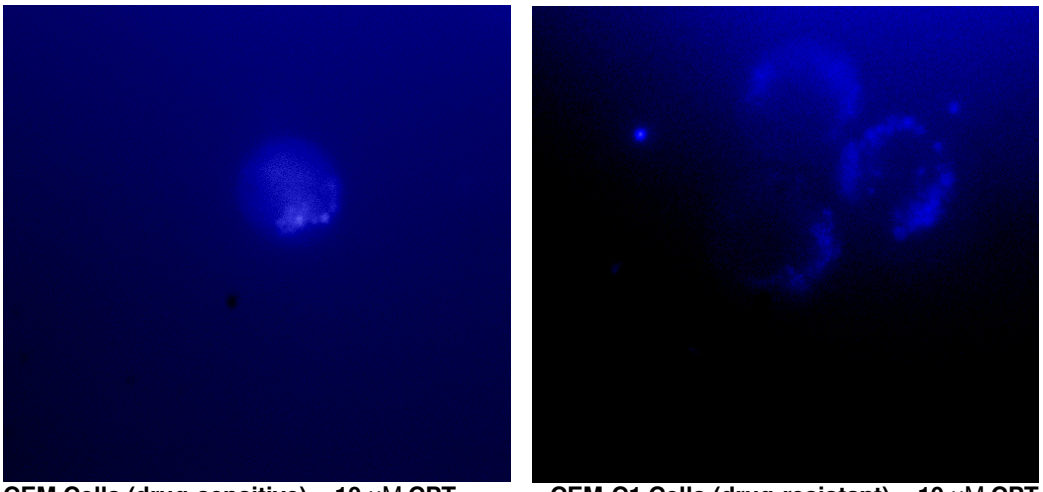

CEM Cells (drug-sensitive) + 10 μM **CPT** **CEM-C1 Cells (drug-resistant) + 10** μM **CPT**

Figure III.6. Visualization of camptothecin distribution in CEM and CEM-C1 cells by fluorescent microscopy.

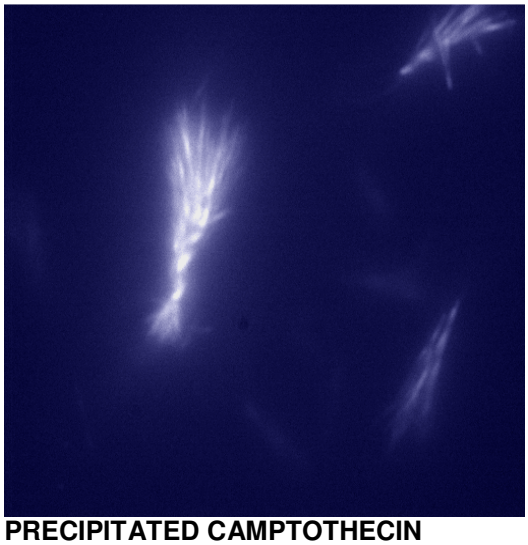

PRECIPITATED CAMPTOTHECIN

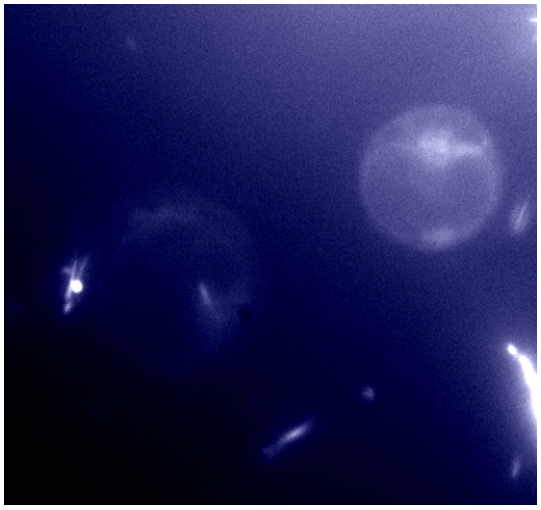

CEM (drug-sensitive) + 50 µM **CPT**

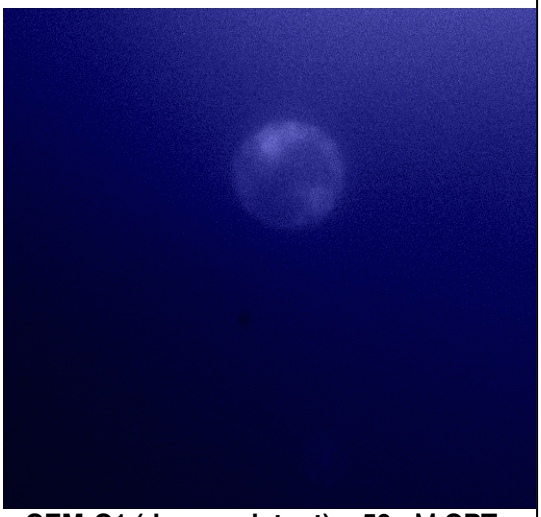

CEM-C1 (drug-resistant) + 50 µM **CPT**

Figure III.7. Upper panel: precipitation of camptothecin. Lower panels: Visualization of camptothecin distribution in CEM and CEM-C1 cells by fluorescent microscopy.

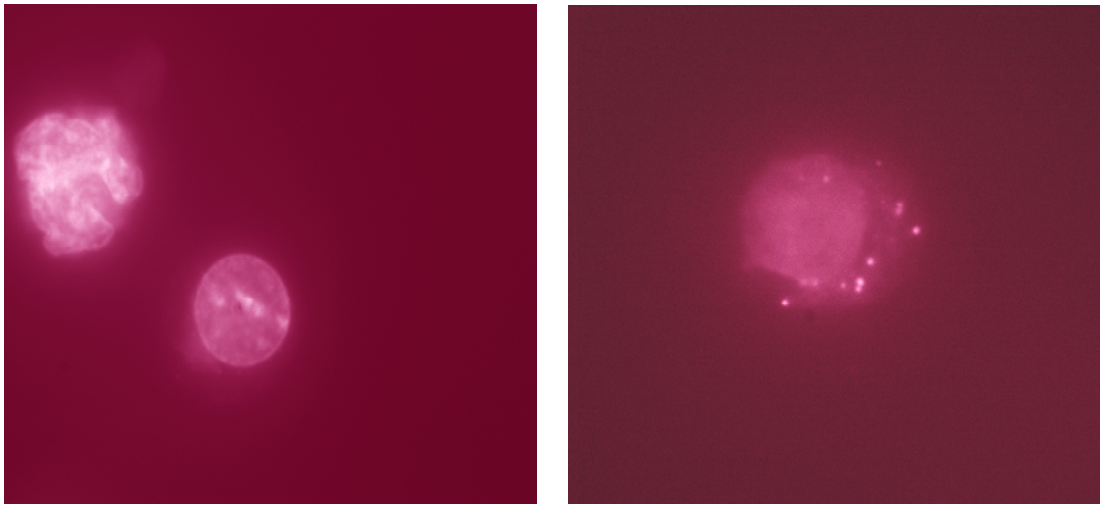

CEM Cells (drug-sensitive) + 1 µM **DNR** **CEM-C1 Cells (drug-resistant)+ 1** µM **DNR**

Figure III.8. Visualization of daunorubicin distribution in CEM and CEM-C1 cells by fluorescent microscopy.

Table III.1. Extraction efficiency for SR-101 in HL60S cells.

Theoretical Conc.	Recovery
50 nM	41.7%
100 nM	50.7%
150 nM	61.4%
200 nM	54.3%
Average	52.0%
SD	8.2%

Table III.2. Extraction efficiency for daunorubicin.

Cell Type	Theoretical Conc.	Recovery
HL60S	200 nM	57.1%
HL60S	400 nM	48.7%
HL60R	200 nM	52.1%
HL60R	400 nM	53.2%
Average		52.8%
SD		3.5%

APPENDIX IV: WHY IS ABSORPTIVE METABOLISM HIGHER THAN SECRETORY METABOLISM IN INTESTINE?

Beverly M. Knight and Dhiren R. Thakker

AAPS 2007

A. ABSTRACT

Purpose

Caco-2 cells are often used to study the interplay between drug transporters and metabolic enzymes in the intestine. It has been reported that B-to-A (basolateral to apical) metabolism is often slower than A-to-B metabolism (Gan et al., 1996) (Paine et al., 2002a) (Raeissi et al., 1999). Therefore, the cause of this effect was investigated.

Methods

Side-by-side diffusion chambers were used to study the transport and metabolism of terfenadine and loperamide in intestinal tissue from P-gp-deficient and P-gp-competent mice during its absorptive transport. Three jejunal segments (0.3 cm^2) were excised from each mouse and immediately mounted between two chambers containing Krebs-Ringer Bicarbonate buffer; viability was maintained by bubbling the solution with oxygen:carbon dioxide (5:95). After a 30-minute equilibration, substrate was dosed into the donor chamber. Samples were collected over 120 minutes. Caco-2 cell monolayers were cultured in Transwell® plates and induced to express CYP3A according to published methods (Schmeidlen-Ren et al., 1999). The transport across Caco-2 cell monolayers of terfenadine and loperamide was characterized in the A-to-B and B-to-A directions and also in the presence and absence of the P-gp inhibitor GW918. During transport of loperamide or terfenadine, CYP3A-specific

metabolites formed over time in all three compartments were quantified using LC-MS/MS.

Results

In Caco-2 and mouse intestine, the rate of metabolism in the A-to-B direction was higher than that in the B-to-A direction for both terfenadine and loperamide. When Caco-2 cells were treated with P-gp inhibitor GW918, the metabolism of loperamide was increased in both directions, but the A-to-B metabolism remained significantly higher (~6 fold) compared to B-to-A metabolism. Accordingly, metabolism of terfenadine by P-gp-deficient mouse intestine showed a polarity in B-to-A vs. A-to-B metabolism: the rate of A-to-B metabolism was about 2-fold higher than B-to-A metabolism.

Conclusions

Some authors have postulated that the enhancement of metabolism observed in the A-to-B direction is due to drug efflux by P-glycoprotein (P-gp). However, since this inequality was not abolished by chemical P-gp inhibition or by genetic P-gp knockout, P-gp is not likely to be responsible. More study is needed to elucidate the mechanisms behind this phenomenon.

B. INTRODUCTION

Oral delivery is the most commonly used method of administering drugs. It is therefore important to understand all of the mechanisms and barriers involved in the oral absorption of drugs. Drug metabolizing enzymes and efflux transporters constitute two important barriers to drug absorption from intestine. Drug metabolizing enzymes, such as the CYP (CYP) enzymes, have been extensively studied in the liver, but their role in intestine is not as well understood. The most important of these enzymes is CYP3A, since it has the highest expression and widest substrate specificity. There are many efflux transporters expressed in intestine, including MRPs (multidrug resistance associated proteins) and BCRP (breast cancer resistance protein) transporters, but the most studied transporter is P-gp. P-gp functions to pump drug out of enterocytes and also has wide substrate specificity.

The way in which these systems interact has been investigated. There is thought to be functional interplay between CYP3A and P-gp in particular, given their overlapping substrate specificities, colocalization at the apical membrane of enterocytes, and similarity of protective function. The first group to pioneer these studies used the Caco-2 cell line, a model of human intestinal epithelium. They noted that metabolism of cyclosporine A was more extensive when compound was dosed on the apical (A) side of the cells than when dosed on the basolateral (B) side. In other words, more metabolites were produced during absorptive (A-to-B) permeation of the compound than during secretory (B-to-A) permeation.

The authors hypothesized that the metabolism was enhanced in the absorptive direction due to P-gp efflux at the apical membrane (Gan et al., 1996). Since then, other authors have noted the same phenomenon for other substrates (Raeissi et al., 1999; Paine et al., 2002a).

This work aimed to examine the underlying cause of these observed results more closely using two dual CYP3A/P-gp substrates, terfenadine and loperamide. Mechanistic studies were carried out to determine whether P-gp efflux increase the extent of intestinal metabolism in the absorptive direction.

C. MATERIALS AND METHODS

C.1. Chemicals and Reagents

Terfenadine, loperamide, sodium selenite, zinc sulfate, all-trans retinoic acid, sodium hydroxide, Kreb's Bicarbonate Ringer and gentamicin were purchased from Sigma Aldrich (St. Louis, MO, USA). Metabolites of terfenadine (azacyclonol and fexofenadine) were generously provided by Dr. Mary Paine. Metabolites of loperamide (monodemethyl- and didemethyl-loperamide) were generously provided by Janssen (Beerse, Belgium). GW918 was provided by GlaxoSmithKline. Methanol, formic acid, ethyl acetate and vitamin E were purchased from Fisher Scientific (Pittsburgh, PA, USA). Ketamine was purchased from Veterinary Medical Supply (Zebulon, NC, USA), and xylazine from Webster Veterinary (Sterling, MA, USA). Eagle's minimum essential medium with Earle's salts and L-glutamate (MEM), Dulbecco's Modified Eagle's Medium with L-glutamine but without sodium pyruvate (DMEM), nonessential amino acids (NEAA, 100X), 0.05% trypsin-0.53 mM EDTA solution, N-Hydroxyethylpiperazine-N'-2-ethanesulfonate (HEPES, 1 M) and penicillin-streptomycin-amphotericin B solution (100X) were obtained from Gibco Laboratories (Grand Island, NY, USA). Hank's balanced salt solution (HBSS) was obtained from Mediatech, Inc. (Herndon, VA, USA). 1α, 25-dihydroxyvitamin D_3 was obtained from Biomol (Plymouth Meeting, PA, USA). Mouse laminin was purchased from BD Biosciences (San Jose, CA, USA).

C.2. Animals

Mice (CF-1 wild type and P-gp mutant) were purchased from Charles River Laboratories (Wilmington, MA) and housed according to AAALAC requirements and protocols accepted by the University of North Carolina Institutional Animal Care and Use Committee. The animal housing facility is under the supervision of the University's Campus Veterinarian, and is in compliance with public laws 89-544 and 91-579. A full-time technician in the Department of Laboratory Animal Medicine is responsible for animal husbandry in this facility. All personnel handling animals must first be certified by the university Institutional Animal Care and Use Committee. Mouse liver and intestinal microsomes were purchased from Xenotech. Human intestinal microsomes were generously provided by Dr. Mary Paine.

C.3. Materials

Corning plates (12-well) with Transwell™ inserts were purchased from Fisher Scientific (Pittsburgh, PA, USA); 6-well-plates and inserts were purchased from BD Biosciences (San Jose, CA, USA). The side-by-side diffusion chamber system (Physiologic Instruments, San Diego, CA, USA) used for the animal studies was loaned by GlaxoSmithKline.

C.4. Caco-2 Cell Culture

The Caco-2 cell line, clone P27.7, was obtained from Mary Paine, Ph.D. and Paul Watkins, MD (Schools of Pharmacy and Medicine, The University of North

Carolina at Chapel Hill, Chapel Hill, NC, USA). Caco-2 cell monolayers were cultured according to the methods of Lee and Thakker (Lee and Thakker, 1999). Except where noted, cell culture medium consisted of 500 ml Minimum Essential Medium (MEM), 50 ml Fetal Bovine Serum (FBS), 5 ml 100X Non-Essential Amino Acids (NEAA), and 5 ml 100X Antibiotic/Antimycotic (final concentrations: 100 U/ml penicillin, 100 µg/ml streptomycin, and 0.25 µg/ml amphotericin B). Cells were grown in 75 cm^2 tissue culture (T75) flasks at 37°C, in an atmosphere of 5% CO_2 and 90% relative humidity, and subcultured at a 1:10 ratio, using 0.05% trypsin/0.02% EDTA solution, upon reaching 90% confluency.

C.5. Transwell® System

For metabolic experiments, 6-well plates containing Biocoat cell culture inserts (4.2 cm^2, 1 µM pore size) were coated with murine laminin (5 µg/cm^2) and then were seeded with Caco-2 cell clone P27.7 (passages 29-42) (Schmeidlen-Ren et al., (Schmiedlin-Ren et al., 1997)) at a density of 5 X 10^5 cells/cm^2. Cultures were grown using growth medium (DMEM containing 20% heat-inactivated FBS, 0.1 mM NEAA, 50 µg/ml gentamicin, and 45 nM vitamin E) until confluence, as assessed by transepithelial electrical resistance values ≥250 Ω·cm^2. After that, the cells were treated for 14 days with differentiation medium (DMEM containing 5% heat-inactivated FBS, 0.1 mM NEAA, 50 µg/ml gentamicin, 45 nM vitamin E, 0.1 µM sodium selenite, and 3 µM zinc sulfate) as described by Schmeidlen-Ren et al. (Schmiedlin-Ren et al., 1997) and

supplemented with 0.5 µM 1α,25-$(OH)_2$-D_3 and 0.2 µM all-*trans*-retinoic acid (Mouly et al., 2004) to induce CYP3A expression.

C.6. Metabolic Studies

To induce CYP3A expression, Caco-2 cell monolayers were grown on laminin-coated inserts in cell culture dishes, and treated with 0.5 µM 1α,25-$(OH)_2$-D_3 for 2 weeks postconfluence, as verified by TEER ≥ 250 Ω·cm^2 (Schmiedlin-Ren et al., 1997; Mouly et al., 2004). After 90 min (loperamide) or 120 minutes (terfenadine), samples were collected from the donor and receiver compartments. Cell monolayers were washed and harvested by scraping into 500 µl of homogenization buffer (100 mM potassium phosphate, 0.25 M sucrose, and 1 mM EDTA, pH 7.4). CYP3A-specific metabolites were identified for each substrate, and metabolite formation over time was characterized by quantification of parent remaining and metabolite formed in all three compartments (donor, cellular and receiver). Parent drug and metabolites were extracted from the lysates samples using a validated extraction procedure. Briefly, samples were vortexed with 1 ml ethyl acetate, then centrifuged and the supernatant removed. The samples were then alkalinized with 50 µl 1 N sodium hydroxide and extracted with an additional 1 ml ethyl acetate. The supernatants were combined, evaporated, and reconstituted in mobile phase.

C.7. Diffusion Chamber Studies

Male CF-1 mice were anesthetized with an IP injection of ketamine (140 mg/kg) and xylazine (15 mg/kg). Just before sacrifice, the intestines were removed and immediately flushed with 10 ml ice-cold Krebs Bicarbonate Ringer (KBR). Three portions of jejunum (~1 inch long) were retained for the analysis. Each section was cut longitudinally and then mounted between the two halves of a diffusion chamber insert and held in place by eight small pins. The inserts were placed in ice-cold KBR until mounted between the chambers. The entire procedure was carried out as quickly as possible, on ice.

Inserts were mounted between two side-by-side diffusion chambers. KBR (3 ml) was added to each chamber and bubbled with oxygen/carbon dioxide gas to maintain viability. After an equilibration period of 30 minutes, the TEER was measured, the buffer in the receiver side was replaced with fresh warmed KBR, and the buffer in the donor side was replaced with warmed dosing solution. Samples were removed from the chambers at the appropriate timepoints and replaced with fresh KBR. At the end of the experiment, the tissues were removed and homogenized in 200 µL of KBR, then extracted with ethyl acetate as described for cell monolayers above.

C.8. Analysis of Terfenadine and Loperamide and Their Metabolites

Terfenadine and its two metabolites, fexofenadine and azacyclonol, and loperamide and its two metabolites, monodemethyl-loperamide and didemethyl-loperamide, were quantified using LC-MS/MS (LC10-ADVP quaternary pumps (Shimadzu, Kyoto, Japan), CTC-PAL autosampler (LEAP Technologies, Carrboro, NC, Sciex API-4000 triple-quadropole mass spectrometer (Applied Biosystems, Foster City, CA).

Mobile phases of 0.1% formic acid in water and 0.1% formic acid in methanol were used with a 5-95% methanol linear gradient. The column used was a Phenomenex Synergy Polar RP, 30 X 2 mm, with 5 µm particle size phenyl-ether linked stationary phase. A flow rate of 0.8 mL/min and injection volume of 15 µL were utilized. Samples were ionized using APCI and ions were monitored at the following transitions: 472/436 for terfenadine, 503/466 for fexofenadine, 268/143 for azacyclonol, 477/266 for loperamide, 463/252 for monodemethyl loperamide, and 449/238 for didemethyl loperamide. Standards were available for each of the metabolites, allowing accurate quantification. Cetirizine was used as an internal standard.

D. RESULTS

The first study was conducted in order to determine whether absorptive permeation of terfenadine across Caco-2 cell monolayers produces more metabolites than that in the secretory direction. At a dose of 20 μM terfenadine, the absorptive metabolic rate was approximately 60% higher than the secretory rate. In contrast, at a higher dosing concentration, the effect seemed to be saturable: absorptive and secretory metabolic rates were more similar (Figure IV.1).

A similar study was carried out for loperamide at a dose of 20 μM. As shown in Figure IV.2, there was a marked difference between A-to-B and B-to-A metabolism for loperamide. More importantly, this effect was not diminished by pretreatment of the cells with P-gp inhibitor GW918; the absorptive metabolic rate remained about 6-fold higher than the secretory rate.

The next set of experiments used fresh intestinal tissue from mice in order to determine whether the effect would be seen in a more physiological system. Indeed, for a 10 μM dose of terfenadine, a 4-fold higher metabolic rate was observed in the absorptive direction (Figure IV.3). At a higher dose (50 μM), the effect was again diminished but the rates were still significantly different. The same results were obtained for loperamide in normal mouse tissue. Even at a dose of 150 μM loperamide, the effect was less but was still apparent (Figure

IV.4). Finally, a P-gp deficient mouse intestine was used to determine whether the effect is mediated solely by P-gp. At a 5 μM dose of terfenadine, the metabolic rate in the absorptive direction remained about 2-fold higher than that in the secretory direction.

E. DISCUSSION

When absorptive metabolism of dual CYP3A/P-gp substrates was shown to be higher than secretory metabolism, it was logically deduced that P-gp may be responsible. This result was confirmed for loperamide and terfenadine in this work, in both the Caco-2 cell model and in fresh mouse intestine. The effect appeared to be saturable, which implies that the cause is not a nonspecific mechanism, such as binding. However, in the Caco-2 cell model, the effect was not diminished by complete inhibition of P-gp, implying that there are other mechanisms at play besides P-gp efflux.

Similarly, in the mouse model, A-to-B permeation of both terfenadine and loperamide produced more metabolites than B-to-A permeation. The effect was somewhat diminished at higher dosing concentrations, again implying saturability of the mechanism involved. When the experiment was performed using P-gp-deficient mouse intestine, absorptive metabolic rate was still 2-fold higher than the secretory rate. Since the difference between the metabolic rates was decreased compared to the wild-type mouse, P-gp may be partially responsible for this interaction. However, there must still be some other process at play that either increases substrate concentration at the enzyme site when the drug is dosed on the apical side, or decreases effective concentrations when the drug is dosed basolaterally.

Another experiment that would help to clarify this issue would be to measure the metabolism of a CYP3A substrate that is not affected by P-gp in the absorptive and secretory directions. This would help to further determine whether P-gp has any involvement in this interaction.

F. CONCLUSIONS

In summary, in the Caco-2 cell system, absorptive metabolism produces more metabolites than secretory metabolism for dual CYP3A/P-gp substrates. Some authors have postulated that the enhancement of metabolism observed in the A-to-B direction is due to drug efflux by P-glycoprotein (P-gp). However, since this inequality was not abolished by chemical P-gp inhibition or by genetic P-gp knockout, P-gp is not likely to be responsible. Instead, another mechanism such as functional coupling of CYP3A to the apical membrane, resulting in better access of the drug to the enzyme from the apical direction, may be responsible.

G. REFERENCES

Gan LS, Moseley MA, Khosla B, Augustijns PF, Bradshaw TP, Hendren RW and Thakker DR (1996) CYP3A-like cytochrome P450-mediated metabolism and polarized efflux of cyclosporin A in Caco-2 cells. *Drug Metab Dispos* **24**:344-349.

Lee K and Thakker DR (1999) Saturable transport of H2-antagonists ranitidine and famotidine across Caco-2 cell monolayers. *J Pharm Sci* **88**:680-687.

Mouly SJ, Paine MF and Watkins PB (2004) Contributions of CYP3A4, P-glycoprotein, and serum protein binding to the intestinal first-pass extraction of saquinavir. *J Pharmacol Exp Ther* **308**:941-948.

Paine MF, Leung LY, Lim HK, Liao K, Oganesian A, Zhang MY, Thummel KE and Watkins PB (2002) Identification of a novel route of extraction of sirolimus in human small intestine: roles of metabolism and secretion. *J Pharmacol Exp Ther* **301**:174-186.

Raeissi SD, Hidalgo IJ, Segura-Aguilar J and Artursson P (1999) Interplay between CYP3A-mediated metabolism and polarized efflux of terfenadine and its metabolites in intestinal epithelial Caco-2 (TC7) cell monolayers. *Pharm Res* **16**:625-632.

Schmiedlin-Ren P, Thummel KE, Fisher JM, Paine MF, Lown KS and Watkins PB (1997) Expression of enzymatically active CYP3A4 by Caco-2 cells grown on extracellular matrix-coated permeable supports in the presence of 1alpha,25-dihydroxyvitamin D3, in *Mol Pharmacol* pp 741-754.

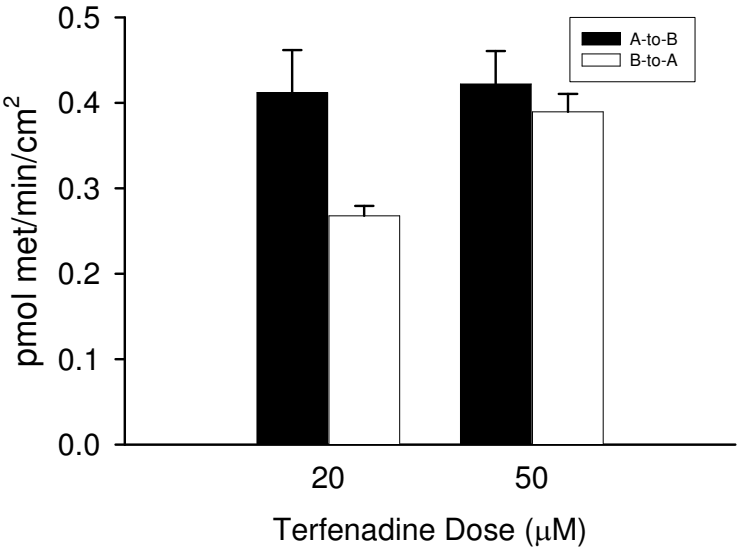

Figure IV.1. Apical to Basolateral (A-to-B) versus Basolateral to Apical (B-to-A) metabolism of terfenadine in Caco-2 cell monolayers. Mean of 3 ± SD. A significant difference was observed between metabolism in the A-to-B and B-to-A directions at the 20 μM dose level only ($p<0.05$, student's t-test).

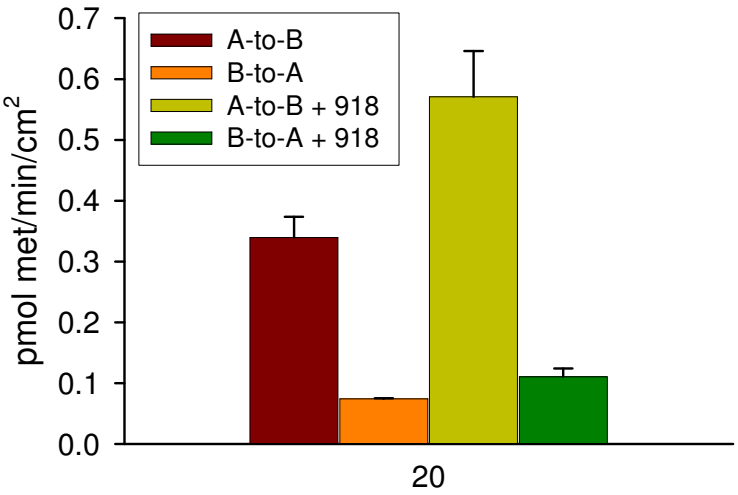

Figure IV.2. Apical to Basolateral (A-to-B) versus Basolateral to Apical (B-to-A) metabolism of terfenadine in Caco-2 cell monolayers, in the presence and absence of 1 μM P-gp inhibitor GW918. Mean of 3 ± SD. A significant difference was observed between metabolism in the A-to-B and B-to-A directions in both treated and untreated groups; a significant difference between treated and untreated groups was observed in the A-to-B direction only ($p<0.05$, student's t-test).

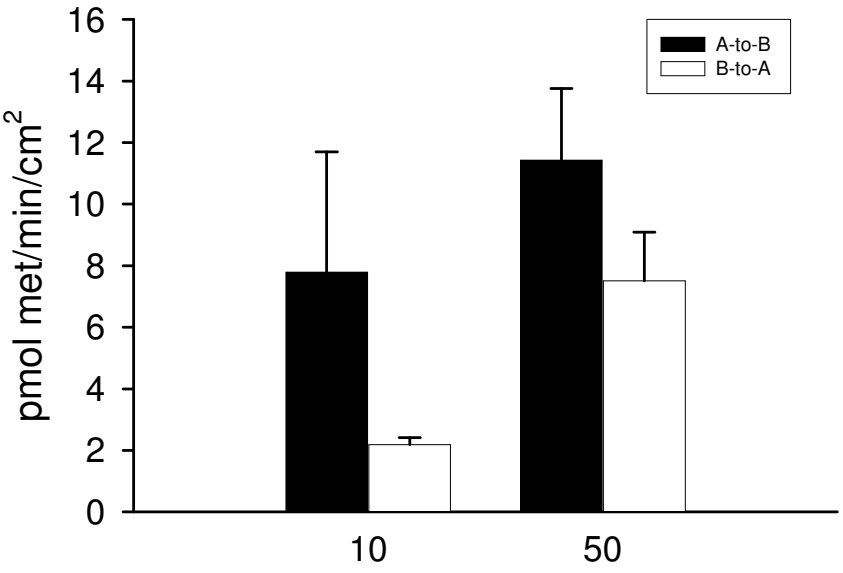

Figure IV.3. Apical to Basolateral (A-to-B) versus Basolateral to Apical (B-to-A) metabolism of terfenadine in P-gp-competent mouse intestine. Mean of 3 ± SD. A significant difference was observed between metabolism in the A-to-B and B-to-A directions at both dose levels ($p<0.05$, student's t-test).

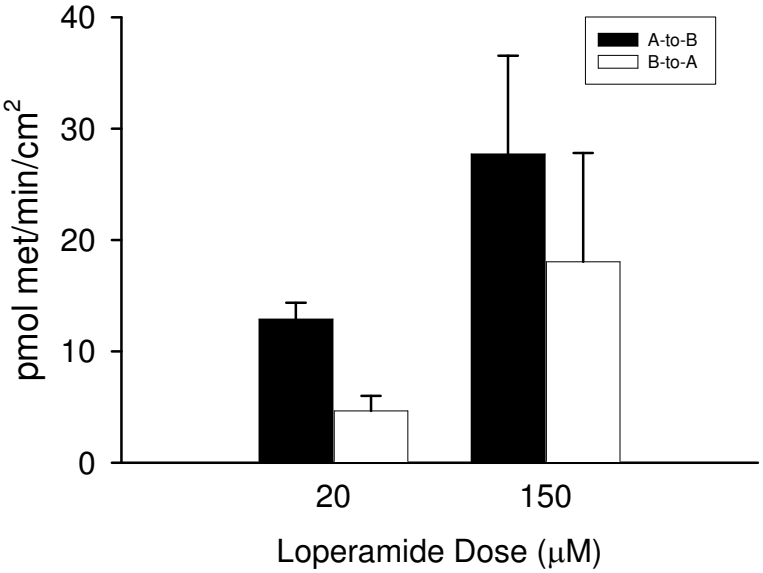

Figure IV.4. Apical to Basolateral (A-to-B) versus Basolateral to Apical (B-to-A) metabolism of loperamide in P-gp-competent mouse intestine. Mean of 3 ± SD. A significant difference was observed between metabolism in the A-to-B and B-to-A directions at the 20 μM dose level only ($p<0.05$, student's t-test).

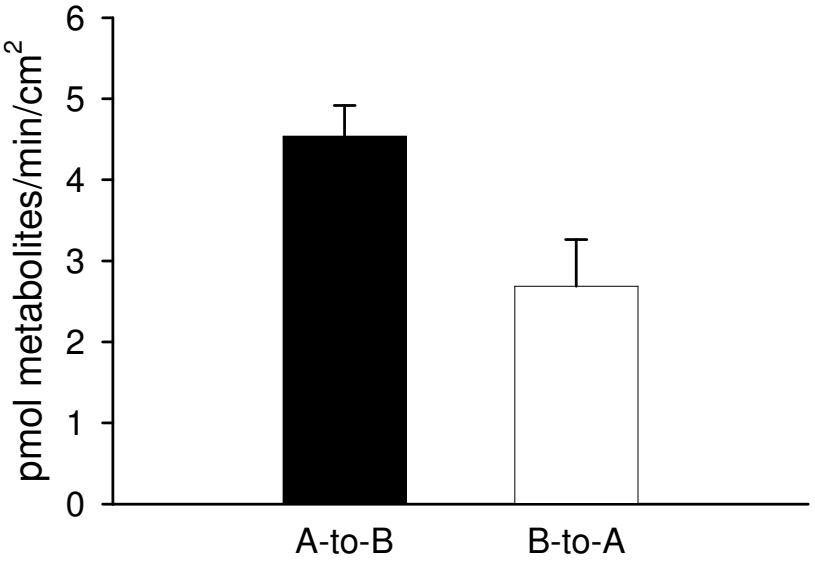

Figure IV.5. Apical to Basolateral (A-to-B) versus Basolateral to Apical (B-to-A) metabolism of terfenadine (5 µM dose) in P-gp-deficient mouse intestine. Mean of 3 ± SD. A significant difference was observed between metabolism in the A-to-B and B-to-A directions ($p<0.05$, student's t-test).